UNIVERSITÉ DE GENÈVE
Département de Chimie
Minérale, Analytique et Appliquée

FACULTÉ DES SCIENCES
Professeur W. HAERDI
Docteur J. BUFFLE

STUDY OF THE FORMATION OF TRUE MERCURY FILMS FOR ELECTROANALYTICAL APPLICATIONS TO SPECIATION

Development of an Iridium Based Electrode

THÈSE

présentée à la Faculté des Sciences
de l'Université de Genève
pour obtenir la grade de Docteur ès Sciences, mention chimique

par

Samuel P. KOUNAVES
de San Diego, California (U.S.A.)

Thèse N^{o} 2151

GENÈVE
1985

"The aim of science is not to open the doors to everlasting wisdom, but to set a limit on everlasting error."

Bertold Brecht

"The Life of Galileo Galilee"

La faculté des sciences, sur le préavis de Messieurs W. HAERDI, professeur ordinaire et J. BUFFLE, maître d'enseignement et de recherche, codirecteurs de thèse (Dpt de chimie minérale, analytique et appliquée) et P. VALENTA, docteur ès sciences (Institut für Chemie der Kernforschungsanlage, D-Jülich)

autorise l'impression de la présente thèse, sans exprimer d'opinion sur les propositions qui y sont énoncées.

GENÈVE, le 12 mars 19 85

Le Doyen :
Armand BUCHS
A. Buchs

Thèse 2151

ACKNOWLEDGMENTS

The work reported in this thesis was carried out in the laboratories of the Department of Chemistry of the University of Geneva, Switzerland.

I would like to thank in particular Dr. Jacques Buffle for his advice, constant interest, and invaluable time, without which this work would not have been possible.

My gratitude is equally addressed to Professor Werner Haerdi who gave me the possibility to undertake this thesis.

I thank Dr. P. Valenta for having accepted to be a member of the thesis committee.

Finally, I wish to thank everyone, who by their professional collaboration or their friendship, have contributed to the realization of this work, and to my wife Aileen for her unfailing support.

REMERCIEMENTS

Les travaux reportés dans cette thèse ont effectués dans les laboratories du Département de Chimie minérale, analytique et appliquée de l'Université de Genève.

Je tiens à remercier tout particulièrement le Docteur Jacques Buffle. Les nombreux conseils qu'il m'a donnés, l'intérêt qu'il a porté à mes recherches et sa disponibilité sont pour beaucoup dans la réalization de ce travail.

Mes remerciements s'adressent également au Professeur Werner Haerdi qui m'a donné la possibilité d'entreprendre cette thèse.

Je remercie le Docteur P. Valenta d'avoir accepté de faire partie du jury de thèse.

Je remercie enfin toutes les personnes qui, par leur collaboration professionel ou leurs relations amicales, ont contribué à la réalisation de ce travail, et à mon épouse Aileen pour son appui infaillible.

ABSTRACT

The purpose of this thesis work was to compare different types of electrode substrates in order to select the best in respect to its ability to maintain a true mercury film on its surface, and show its potential applicability for the speciation of trace metals.

The complete system, as developed for this research, permits the simultaneous control of potential and current at an electrode, while microscopically observing in-situ its surface. In addition, a flow through configuration allows for the exchange of test solutions without interrupting the electrode-solution contact. The system is constructed so that it may easily be adapted to a variety of electrochemical experiments.

A selection of substrate test materials was made based on their low solubility and non-chemical interaction with mercury as defined by the electrochemical work function.

This study has allowed the development of a complete procedure for preparing a mercury film electrode on Ir (IrMFE). An application is demonstrated where the iridium-MFE is used for quantitative analysis of cadmium in model water, and zinc in natural sea water. At the same time, a simple theory for "stripping polarography" at a mercury film is tested and shown to be valid.

RÉSUMÉ FRANÇAIS

Le but de ce travail de thèse est de comparer différents types de substrats, de sélectionner le meilleur par rapport à se facilité à maintenir un vrai film de mercure sur sa surface et de montrer son applicabilité potentielle à la spéciation de métaux en trace.

Le système complet, comme structuré pour cette recherche, permet de contrôler simultanément le courant et la potentiel à une électrode, pendant l'observation microscopique "in-situ" de sa surface. D'autre part, la circulation de flux permet l'échange des solutions testées sans couper le contact électrode-solution. Le système est surtout construit pour être facilement adaptable à une variété d'expériences électrochimiques.

Une sélection des matériaux a été faite en se basant sur la faible solubilité, et sur l'interaction non-chimique du substrat avec le mercure comme défini par la fonction de travail électrochimique.

Cette étude a permis de développer un procédé complet pour préparer une électrode à film de mercure sur Ir (Ir-MFE). Les applications ont démontré que l'iridium-MFE peut être utilisée pour l'analyse quantitative du cadmium dans l'eau modèle, et du zinc dans l'eau de mer naturelle. En même temps, une théorie simplifiée pour la "stripping polarography" sur un film de mercure est testée et se révèle valable.

TABLE OF CONTENTS

APPENDICIES

FRENCH RESUME

1. INTRODUCTION AND BACKGROUND

1.1 USE OF VOLTAMMETRIC STRIPPING TECHNIQUES IN TRACE METAL ANALYSIS AND SPECIATION

With the arousing of environmental consciousness has come the increasing demand on analytical chemistry to provide the means, not only to determine which and how much of an element is present, but also to characterize the role and reactivity of the different forms in which it occurs [1,2] . The distribution of an element or component into all its physico-chemical forms or species is referred to as its *speciation*.

The speciation of a trace metal is very important since it can drastically affect its toxicity towards aquatic organisms, or alter its role in the geochemical environment. For example, studies have shown that free metal ions and lipid-soluble complexes are the most toxic, while most stable complexes and colcolloidally associated species are not [3].

Speciation analyses normally require the use of several techniques before complete speciation of an element can be made [4]. Currently available techniques include ion-exchange, solvent-extraction, spectrometry, neutron-activation, dialysis, ultrafiltration and electrochemical. The use of these methods allows the components to be divided into fractions or groups for more efficient characterization. In practice they are often arbitrarily divided into several major groups, such as *soluble* and *particulate*, or *inert* and *labile*.

Electrochemical methods offer versatile and efficient approaches for measurement and characterization of the dissolved trace metal species [5-8]. Table 1.1 shows a list of the currently available electrochemical methods.

TABLE 1.1 Sensitivity of Electrochemical Methods for Trace Metal Determinations

ELECTROCHEMICAL METHOD	LOG SENSITIVITY (M)
Ion selective electrodes	-6
Classical Polarography	-6
Linear-sweep voltammetry	-6
Differential Pulse Polarography	-7
ASV with hanging mercury drop	-8
DPASV with hanging mercury drop	-9
DPASV with mercury-film electrode	-11

Since many metals of interest occur at total concentrations between 10^{-8} to 10^{-10}M, most speciation studies in natural waters have been done using ASV. The remarkable sensitivity of ASV is due to a pre-deposition step during which the metal ions in solution are reduced and concentrated in a mercury drop or film electrode. Reoxidation and measurement of the metal ion is then performed by either an anodic potential sweep or by chronopotentiometry.

The work using ASV has primarily progressed in two major directions: studies of the shift in peak potentials with changing concentrations of ligands [9-11] and studies of changes in peak height or peak area under differing experimental conditions. Variants of the second approach include pH titrations [8,11] and complexometric titrations [12] in which ligands are quantitatively titrated with metal ions or, alternatively, metal ions are titrated with ligands [13,14]. In this technique, the electrolysis potential is set at a value which presumably discriminates between the "free" metal ion and its complexes, since at that potential, the complexes are supposedly reduced at a slower rate, or not at all (see Fig.1.1).

Techniques based on the shift of the ASV peak potential depend on the degree of reactivity of the oxidized metal with the ligand of interest in the reaction layer. They can describe the species undergoing reduction, i.e., the speciation in the natural medium, only indirectly since only the ratio of the concentrations of ASV labile metal to the total metal, is measured. Furthermore, reversibility must usually be assumed in order to enable simple interpretation of the data. Thus, they

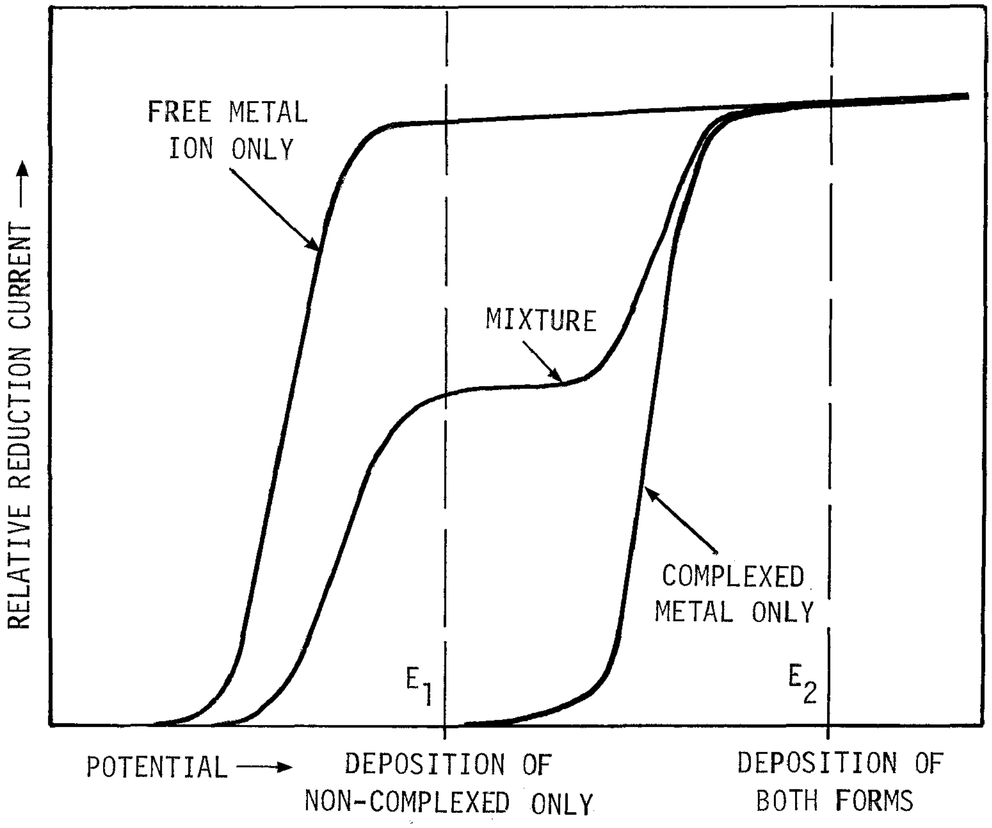

FIGURE 1.1 Potential at which deposition is set in order to discriminate "free" and complexed species.

are more suitable for model studies and for determination of stability constants in known media than for direct measures of natural speciation. On the other hand, methods dependent on peak height or peak area can give direct information on the natural species as long as a direct proportionality exists between the quantity of the species reduced during the electrolysis step and the peak current or area during the oxidation step.

One relatively novel form of ASV, which gives information about the species undergoing reduction, is known as Stripping Polarography (SP) [15,16]. In stripping polarography, peak current or charge obtained by ASV or chronopotentiometry are plotted against the applied electrolysis potential. These plots, as shown in Figure 1.2, have the sigmoidal shape of ordinary d.c. polarograms but without the residual current component, and present the possibility of extending classical polarographic methodology to trace metal speciation at the 10^{-10}M level. As will be shown in Sec.2.4, one may obtain from the stripping polarogram, $E_{1/2}$, the slope of the reduction wave, the equilibrium constant, and the number of ligands, determined from the variation of $E_{1/2}$ with the amount of added ligand.

1.2 PROBLEMS ASSSOCIATED WITH ELECTRODES USED FOR VOLTAMMETRIC STRIPPING TECHNIQUES IN SPECIATION

As was mentioned earlier, there are two main types of electrodes currently used with stripping techniques, the HANGING MERCURY DROP (HMDE) and the MERCURY FILM (MFE) (see Fig.1.3). Since the main topic of this thesis is the latter, a more detailed description of it, and its problems, will be covered in the following sections. What will be briefly discussed here, are the limitations of the HMDE [17,18] as compared to the MFE and some of the major problems that are common to both types.

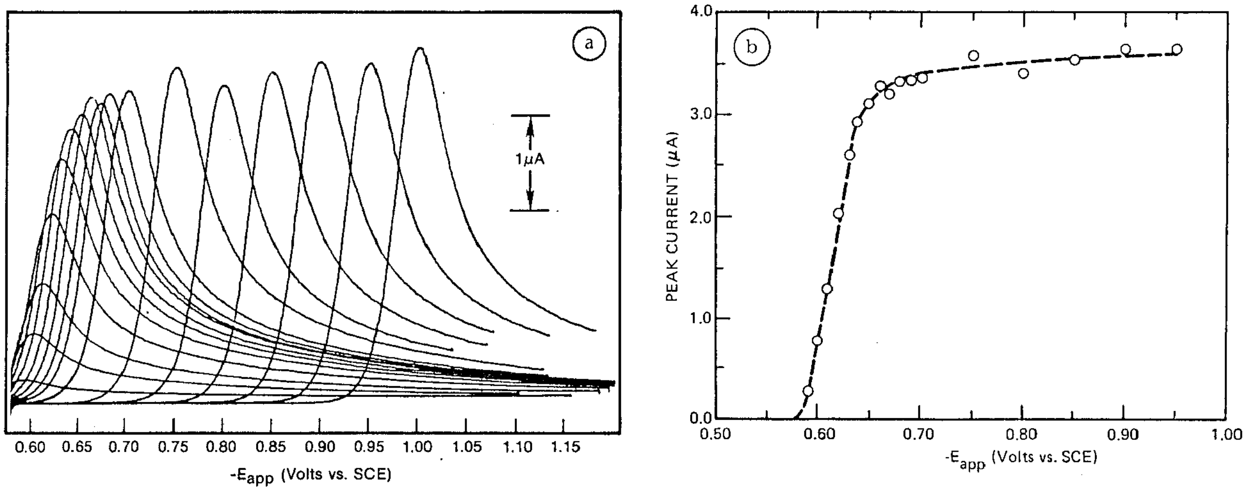

FIGURE 1.2 (a) ASV current peaks obtained at each indicated potential. (b) Stripping polarogram constructed from ASV peaks. (10^{-8}M cadmium(II) in seawater)

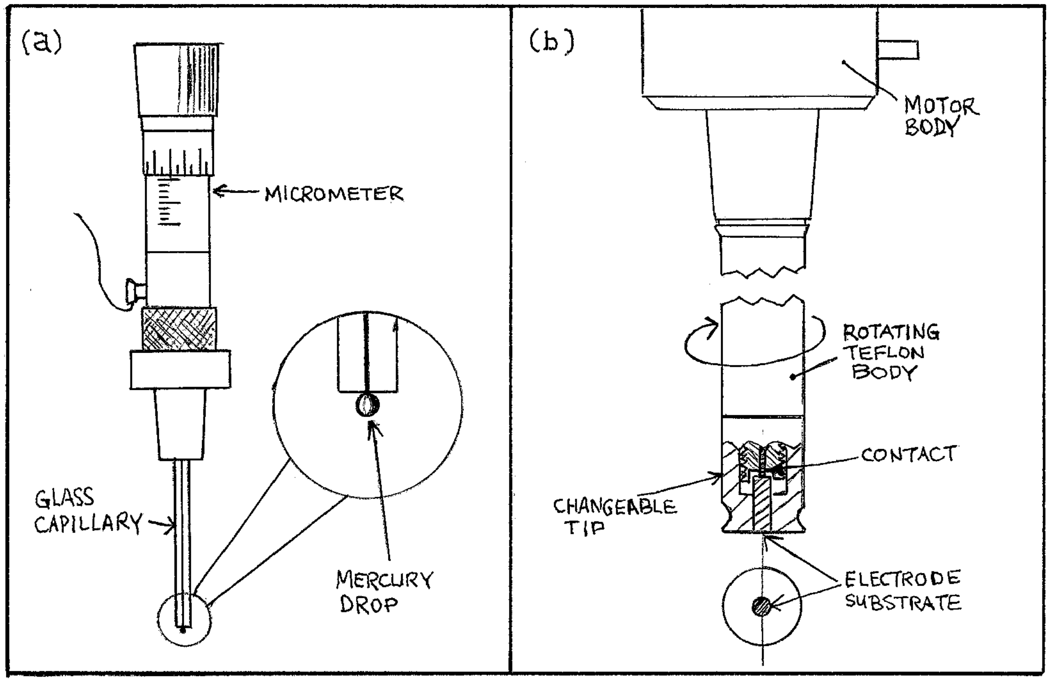

FIGURE 1.3 (a) Hanging mercury drop electrode with micrometer and capillary delivery system. (b) Mercury film as part of a rotating disk electrode configuration.

HMDE vs. MFE. The HMDE consists of a drop of mercury suspended from a mercury thread formed in a glass capillary, with a calibrated micrometer for control of drop size. Because of its spherical shape it has a low surface-area/volume ratio. This implies a dilution of the metal reduced into the drop and consequently necessitates longer deposition times than for the MFE. It also means that a finite time is required for dissolved metals in the mercury to diffuse to the surface during the stripping step. The end result of the slow diffusion is broader stripping peaks, leading to loss of resolution in multimetal analysis. The hanging of the drop from the capillary results in: *i)* having to use slower stirring in order to avoid dislodging, *ii)* a deformation of the spherical shape, and *iii)* effectively shielding part of the drop surface. The spherical geometry makes it difficult to have any type of defined, homogeneous, hydrodynamic conditions in relation to the diffusion at the surface.

After such an array of disadvantages, one may wonder why the HMDE is used at all. Most of these problems however are not important for purely quantitative analysis; where its excellent negative potential range, the ease and reproducibility of obtaining a new drop with a totally new surface, and the very low residual current, account for its being the most popular electrode for ASV.

Limitations Inherent to Both HMDE and MFE. There are three important limitations for both HMDE and MFE which would apply even to the "ideal" electrode. The first two could be overcome by modifying the geometry or cofiguration of the electrochemical cell. Although solving these problems was not the primary goal of this thesis work, it is worthwhile to mention them:

- _adsorption effects on mercury_, which have been shown to cause major changes in polarographic results when organic matter, colloidal particles or any other surface active substances are present to coat the mercury surface. [19,20].
- _surface concentration effects_, which result from the fact that there is a larger concentration of the metal ion at the electrode surface during the stripping step than in the bulk solution. Any ligand with which the metal may combine, and that has a concentration < 1000 times that of the metal, may be easily saturated with the reoxidized metal at the surface [21]. The net effect is a distortion of the stripping peaks, and a possible misinterpretation of the speciation data [22,23].
- _number of analyzable metals_, which is normally limited to about fifteen. Among these however, we have Cd, Pb, As, Cu, and Zn, which are currently of great environmental interest.

A good comparative study of the HMDE and MFE has been done by Batley and Florence [24].

Stripping techniques have also occasionally been used in conjunction with solid electrodes such as _graphite_ and _platinum_ [25,26]. Unlike the mercury electrodes, however, the metal ion is reduced directly onto the solid surface. Generally speaking, such electrodes have been of little use mainly because of the poor results obtained. Problems associated with surface contamination, reproducibility and intermetallic interactions between the different metals in the deposited film are often encountered and give rise to irregularities in the stripping peaks, such as frequent overlapping and multiplicity.

1.3 THE MERCURY FILM ELECTRODE

The advantages of the MFE for stripping techniques became apparent in the early 50's, and have since prompted its wide-spread use [27]. Despite this, we still have the situation today where:

1) there are as many methods for the preparation of a MFE as there are papers describing them,
2) the theoretical basis for the wetting of metals by mercury is poorly understood and the experimental literature on the subject contains many contradictory statements and results,
3) no one has yet produced an "ideal" or even "near ideal" mercury-film electrode,

1.3.1 The Literature

The earliest attempts to construct a MFE were made by Gardiner and Rogers [28] who used mercury coated platinum and silver to determine cadmium and zinc. However, even with this premier investigation it was noted that both electrodes presented problems in respect to stability and reproducibility. All attempts since then [29-34] to use silver as a substrate have all basically ended with the same conclusion. In the very rigourous and complete study by Stojek and his group [32,33], the general characteristics, stability, and aging of the silver based electrode were investigated. Although attempts were made to diminish the problems, it was clear that for all of the metals used in the study (Sb, Tl, Sn, Cu, Bi, Zn, Cd and Pb), some degree of metal-silver compound formation occurred in the mercury, giving pre-peaks and generally irreproducible results for films older than a few hours.

The platinum based MFE has been the most widely used and investigated of the metallic based electrodes. Rogers et al. [28,35] were the first to use it for determination of cadmium and zinc. Several groups during the years that followed did extensive studies and developed many methods for the preparation and uses of the platinum-MFE [36-44]. Although the platinum-MFE does not show intermetallic compound formation to the same extent, for example that silver does, it has became apparent that interactions between the platinum base, the mercury, and certain metals (Cu, Sn, In, Al, Zn) do occur [43-45] and that the "film" is not even a true film in some cases [46].

Two other metals which have been tried as substrates for the MFE are nickel [47-49] and gold [50]. In both cases nonuniform films and intermetallic compound formation were noted.

The glassy-carbon-MFE is now the most widely used in voltammetric analyses, supposedly because it is inert, mechanically strong and has good electrical conductivity.

This MFE is usually prepared in one of two ways: either by plating from a mercury(II) solution and then transferring to the sample solution [51,52], or by simultaneous in situ deposition of the mercury and the trace metals to be analyzed, ie. by adding mercury(II)-nitrate to the sample solution and plating at a potential where both the mercury and metal are reduced. For another sample, the mercury-film is removed by wiping off with a tissue [53,54].

Although both methods are very satisfactory for quantitative analytical work, certain drawbacks exist for both when used in speciation studies. Firstly, the sample solution may have its species distribution drastically modified by addition of mercury(II) ions. Since we wish to measure the original speciation, this makes the in situ method impractical. Furthermore, both methods have a more serious problem, since speciation interpretations require a MFE surface that is not only empirically reproducible (as they must also be for quantitative analyses), but in addition, more rigorously defined. Most voltammetric stripping analyses assume the existence of a thin, homogeneous mercury film. It is now clear that this is not the case. Microscopic examination of the glassy-carbon surface after mercury deposition shows it to be covered by a large number of spherical mercury drops [55]. For deposition of very thin mercury films (< 0.1µm), these droplets are small enough and close enough in comparison with the diffusion layer thickness, that they appear as a flat surface electrode. Thus, an agreement with the theory for diffusion controlled currents is to be expected. Use of this type of electrode has shown it to be reproducible for quantitative analysis [51]. However, since the carbon surface is exposed between the drops, and it is well known that the surface of the glassy-carbon is particularly suitable for adsorption of organic material [56,57], both theoretical studies and natural media speciation must deal with possible interferences from such adsorption.

It should be mentioned at this point that a number of different versions of the carbon based electrode have been prepared. These include, in addition to the already mentioned glassy carbon, impregnated-graphite [58-60], pyrolytic-graphite [61], and graphite-spray [62]. All of these suffer from the same problems as glassy-carbon in terms of film formation and adsorption.

1.3.2 The Contradictions

To allow a better understanding of the problems involved in preparing and using a MFE, it may be of some value to briefly mention some of the contradictory statements that have appeared in the recent literature.

Structure of the Film. One of the problems with the MFE can be best illustrated with the glassy-carbon substrate. For many years this electrode was plated with mercury, and since a visual observation of the surface showed a dull gray layer, it was assumed that a mercury film covered the surface.

Florence [53] and Stojek et al. [63] have both described mercury deposition on glassy-carbon as resulting in a uniform spread over the electrode surface for thicknesses of 0.001µm to 1µm. Both authors found "excellent agreement" between the experimental data (for peak heights, half-width and shifts) and the De Vries-Van Dalen theory [64,65] for thin film electrodes. Perone and Brumfield [66] obtained excellent correlation between experimental and theoretical behavior using chronopotentiometric stripping and films from 0.5µm to 5µm thick, but when stripping with a linear sweep potential, poor correlation was obtained. In complete disagreement with the opinion of the above authors in relation to the film structure, Stulikova [55], Hume and Carter [59], and Mataon et al. [52] all report that the mercury deposited on glassy-carbon always consists of an "aggregate of tiny mercury spheres" whose size and number depends on the mercury deposition potential. It is interesting to note that Cox [39], who assumed the existence of a true film on a platinum-MFE, found poor correlation with theory. It is ironic that the few investigations carried out to confirm the De Vries-Van Dalen "thin film" theory have used as substrates, either glassy-carbon [63,66], platinum [39], or nickel [47]. On all of these substrate surfaces, one may question the existence of a true and pure mercury film.

Film Preparation. Another main area of "nonagreement" is over the type of pretreatment required to enhance the ability of a substrate to support a thin mercury film. That such a wide variety of pretreatments have proliferated is related to a relatively poor understanding of the nature and reactivity of the electrode surface before and after pretreatment.

The case of platinum is a good example. The work of Heumann and Forch [67] showed that the formation of a mercury film on the surface of most solids, including platinum was facilitated by the existence of an oxide layer. Indeed, many current pretreatments include an anodization step previous to mercury deposition [eg.45,68]. In contrast to this, the work of Maslentskii and Zverevich [69] and Barlow and Planting [70] showed that wetting by mercury takes place more easily on clean and reduced metal surfaces. Based on these results, many pretreatments include a cathodization step [eg.38,40].

Other Areas of Contradictory Data. In addition to the ones already mentioned above, we can add:

- Mechanical Strength; glassy-carbon has been described as being "mechanically strong" [53], in contrast to "possess the tendency to develop cracks" [72].
- Activation with Hydrogen Gas; it has been shown that "gassing a nonpolarized platinum surface with hydrogen does not increase the tendency of mercury to wet its surface" [73], while another author claimed that "wetting the surface of metals with mercury is produced after the surface is pretreated with hydrogen gas" [74].
- Inertness; glassy-carbon has been generally described as being "inert" [53] but evidence has been found that there are functional groups on the surface which undergo redox reactions [57,71,75].
- Deposition Conditions; for such items as, the solvent, temperature, pH, potential, and current, the choices are as many as there are electrochemists to make them.

It is evident from the above, why many electrochemists consider the formation of a mercury film more of an "art" rather than an established technical procedure.

1.4 PURPOSE

The endeavors to underatand the distribution of chemical species in the aquatic environment could substantially benefit from improvements in the abilities of voltammetric stripping techniques.

The most important limitations for the interpretation of data obtained from such techniques are linked to the electrode geometry and hydrodynamics, especially during the deposition step. An ideal electrode should be stable both mechanically and chemically and possess a high hydrogen overvoltage. Mercury drop or film electrodes possess some of these properties and have therefore been generally used in voltammetric studies. However, as was previously mentioned, serious limitations exist for the mercury drop electrodes in speciation studies, particularly in terms of their relative "massiveness" in respect to internal diffusion and their rather uncontrolled and nonuniform hydrodynamics and diffusion at their spherical surface.

The ideal configuration would be a thin mercury-film with a controlled flow over its surface. One hydrodynamic system that comes close to uniform surface hydrodynamics is the rotating disk [76,77]. The combination then of a thin mercury-film on a rotating disk should provide some of the desirable properties of an "ideal electrode". It seems though that finding an "appropriate" substrate on which to form a mercury film has been, to the frustration of many electrochemists, a rather unattainable goal.

This substrate should: *i)* possess good wettability by mercury, in order to promote film formation and mechanical stability, and *ii)* be chemically inert in respect to mercury and all metals to be reduced into the mercury. As we have seen, neither of the currently used substrates, <u>platinum</u> and <u>glassy-carbon</u>, possess both of these properties. The first is in reality an amalgam film electrode, while the latter is a mercury droplet monolayer electrode.

Seeing that only a limited number of materials have been tested as mercury film substrates, the first aim of this thesis work was to compare a number of different types, and select the best one in terms of its ability to maintain a mercury-film on its surface.

At the same time a second objective of this work was to bring to light some of the current discrepancies and problems that must be addressed, in order to use such a mercury-film electrode to correctly measure speciation parameters in natural conditions.

The present study is composed of three experimental parts. The first part, described in Chapter 4, is an investigation of various materials in relation to their suitability as possible substrates for mercury-film formation. An iridium substrate is proposed as the best choice. The second part, described in Chapter 5, concentrates on the optimum conditions for the preparation and study of the properties of an iridium mercury-film electrode. The third part, described in Chapter 6, demonstrates the application of an iridium-substrate mercury-film rotating-disk electrode to: *i)* the evaluation of the De Vries and Van Dalen ASV mercury-film theory, and *ii)* to the analysis of cadmium, lead, and zinc in both model and natural water systems.

2. THEORY

This thesis work deals with several areas of electrochemistry. It encompasses electrode geometry and hydrodynamics, formation and characterization of thin mercury films, and several voltammetric techniques used in making speciation analyses.

The goals of this chapter are, therefore, to briefly set forth the theoretical aspects necessary for the understanding of the material that follows, and to allow the reader to proceed without needing to consult other texts.

2.1 ROTATING DISK ELECTRODE

The rotating disk electrode (RDE) is one of the few convective electrode systems for which the hydrodynamic and the convective-diffusion equations have been rigorously solved. A detailed description of the hydrodynamic theory for the rotating disk can be found in several special books [78-80]. Only the simplest concepts will be discussed here which may be needed later for interpretation of experimental data.

The electrode usually consists of a disk of the conducting material imbedded in a rod of insulating material, such as Teflon or some type of plastic, which is then rotated at high speed by an electric motor (see Fig.1.3a). As the disk rotates, it drags the fluid at its surface along with it and, due to the centrifugal force, develops a radial velocity outwards from the center of the disk. Consequently, the fluid pressure at the surface is decreased, and is replenished by a flow normal to the surface. A diagrammatical representation of this process is shown in Figure 2.1.

2.1.1 Velocity and Concentration Profiles

Velocity Profile. The velocity profile of a fluid near a rotating disk was analytically solved by Cochran [81] and later numerically by Clarenbach and Grabner [82]. The values calculated by the the former are shown in Fig. 2.2a. At the surface (ie. $x = 0$), $v_r = 0$, $v_x = 0$, and $v_\phi = \omega r$, where v_r, v_ϕ and v_x, are the radial, tangential and axial velocity components, ω is the angular disk velocity (rad/sec) and r is the radial distance from the rotation axis. In the bulk solution (ie. $x = \infty$), $v_r = 0$, $v_x = -v_0$, and $v_\phi = 0$. Thus, far from the surface, there is no flow in the radial and tangential directions, but the solution flows at the limiting velocity, v_0, toward the disk with v_0 being determined by ν and ω. It should be noted that at $x(\omega/\nu)^{1/2} \approx 3.2$, we have $v_x \approx 0.8v_0$ while $v_\phi \rightarrow 0$. The corresponding distance:

$$x = 3.2(\nu/\omega)^{1/2} = \delta_H \qquad (2.1)$$

where ν is the kinematic viscosity of water (cm^2/sec), is taken as the thickness of the hydrodynamic boundary layer, δ_H (ie. the layer of liquid dragged by the rotating disk), and is constant over the entire surface of the disk. For water, with $\nu = 0.01$cm^2/sec, and $\omega = 100$ rad/sec ($\approx$1000rpm), δ_H is of the order of a few hundredths of a centimeter.

Concentration Profile. The above discussion is only concerned with the liquid-flow and applies to any rotated disk whether or not it is used as an electrode. In the usual

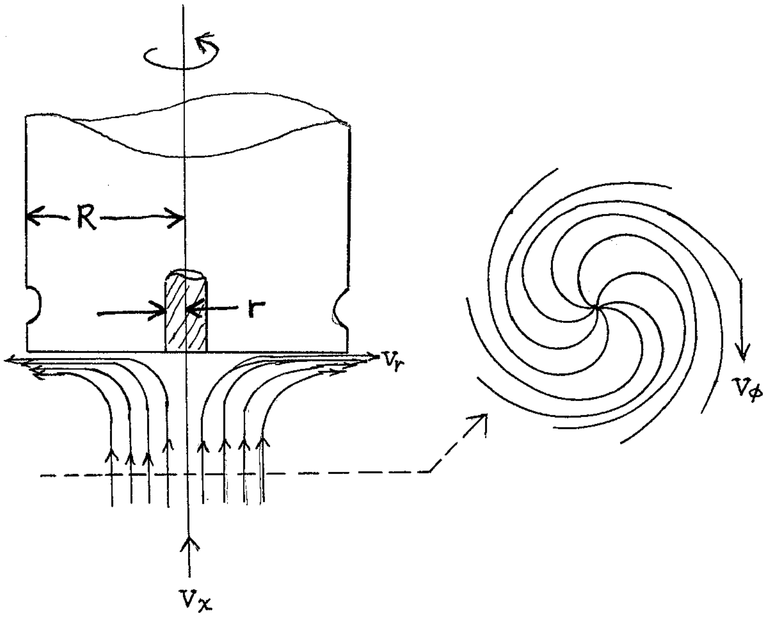

FIGURE 2.1 Rotating disk electrode showing the hydrodynamic fluid flow and velocity vectors.

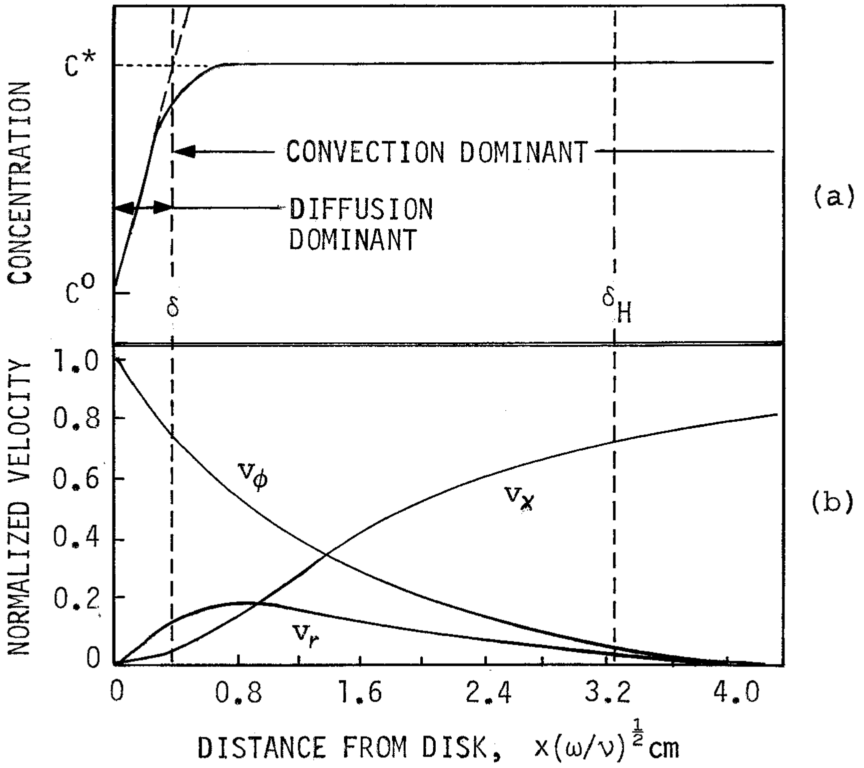

FIGURE 2.2 (a) Velocity distribution around the rotating disk electrode where v_x, v_ϕ and v_r, are the axial, tangential and radial components. (b) Concentration profile at the surface with δ being the thickness of the Nernst diffusion layer and δ_H being that of the hydrodynamic layer.

electrochemical case, the concentration of the electroactive species must also be taken into account.

As is illustrated in Figure 2.2b, between δ_H and the surface, the concentration is essentially equal to the bulk concentration <u>except</u> for a thin portion next to the electrode surface, where it varies "almost" linearly between the bulk value, C^* and the surface value, C^o. If two straight lines are drawn, their intersection will define the thickness of the <u>Nernst diffusion layer</u>, δ. According to theoretical calculations [79] the value of δ is given by:

$$\delta = 1.6\ D^{1/3}\ \nu^{1/6}\ \omega^{-1/2} \tag{2.2}$$

For values of $D = 10^{-5}$ cm^2/sec and ω=32 radians/sec (≈ 300 rpm), the thickness of the diffusion layer, δ, will be ≈ 0.05 mm, or only about 1/20 that of the hydrodynamic layer, δ_H. This fraction does not change much from experiment to experiment, since both D and ν tend to remain constant.

There is one very important fact that should be noted about the diffusion layer thickness. Since the fluid at the surface is moving radially, δ_H should <u>increase</u> proportionally to $(r_o)^{1/2}$, where r_o is the radial distance from the center of the disk [79]. However, at the same time, δ_H is proportional to $1/(v_\phi)^{1/2}$ and v_ϕ is proportional to r_o, so that in this case δ_H should <u>decrease</u> proportionally to $1/(r_o)^{1/2}$. As can be seen, these two effects cancel each other, and as a result, δ_H is constant over the entire surface of the disk as long as the conditions for laminar flow are met (see Sec.2.1.2). The constant thickness of δ_H means that δ is also constant over the entire surface. This property of the RDE, which sets it apart from most types of electrode configurations, is known as <u>uniform accessibility</u> [76,79]. On a uniformly accessible electrode, the flux of material reacting on the surface is the same at all points.

Limiting Current for the RDE. The mass transfer and limiting diffusion current can be estimated by means of the model and concentration profile shown in Figure 2.2.

For a simple one-dimensional flux, F_o Fick's law can be written as:

$$F_o = D(\partial C/\partial x) \tag{2.3}$$

The flux can also be expressed in terms of the current i:

$$F_o = i/nFA \tag{2.4}$$

Using the approximation that $\partial C/\partial x \approx C^{*}-C^{o}/\delta$

$$i = nFAD(C^{*}-C^{o})/\delta \tag{2.5}$$

Then, assuming the application of a potential which assures that $C^{o}=0$, and substituting δ from Eq.(2.2), the limiting current i_L is given by the equation:

$$i_L = 0.62nFAD^{2/3}C^{o}\nu^{-1/6}\omega^{1/2} \tag{2.6}$$

where the symbols all have their usual meanings.

Surface Potential Distribution. For a disk electrode of radius r, which is embedded in an "effectively" infinite insulating plane, and for which the solution adjacent to its surface can be taken as an equipotential surface, the current distribution, I/I_o, has been shown [84] to be:

$$I/I_o = 0.5/\{1 - (r_o/r)^2\}^{1/2} \tag{2.7}$$

where I is the normal current density component (A/cm^2), I_o is the average of I, and r_o is the radial position. The equipotential and current lines for such an electrode are shown in Figure 2.3a. The equipotential lines are closer near the edge, and, at this point, the current density approaches infinity. However, polarization of the electrode promotes a more uniform current distribution, to a degree determined by the electrode reaction kinetics. In effect, slow kinetics impose additional ohmic resistance at the electrode surface, which eventually results in an almost linear current distribution. Figures 2.3b and 2.3c show the current and potential distributions, respectively, when going from a system

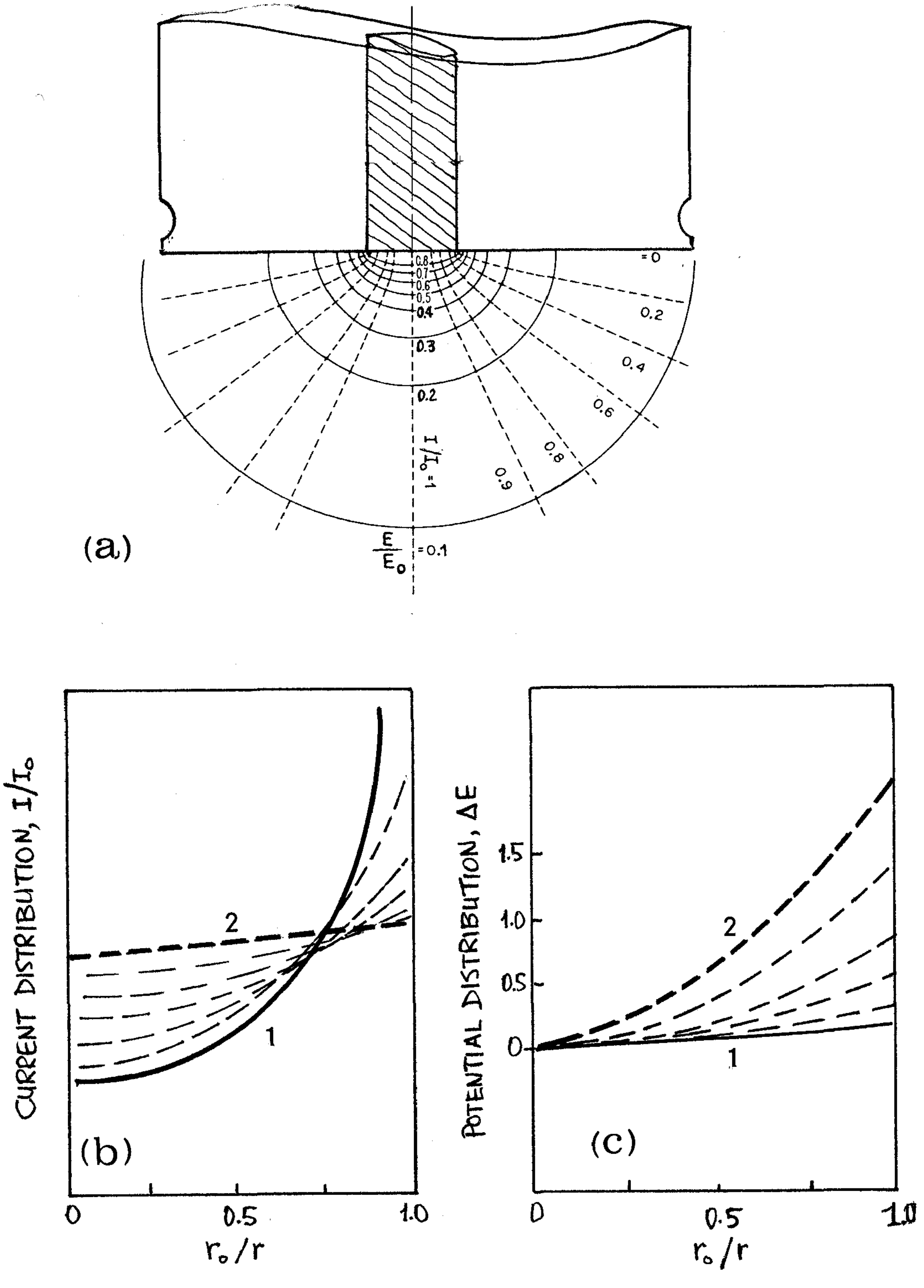

FIGURE 2.3 (a) Current and potential distributions for a disk electrode. The current lines are represented by dashed curves and the equipotential surfaces by solid curves. (b) Current and (c) potential distributions, as a function of radial position and kinetics. (1 = primary distribution, controlled by geometry 2 = secondary distribution, controlled by reaction kinetics)

controlled only by geometry (primary distribution), to one controlled by slow kinetics (secondary distribution).

The situation of a uniform current density (Fig.2.3b curve 2), corresponds to a significant variation of potential adjacent to the disk (Fig.2.3c curve 2). The maximum potential difference between the center of the disk and the edge is:

$$\Delta E = E(r_o{=}0)-E(r_o{=}r) = 1.45r^2 I_o/R_S \qquad (2.8)$$

where R_S, the resistance (ohms) = $4\kappa r$, κ being the conductivity (mho/cm). This equation has important implications in regard to the size of the active electrode area, the composition of the solution, and the kinetic reaction parameters. For example, in a 0.1M KCl solution, with κ = 0.013 mho/cm, r = 0.1cm, and I_o = 6x10^{-3} A/cm^2, the potential at the edge of the electrode, for a cathodic reaction, would be approximately 170 mV more negative. This means that even though the potential may be set 100 mV below the potential for the reduction of water to hydrogen gas, this reaction could still be taking place on a significant portion of the disk perimeter.

2.1.2 Theoretical Design Factors

Before ending the theoretical discussion for the RDE, it is desirable to consider some of the design factors which must be taken into account in order to insure conformity with theory.

In terms of fluid flow, a disk of radius R can effectively be considered of infinite diameter provided R >> δ_H. For a disk with a concentric "active electrode area" of radius r << R, it suffices that only r >> δ_H. The flow on the surface of such a RDE can be considered laminar if:

i) the Reynolds number, Re = $r^2\omega/\nu$, does not exceed the critical value for the onset of turbulence. For water, with Re < 2x10^5, we can theoretically have laminar flow as long as the product of $r^2\omega$ < 2000. For a mirror finished surface, rotating in water, with $r \approx 1$mm, the rotation rate is limited to 100 rpm < ω < 10000 rpm. Turbulent flow however, can occur at much lower values, for example; when the surface of the disk is not sufficiently polished, the RDE shaft is eccentric, or the cell walls are too close to the electrode surface.

ii) no serious edge effects are present. This requires that the flow in the upper half of the system does not interfere with that in the lower half. To meet this condition a practical RDE requires that all bounding surfaces be "effectively" at an infinite distance from the disk. These include the liquid/air interface, the walls of the cell, the reference and counter electrodes, and gas inlet/outlet. The shape of the RDE itself also plays a major role, and many different shapes are possible depending on the individual system [83].

Any RDE which satisfies the fluid-flow / mass-transport requirements discussed above will be satisfactory also from the standpoint of the surface potential distribution. The counter electrode is usually chosen so that it is much larger than the disk electrode in order to confine any polarization changes to the RDE itself, but the shape and size of the counter electrode should be irrelevant provided that it is "effectively" at an infinite distance from the disk.

2.2 NUCLEATION AND WETTING IN THE ELECTRODEPOSITION OF MERCURY

According to the classical theory of nucleation [85], if constant supersaturation is maintained for a given time, a certain number of stable nuclei will form. Electrochemical nucleation has the advantage of being able to control the degree of supersaturation and hence nucleation, simply by controlling the overpotential, η, at the electrode surface.

The overpotential, η, is defined as the difference between the applied potential, $E_{a}pp$, and the equilibrium potential, E_{o}.

The exact relationship between η and the nucleation process is usually established by directly or indirectly determining the density of nuclei formed during a potentiostatic or galvanostatic experiment. The number of nuclei can be directly evaluated by visual microscopic observation [86,87], or indirectly by measuring the faradaic current at some time and relating it to nuclei density [88,89].

Both nucleation (the initial formation of a small volume of liquid mercury from the solvated mercury(II) ions) and growth (the increase in size of the original nuclei) require that the accompanying total free energy change, ΔG, decrease [90]. Consequently the existence of an overpotential necessary for a phase change is to be expected. This transformation can not take place precisely at the equilibrium potential becauae, by definition, this is the potential at which the free energies of the phases are equal.

The formation of a mercury nucleus, in a reaction such as $Hg^{++} \rightarrow Hg^{o}$, leads to a decrease in free energy due to the difference in volume between the liquid mercury and the solvated mercury ions. Simultaneously, there is an increase in free energy because of the creation of a new surface between the solution and the liquid mercury. The volume and surface related energy terms for the above cases, can be expressed as; the electrical energy required to bring about a unit molar volume change, $\Delta G_V = V(nF\eta/m)$, and; the surface energy acquired per unit surface area, $\Delta G_S = A\gamma$. Combining both terms gives the total free energy change:

$$\Delta G = \Delta G_V + \Delta G_S = V(nF\eta/m) + A\gamma \qquad (2.9)$$

where V is the volume of the nucleus, n and F have their usual meanings, η is the overpotential, m is the molar volume of mercury, A is the surface area of the nucleus, and γ is the surface free energy of mercury.

As shown in Figure 2.4, ΔG increases until the nucleation <u>activation energy barrier</u>, ΔG_c, is reached at the <u>critical radius</u>, r_c. For $r > r_c$, the nucleus can spontaneously increase in size since this is accompanied by a decrease in ΔG, and the ΔG_V term dominates. For $r < r_c$, the nucleus has a tendency to decrease in size since ΔG is also decreased by this process. This critical radius can be found by substituting the appropriate formulas for volume and surface area into Eq.(2.9), taking the derivative $d\Delta G/dr$, setting it equal to zero, and solving for r_c. We thus obtain:

$$r_c = 2m\gamma/nF\eta \qquad (2.10)$$

Note that r_c is a meaningful quantity only when $\eta > 0$, and nucleation should therefore be impossible at the equilibrium potential. As will be disscused below, however, this is only the case if no reaction of any type occurs between the substrate and the mercury. It is also interesting to note that r_c is applicable to any spherical or spherical segment shaped nucleus, since it is only the radius or circumference which is critical.

In order to form a nucleus, the ΔG_c barrier can be surmounted only with the expenditure of reversible work. The <u>work of nucleation</u>, $W \approx \Delta G_V$, can be found by substituting Eq.(2.10) back into Eq.(2.9). In this case, however, the value of W depends on the spherical segment used. Assuming a whole sphere:

$$W = 16\pi\gamma^3 m^2/3n^2F^2\eta^2 \qquad (2.11)$$

where all symbols have their previous meanings. This value can be thought of as the amount of work necessary to bring about the deposition of a certain volume of mercury at an overpotential $\eta > E_o$, in the form of a nucleus of radius r_c.

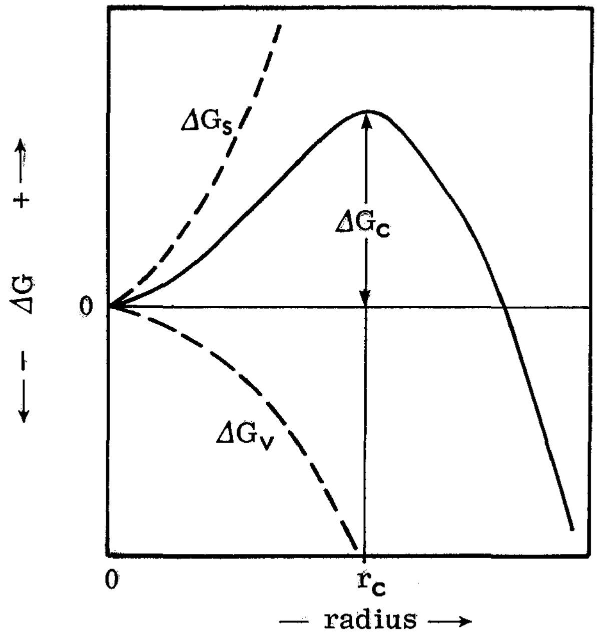

FIGURE 2.4 The change in the free energy accompanying the formation of a nucleus of radius *r*.

The rate of nucleus formation dN/dt can be found by using the Boltzmann statistical distribution expression, which gives the fraction of nuclei that can surmount the ΔG_c barrier, as a function of the exponential term $e^{(-W/RT)}$. Substituting Eq.(2.11) for W we obtain:

$$dN/dt = N_0 \exp[-16\pi\gamma^3 m^2/3RT(nF\eta)^2] \qquad (2.12)$$

where dN/dt is the number of nuclei formed per second per unit area, and N_0 is the nucleation rate constant. The determination of N_0 can present considerable difficulty since it is controlled by several variables such as surface quality, overpotential, deposition solution, and the material from which the electrode is made.

In addition, and more importantly, once the nuclei are formed, their growth is limited by diffusion zones. The growth of the mercury nuclei, randomly distributed over the electrode surface, is controlled by mass-transfer and the diffusion rate.

As shown in Figure 2.5, a hemispherical diffusion pattern develops around each nucleus. This diffusion zone grows outwardly at a rate proportional to $(Dt)^{1/2}$. As radii increase and the hemispherical diffusion zones begin to overlap, replacement of mercury ions in the planes near the electrode surface becomes restricted and eventually the only diffusion source is that which is perpendicular to the surface.

Wettability and Contact Angle. It has been found that, very often, the overpotential at which nucleation sets in is much lower than the calculated values [91,92]. This situation arises due to wettability of the electrode surface by mercury. The index of this effect is the contact angle, θ, which the mercury forms with the surface and is illustrated in Figure 2.6. The shape of the mercury in contact with the electrode depends on the relative values of surface energy components. In the electrode plane, force equilibrium must exist at the various

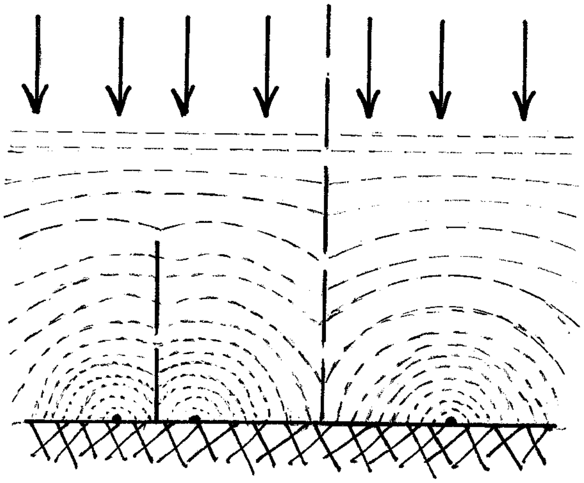

FIGURE 2.5 Diagrammatical representation of the growth of the diffusion zones and their eventual overlap. The extended vertical lines represent effective boundaries between columns.

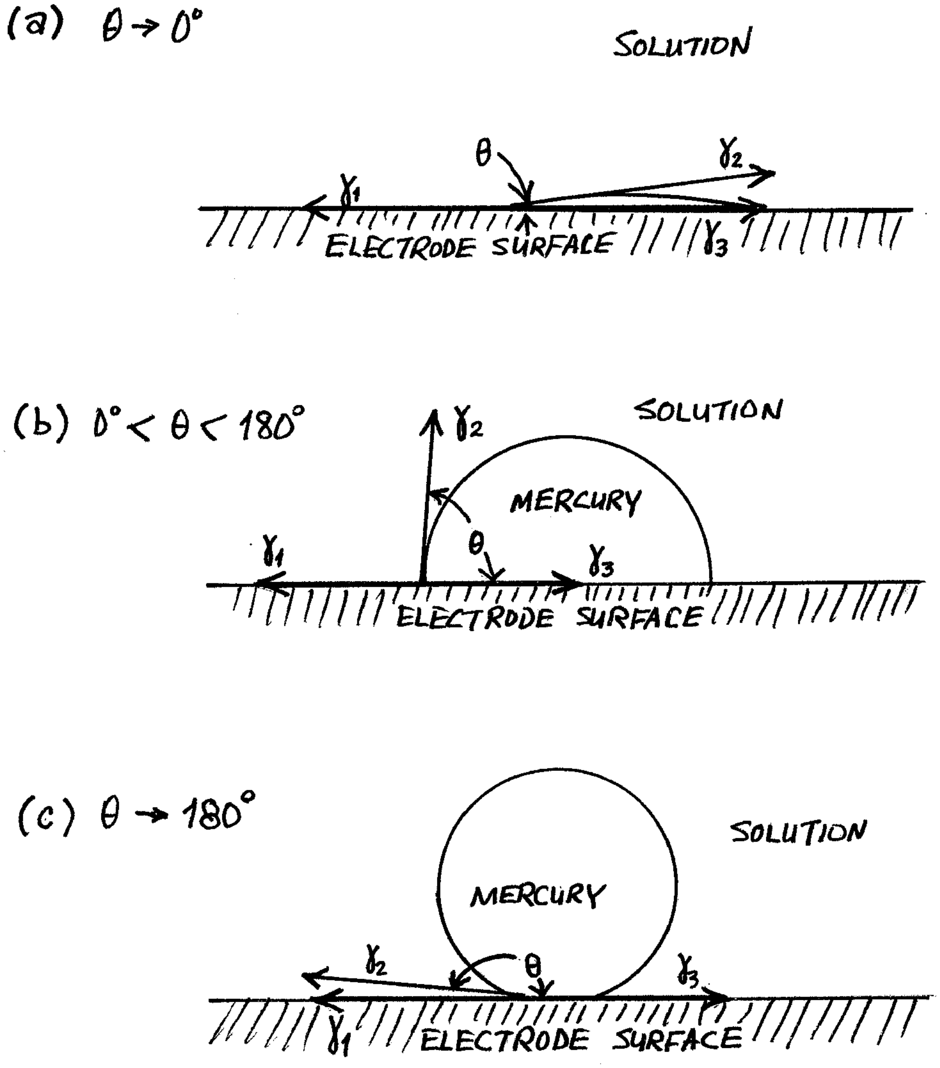

FIGURE 2.6 (a) Wetting of the surface occurs when the sum of the mercury-solution and electrode-mercury surface energies γ_2, and γ_3, is less than the solution-electrode energy, γ_1. (b) Partial wetting of the electrode by mercury occurs when the surface energies in the horizontal plane are balanced.

(c) No wetting occurs when $\gamma_3 > \gamma_1 + \gamma_2$

interfaces, since the mercury is free to move laterally until equilibrium is established. For an ideal horizontal solid surface it can be shown that:

$$\cos\theta = (\gamma_1 - \gamma_3)/\gamma_2 \tag{2.13}$$

where θ is the contact angle measured between the electrode surface and the tangent to the mercury, drawn from the intersection point of the three phases (see Fig.2.6); γ_1, γ_2, and γ_3 are the solution-electrode, mercury-solution, and mercury-electrode surface energies, respectively.

As shown in Fig.2.6a, the mercury will completely wet the surface ($\theta \rightarrow 0^\circ$) if the mercury-electrode and mercury-solution surfaces formed have less energy than the original solution-electrode interface (i.e., $\gamma_2\cos\theta + \gamma_3 < \gamma_1$). Complete lack of wetting ($\theta \rightarrow 180^\circ$), as shown in Fig.2.6c, occurs under the condition when we have $\gamma_3 > \gamma_1 + \gamma_2\cos\theta$. In terms of nucleation, ΔG_c becomes progressively smaller as θ decreases, and for complete wetting, it approaches zero since the new interface has less total surface energy than the previous one.

In practice, the term "wetting" has often had a very imprecise meaning. Usually, if $\theta > 90^\circ$, wetting is not considered to occur, and does not do so unless $\theta = 0^\circ$. However, Eq.(2.13) does not hold if $\theta = 0^\circ$, and the imbalance of the surface free energies must then be defined by the spreading coefficient:

$$S = \gamma_1 - (\gamma_2 + \gamma_3) \tag{2.14}$$

The value of S is positive for spontaneous spreading and negative for non-spreading systems.

2.3 ANODIC STRIPPING VOLTAMMETRY WITH THE MERCURY FILM ELECTRODE

The technique of Anodic Stripping Voltammetry (ASV) with a mercury film electrode (MFE) was briefly mentioned in Sec.1.1. In this section we will look at the theoretical equations for the current-potential curves, as derived by DeVries and VanDalen [64,65], for the three ASV steps; (1) pre-electrolysis with stirring; (2) an equilibration period to allow all forced convection to stop; and (3) dissolution by a linear anodic potential scan.

Pre-electrolysis. If we assume linear diffusion for the metal reduced in the mercury film, then the concentration C_R must be determined from:

$$\partial C_R(x,t)/\partial t = D_R \partial^2 C_R(x,t)/\partial x^2 \qquad (2.15)$$

where D_R is the diffusion coefficient of the reduced metal in the mercury, x is the distance from the substrate, and t is the electrolysis time. Applying the boundary conditions that:

$$C_R(x,0) = 0, \text{ with } 0 < x < \ell$$
$$D_R(\partial C_R/\partial x)_{x=0} = 0, \text{ with } t > 0$$
$$D_R(\partial C_R/\partial x)_{x=\ell} = F_o = i/nFA, \text{ with } t > 0$$

where ℓ is the mercury film thickness, and all other symbols have their usual meaning, the following approximate solution is valid for values of $\ell < 10^{-2}$cm and $t > 2$ seconds:

$$C_R(x,t) = (F_o t/\ell)+(F_o \ell/6D_R)[3(x/\ell)^2-1] \qquad (2.16)$$

During pre-electrolysis the concentration is thus essentially parabolic.

Rest Period. At the end of the pre-electrolysis time, t_p, the stirring or rotation of the electrode is stopped. Almost instantly, the flux decays to practically zero. If at the beginning of the rest period there is a concentration function

$C_R(x,t_p)$, then after a rest period, t_R, the concentration $C_R(x,t_R)$ can be calculated by solving Eq.(2.15) with the initial and boundary conditions that at $t_R = 0$ and $0 < x < \ell$, we have:

$$D_R(\partial C_R/\partial x) = 0, \text{ at } x=0 \text{ and } t_R>0$$

$$D_R(\partial C_R/\partial x) \approx 0, \text{ at } x=\ell \text{ and } t_R>0$$

The result obtained for a rest time of $t_R > 2$ secs is:

$$C_R(x,t_R) = (F_0 t/\ell)+(2F_0\ell/D_R\pi^2) \tag{2.17}$$

and since all quantities on the right side are constant, the concentration of reduced metal in the mercury can be considered to be homogeneous.

Dissolution Step. The exact treatment of the dissolution step involves some rather lengthy integral equations which are usually solved with the aid of Laplace transforms and the method of Huber for numerical integration. For this reason, only the graphical results are given here, and the original paper by DeVries [65] should be consulted for exact details.

Figures 2.7 and 2.8 illustrate the general trend of the peak current, i_p, peak potential, E_p, and half-width, $b_{1/2}$, with the scan rate, v, and film thickness, ℓ. For $\ell < 10\mu$m, i_p is directly proportional to v for values of $v < 30$ mV/sec. As ℓ increases, i_p increases faster than v. At the limit, i_p increases with $v^{1/2}$, as it does for a large volume mercury electrode.

The dependence of i_p on ℓ is seen to be a function of v. For $v < 2$ mV/sec., i_p is essentially independent of ℓ for values of up to 100μm, while for $v = 30$ mV/sec. i_p decreases rapidly with ℓ.

The value of E_p, is seen to shift in a positive direction with increasing ℓ and v, although the derivation is based on an ideally reversible couple. This illustrates that quoting specific values of E_p for a given couple is not very meaningful when dealing with mercury film electrodes.

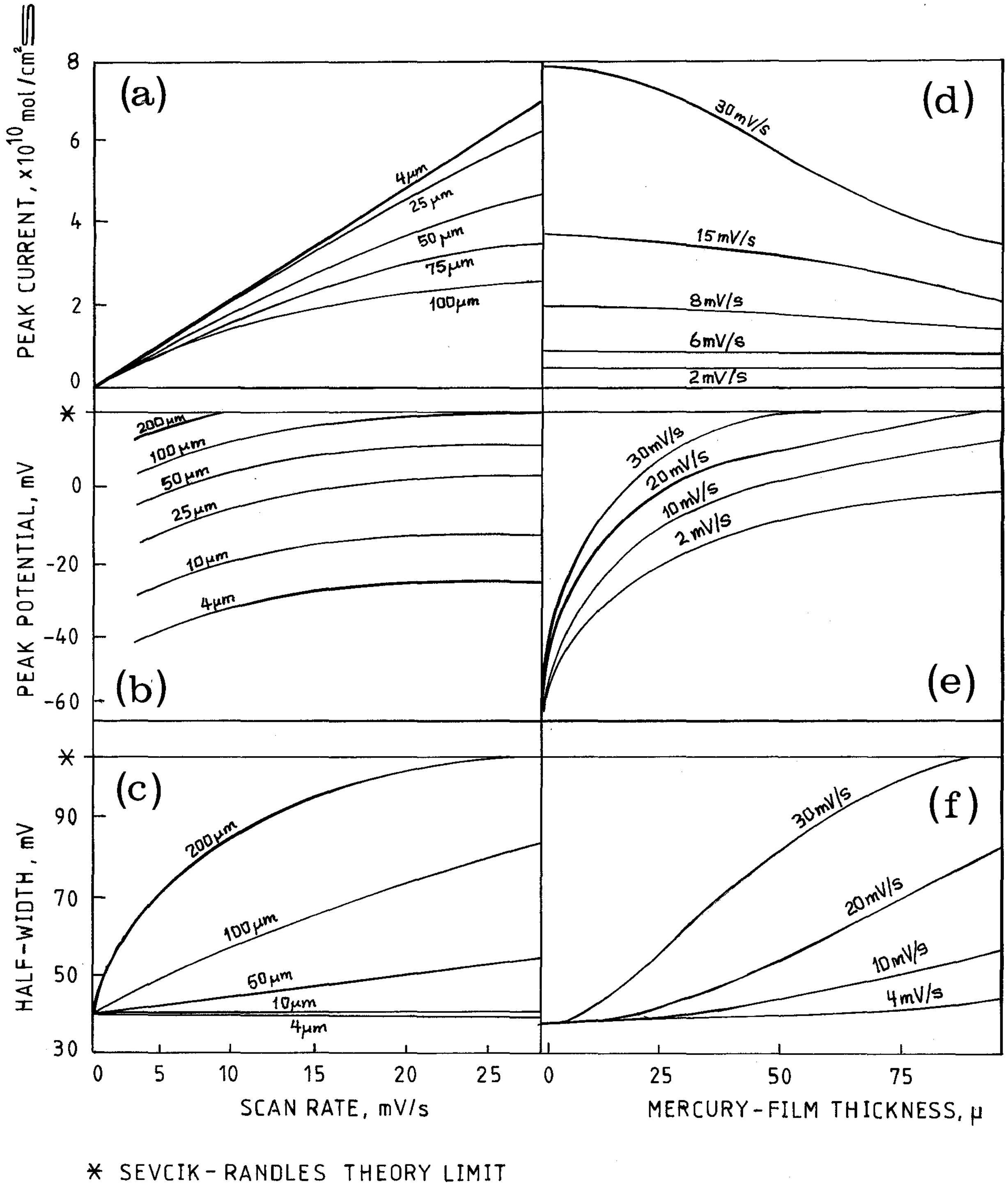

FIGURE 2.7 The dependence of peak current, peak potential and half-width on; (a,b,c) scan rate, and; (d,e,f) mercury film thickness, respectively.

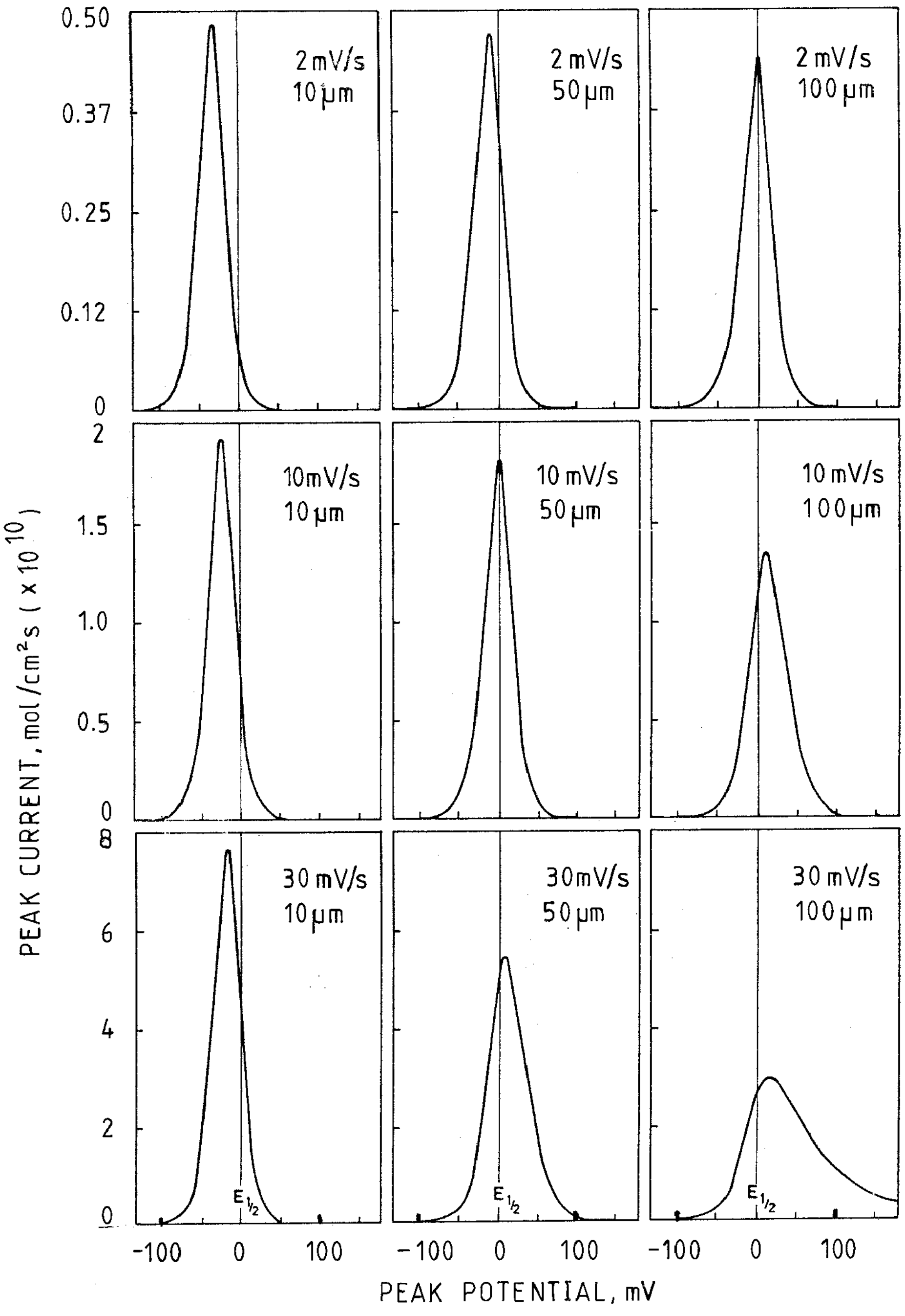

FIGURE 2.8 The shape of the ASV peaks obtained for several values of scan rate and film thickness.

Of importance when considering the resolution of mixtures is $b_{1/2}$. If $\ell < 10\mu m$, then $b_{1/2}$ is independent of v for values up to 30 mV/sec. The value for a $2e^-$ oxidation is about 35 mV. With thicker films, $b_{1/2}$ increases with v, and approaches 102 mV for the most non-ideal case. As n increases, $b_{1/2}$ decreases.

On the basis of the exact treatment given by DeVries [65], the values of i_p, E_p, and $b_{1/2}$ may be quantitatively evaluated, provided that the value of $H = nF\ell^2v/RTD_R$ is less than $1.6x10^{-3}$ (eg. if $D_R = 1.8x10^{-5}cm^2/sec.$, $n = 2$, $\ell = 10^{-4}cm$ and other symbols having their normal values, this implies that we must have $v < 40$ mV/sec.), to give:

$$E_p(mV) = (E_{1/2}-1.4+29.5\log(H))/n \qquad (2.18)$$

$$i_p(Amp) = 1.12x10^{-6}\ n^2AC_R\ell v \qquad (2.19)$$

$$b_{1/2}(mV) = 75.5/n \qquad (2.20)$$

where A is the electrode area in cm^2, ℓ is the film thickness in cm, the rest of the symbols haveing their usual meaning.

2.4 STRIPPING POLAROGRAPHY

The reduction of a metal ion from solution has been shown to be sensitive to its complexation. This is reflected through changes in the amount of metal deposited as a function of deposition potential. The technique of Stripping Polarography (SP), described in Sec.1.1, makes use of ASV stripping peak currents as a function of deposition potential, to obtain complexation values at very low concentrations. In this section we will discuss the theoretical basis of the SP technique.

In the course of the past ten years several derivations have been made of the SP theory equations. The first, made by Zirino and Kounaves [93], was for a reversible, simple ion system using an HMDE or MFE. This was then extended by

Kounaves and Zirino [15] to include labile complexes.

Brown and Kowalski [94] derived a set of equations for the MFE which took into account the effect of nonuniform distribution of the reduced metal in the mercury. Their resulting equations however, were, for all practical purposes, the same as those previously derived [93,15].

Shuman and Cromer [95] developed equations for the HMDE which were applicable to reversible and nonreversible reactions, however, after long and complicated equations, for deposition times of >10 seconds their result is the same as that of Zirino and Kounaves [93]. During the same time period Zirino and Kounaves [96] presented an approximate but general treatment for reversible and irreversible systems for the HMDE.

Finally, Huizenga and Kester [97] described equations applicable to the MFE for a reversible reduction. They used an exact expression for the distribution of C_R and considered both thick and thin mercury films. Their resulting equation for the half-wave potential does not give $E_{1/2}$ explicitly, but must be calculated by an iterative method, thus making it difficult to use for practical work. Their use of a nonuniform term for the reduced metal, as will be shown below, is also not necessary for mercury film electrodes.

We give here a derivation for the MFE based on the original by Zirino and Kounaves [93] but with the assumptions that C_R is uniformly distributed in the film, and that the film is formed on a RDE.

For a reversible reaction in which substance O is reduced to a metal R and forms an amalgam with mercury, i.e.:

$$\mathrm{O} + ne^- \longleftrightarrow \mathrm{R}$$

the Nernst diffusion layer theory assumes that there is a stagnant layer with a thickness, δ, through which transport occurs only by linear diffusion, so that:

$$C_O(\infty) - \bar{C}_O(o,t) = \delta \bar{F}_O / D_O \qquad (2.21)$$

where $\bar{F}_O$ is the average flux of O at the surface, $C_O(\infty)$ is the bulk concentration (considered as constant), and $\bar{C}_O(o,t)$ is the average concentration of O at the surface as a function of time.

At any time t, $\bar{C}_O(o,t)$ is related to the average concentration of R at the surface, $\bar{C}_R(o,t)$, by the Nernst equation:

$$\bar{C}_O(o,t)f_O/\bar{C}_R(o,t)f_R = \exp[nF/RT(E-E^o)] \qquad (2.22)$$

where E is the potential of the electrode, E^o is the standard potential for the amalgam electrode, f_O and f_R are the activity coefficients of O and R respectively, the other symbols having their usual meaning.

It has been shown [64] that for times >2 seconds, (eg. the common value for the rest period being 30 sec.) the concentration of reduced metal in the mercury is practically homogeneous, and that $C_R(o,t) = \bar{C}_R(o,t)/2$ [93],so we then have:

$$C_R(o,t) = \bar{F}_O t/2\ell \qquad (2.23)$$

Combining Equations (2.21)-(2.23), and then subatituting $\bar{F}_O = q/nFAt$, the limiting charge q_L for $nFA(D_O/\delta)tC_O(\infty)$ and $\theta = \exp[nF/RT(E-E^o)]$, we get:

$$\theta = (q_L-q/q)(2\delta\ell f_O/D_O f_R t) \qquad (2.24)$$

Since we are using a RDE, we can substitute Eq.(2.2) for δ, and, change q to it. Combining and simplifying, we get:

$$\theta = (i_{pL}-i_p/i_p)(0.032D_O{}^{-2/3}f_O\ell/tf_R\omega^{1/2}) \qquad (2.25)$$

when $i_p = i_{pL}/2$, the expresion for the half-wave potential is obtained:

$$E_{1/2} = E^o + (RT/nF)\ln(0.032D_O{}^{-2/3}f_O/f_R)$$
$$+ (RT/nF)\ln(\ell/\omega^{1/2}t) \qquad (2.26)$$

Thus $E_{1/2}$ (for a stripping polarogram of a simple metal ion, reversibly reduced at the mercury film) varies linearly with the natural-log of the RDE rotation rate $\omega^{1/2}$ and the deposition time t, and inversely with natural-log of the mercury film thickness ℓ.

In the manner of the complexed ion relationship given previously [15], Eq.(2.26) can be extended to reduction of complexed metal ions at a MFE. Assuming that the complexed species is in excess of the simple metal ion, we have:

$$E_{1/2c} = E_{1/2} + (RT/nF)\ln(K_c) - (RT/nF)p\ln(C_L f_L) \qquad (2.27)$$

where $E_{1/2c}$ is the half-wave potential of the stripping polarogram for the complexed species, K_c is its dissociation constant, p is the stoichiometric coefficient of the ligand with the metal ion, C_L is the total concentration of the ligand, and f_L is its activity coefficient. For values of $p\ln(C_L) \geq \ln(K_c)$, Eq.(2.27) can be used to predict the change of $E_{1/2}$ with added ligand, or determine the values of p, n, K_c, or C_L, depending on the variables already known or controlled.

3. DESIGN AND DEVELOPMENT OF ANALYTICAL SYSTEM

During the initial phases of this research it became evident that no single commercially available electrochemical system could fulfill all the foreseen requirements. In order to meet our needs, the major portion of the equipment described in the following sections, was either designed and constructed "in-house" or purchased and modified.

The complete system, as configured for this research, is shown in Figure 3.1. It basically consists of a microcomputer, with two custom-built interfaces for data acquisition and control, a potentiostat/galvanostat, a plexiglas flow-through cell, and a reflecting microscope.

Unlike existing systems, it enables us to simultaneously control the current-potential at an electrode while microscopically observing its surface. It also allows flow-through exchange of test solutions without breaking electrode-solution contact. The system is overall designed to be easily adaptable to a variety of electrochemical experiments.

3.1 MICROCOMPUTER CONTROLLED ELECTROCHEMICAL SYSTEM

It has become apparent that computer controlled techniques are indispensable in the collection, manipulation and evaluation of the large amount of data which can be generated in many electrochemical experiments. For example, in constructing

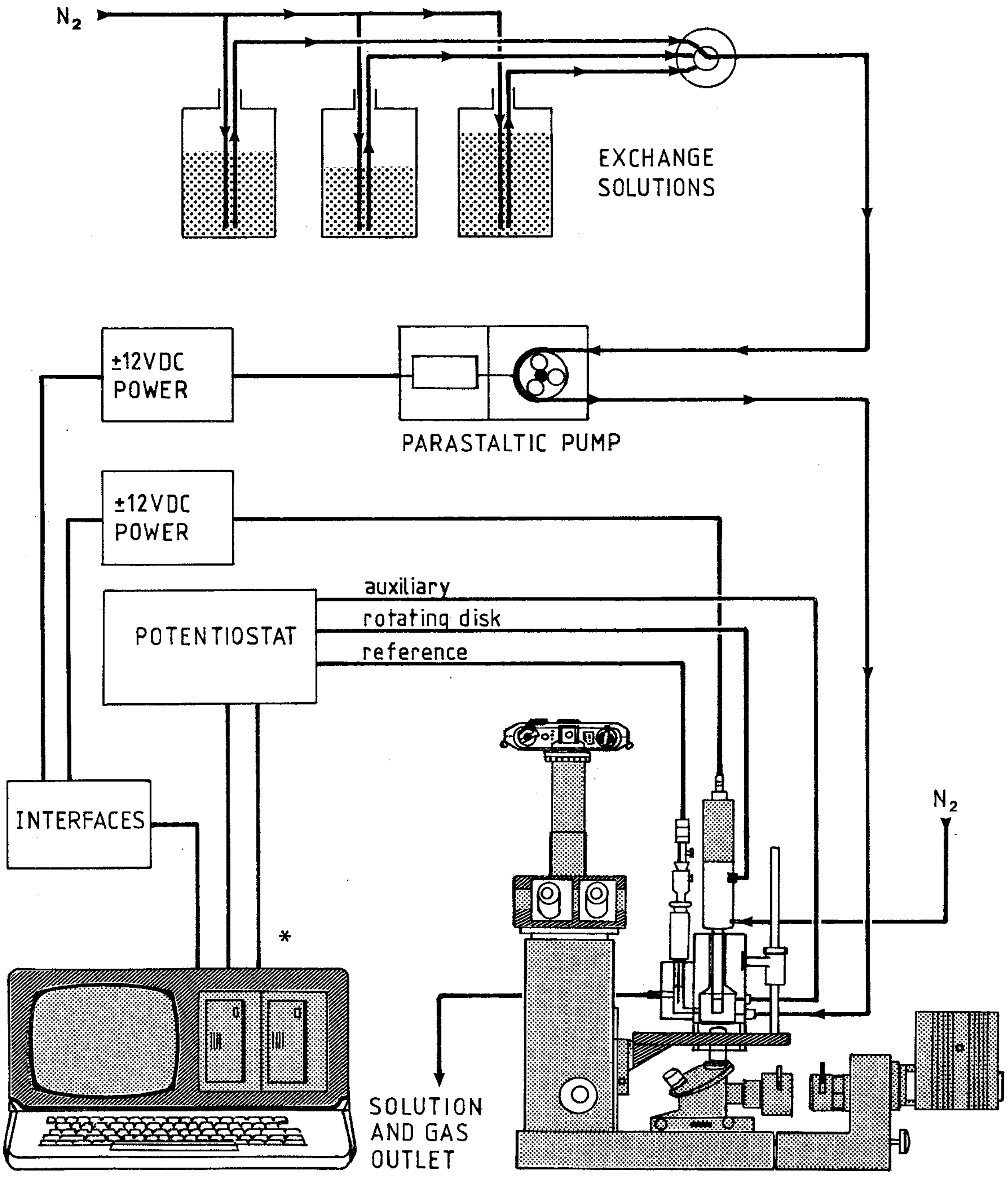

FIGURE 3.1 General view of the medium exchange flow-through cell system and its electrical and solution-flow connections. (* - for computer system interconnections, see Fig.3.2)

stripping polarograms (SP), a minimum of 15 to 20 separate points is required, each point being at least one normal ASV experiment. Under usual conditions, with deposition times of 10 to 30 minutes, obtaining a complete set of ASV curves for constructing a SP curve can take from 2 to 10 hours. During this time the operator has to constantly monitor the instrument, setting deposition potentials, purging with nitrogen gas, timing, initiating scans, changing mercury drops (for HMDE), and so on.

Previous investigations [15,98-101] have shown the utility of on-line microcomputer systems for controlling electrochemical analysis. Timing, control of gases/solutions, processing data such as peak heights, areas, subtraction of base-lines and curve smoothing, can be done accurately and rapidly.

Our microcomputer interface system can also accommodate other inputs such as sensors for pH and temperature, and can control switches, valves, or other electrochemical instrumentation, with only minor changes in software and/or hardware. Figure 3.2 shows the basic layout of the microcomputer system's hardware and interface connections.

3.1.1 Hardware

<u>EXORset-30 microcomputer</u>. The EXORset-30 is a development system microcomputer (Motorola Inc.) consisting of a full size ASCII keyboard, 23 cm CRT monitor capable of displaying normal or graphic data, memory consisting of 56K bytes of RAM and 8K bytes of ROM, and dual mini-floppy disk drives providing 160K bytes of mass storage. Two extension card slots and outputs for a cassette recorder and a printer are also available.

<u>Analog/Digital Conversions</u>. The analog-to-digital (ADC) and digital-to-analog (DAC) conversions are performed by an RTI-1231-R DAC-ADC (Analog Devices, Norwood Mass./USA). This is

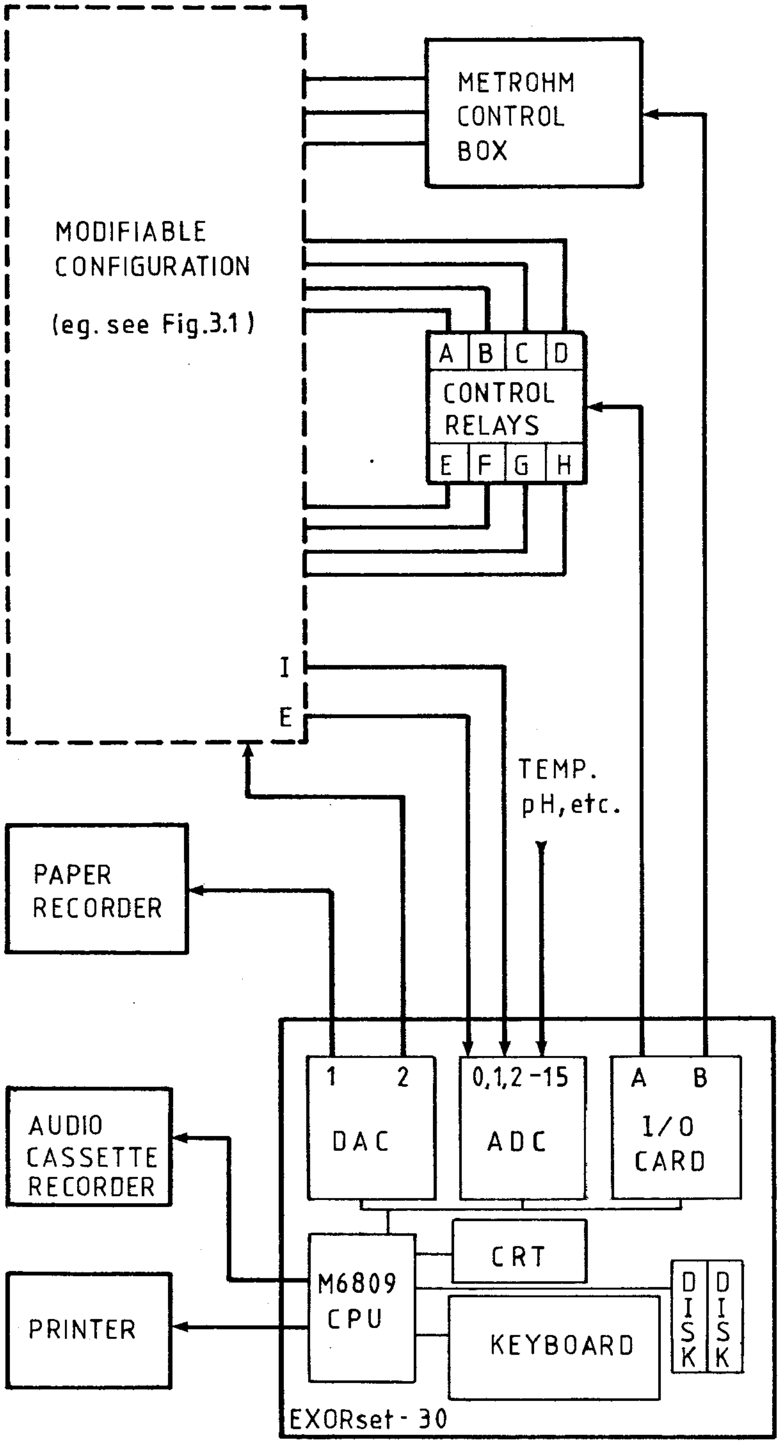

FIGURE 3.2 Block diagram of microcomputer system and interface connections.

an integrated circuit board which can be plugged directly into a slot of the EXORset-30. The card includes both ADC and DAC circuitry. The ADC's have 16 inputs and the DAC's have 2 outputs.

The two DAC's are used to output a given voltage to two circuits. The DAC-1 is set to output ± 5 V to the external pilot of the potentiostat. The applied potential to the cell can be controlled to within 1 mV in the range ± 2 V. The DAC-2 is set to output ± 5 V to an analog paper recorder, thus allowing a hardcopy record of any output signal.

In their current configuration the ADC's are set up for differential input in the bipolar range of ± 5.12 V. The ADC resolution is 12 bits with a conversion time of 25 µs maximum. This allows for a theoretical sampling rate of 40 KHz (the actual rate being determined by the user's software data handling capability).

I/O Control Interface. I/O control is implemented by the use of a Motorola Universal Support Module MEX68USM (Motorola, Inc.) containing one Periferal Interface Adaptor (PIA). The PIA has two 8-bit bi-directional peripheral data-buses for interfacing (see APPENDIX A for outputs). The "A" data-bus is used for control of a Metrohm E607 (Metrohm, Switzerland), described below. The "B" data-bus is used to control eight relays. Two of the relays are used for control of the cell (on/off) and potentiostat/galvanostat mode selection (P/G). The other six relays are available for control of other valves or equipment such as an automatic sampling system or a pump for the flow-through cell.

Metrohm E607 Control Unit. This unit allows for control of three cell functions by activating: (1) a gas control valve which determines whether the nitrogen gas is to purge or blanket the cell solution; (2) a 220 VAC outlet for controlling either stirring or the RDE motor; and (3) a drop dispenser / dislodger (used in conjunction with a HMDE), which consists of a stepper-motor which has been modified to respond to pulses generated by the stand-control-box under software control.

<u>Potentiostats and Galvanostat</u>. Depending on the experiment, two different Tacussel units were used, either a CORROVIT combination potentiostat/galvanostat or a PRG5 potentiostat (both from Tacussel-SOLEA, Lyon, France). The following modifications were made to both units to allow for computer control.

Two relays were added internaly to the CORROVIT, one for control of the cell on/off function, and the other for control of the potentiostat/galvanostat (P/G) switch. Both of these relays are in turn connected to two relays on the control-relay box. Three special connectors were added to the rear panel. Two are for output of current and potential values, and one is for computer control of applied potential. All switches on the front panel of the CORROVIT must be set to the specific positions listed in APPENDIX B, when used under computer control.

The CORROVIT was used mainly for chronopotentiometry or staircase voltammetry.

The only modification made to the PRG5 consisted of making available (for computer control) the STOP SCAN function at pins 24 and 25 of connector J-17 (rear panel). The PRG5 was used for linear scan voltammetry.

3.1.2 Software

<u>Operating System Software</u>. The XDOS operating system controls all disk operations and file directory management. The XDOS is initially loaded by placing the system disk in DRIVE 0 and entering the command XDOS. Once XDOS is loaded, the XDOS prompt "=" will appear on the screen.

The high-level programming language is a Motorola extension of standard BASIC called BASICM, which can be used in both compiler or interpreter modes. It also contains many features similar to those found in FORTRAN and PASCAL.

All system software is fully documented in the Motorola user's manuals for XDOS and BASICM.

Process Control Programs. Several programs have been written to allow for control of various electrochemical processes. These programs are written in BASICM and can be run after loading the XDOS system. Their purpose is to run the desired experimental procedure, while at the same time making all instrument operations transparent to the user.

PROGRAMS ASV/ASV5: (Appendix C) These programs are used for conducting an ASV experiment sequence with either the CORROVIT or PRG5 respectively. The programs are run by inputing the command "BLOAD XXX.LO:1;G", where XXX = ASV or ASV5. As shown in Figure 3.3, they allow the user to set all the parameters (potential, time, etc.) required to conduct one complete ASV experiment.

Once all parameters have been set, the special function key F9 (START) on the keyboard is pressed. From this point on, the program is in control. The solution will be purged with N_2 for the requested time, after which, the deposition and equilibriation will be carried out for the requested times. A potential scan will be made within the range and at the rate specified. The program will then display "READY-MAKE SELECTION". At this point the user may continue on to another experiment or may save the data from the experiment to the disk. If saved, the data will be composed of 1010 data points. The first ten values are the input parameters and instrument settings, and the remaining 1000 are the current measurements.

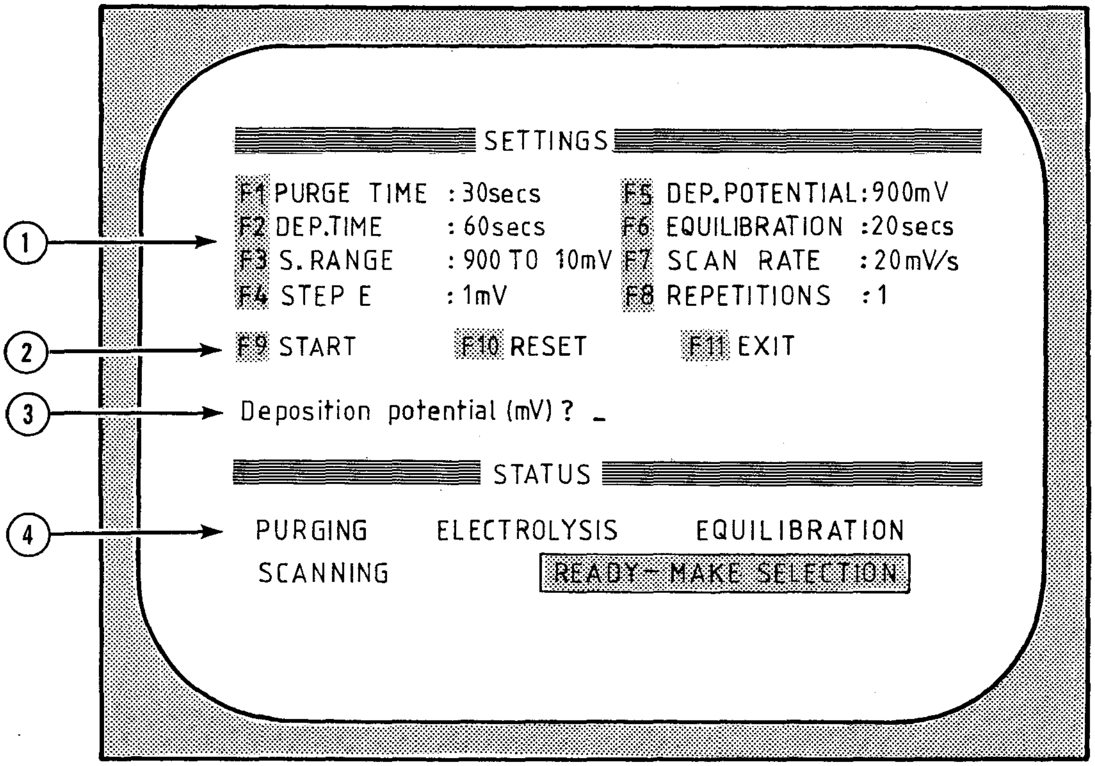

```
SETTINGS
F1 PURGE TIME  :30secs         F5 DEP.POTENTIAL:900mV
F2 DEP.TIME    :60secs         F6 EQUILIBRATION :20secs
F3 S.RANGE     :900 TO 10mV    F7 SCAN RATE    :20mV/s
F4 STEP E      :1mV            F8 REPETITIONS  :1

F9 START          F10 RESET          F11 EXIT

Deposition potential (mV) ? _

STATUS
  PURGING       ELECTROLYSIS       EQUILIBRATION
  SCANNING              READY-MAKE SELECTION
```

FIGURE 3.3 Screen display used by program ASV and ASV5 to set up an experiment: (1) parameters as currently set by user or default, (2) request program to take indicated action, (3) parameter selected by special function-key to allow entry of a new value, (4) current action being carried out by system.

For the CORROVIT, the values for the potential are assumed to start at the initial potential with increments of 1 mV for each data point. For the PRG5, each increment is 1/1000 of the total scan range.

PROGRAM CHRPOT: (Appendix D) This program has a similar structure to the ASV programs, but is used for controlling the CORROVIT when doing chronopotentiometry(CP), either normal or with predeposition and anodic stripping (ACP). Due to technical reasons involving the CORROVIT electronic circuitry, the required constant current cannot be controlled by the microcomputer and must be manually set on the CORROVIT front panel.

The data collection for this program is accomplished in a rather novel manner for an ACP procedure [102]. As shown in Figure 3.4a, a normal plot for ACP data can be obtained by recording the potential over the time it takes for it to reach certain values. In this program, since we have a limited amount of memory available for each experiment (1000 bytes), the collection of neither the potential nor time data can be allowed to "run free". In order to accomplish this, the 1000 bytes of memory are assigned to a 1000 mV potential range, giving one thousand 1mV potential intervals. Each potential interval can accumulate 32768 counts, taken at the rate specified in the program; the smallest being 1 count each 25 ms. Since the potential scan is made at a constant rate, the number of potential measurements falling into one specified potential interval, is

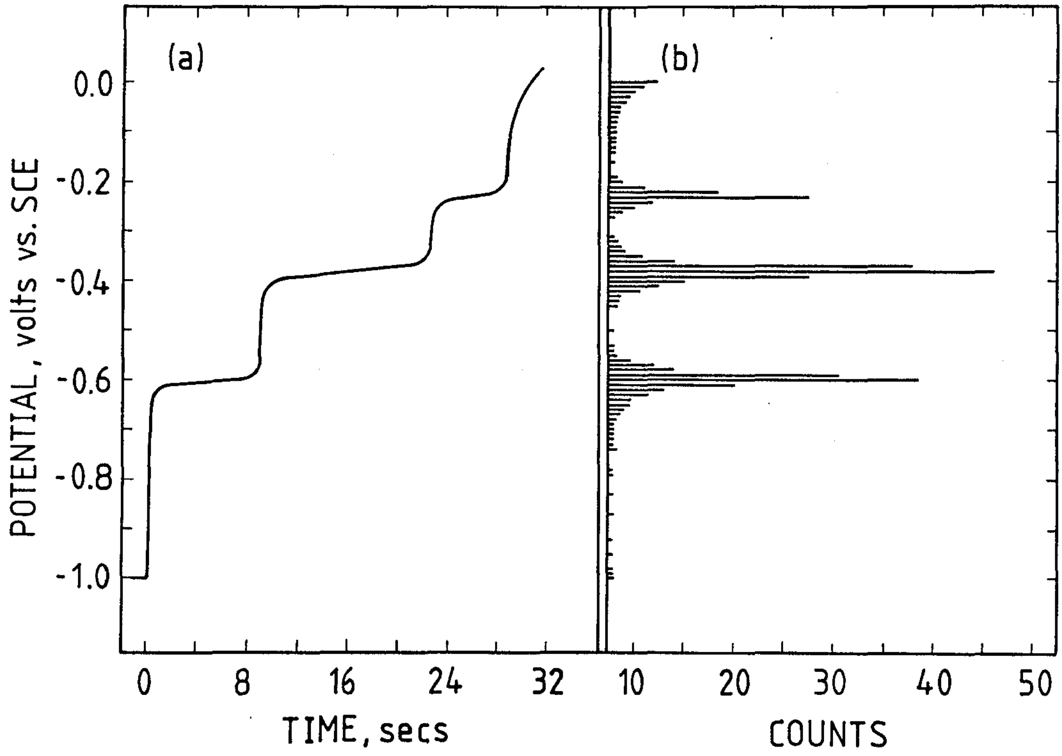

FIGURE 3.4 (a) Normal curve resulting from an ACP experiment. (b) Output used by program CHRPOT to display same data.

in effect, a measure of the time the electrode potential rests within this interval. The result of displaying this "count" vs. potential data is shown in Figure 3.4b. The peaks correspond to the potentials at which the greatest amount of time is spent. The area under the peak corresponds to the transition time. For analytical purposes, where the transition time is the important parameter, it would of course be more practical to use the distance between the peaks of the dE/dt curve to determine it. However, in speciation studies a dissymmetric $E = f(t)$ curve may be of greater interpretive value than the transition time. As can be seen below in Figure 3.5a, the $E = f(\text{counts})$ curve gives a better display of the dissymmetry than does the normal $E = f(t)$ curve in Figure 3.5b, for the same data. This type of process could be useful for interpretation of electrode reaction mechanisms (e.g., complexation).

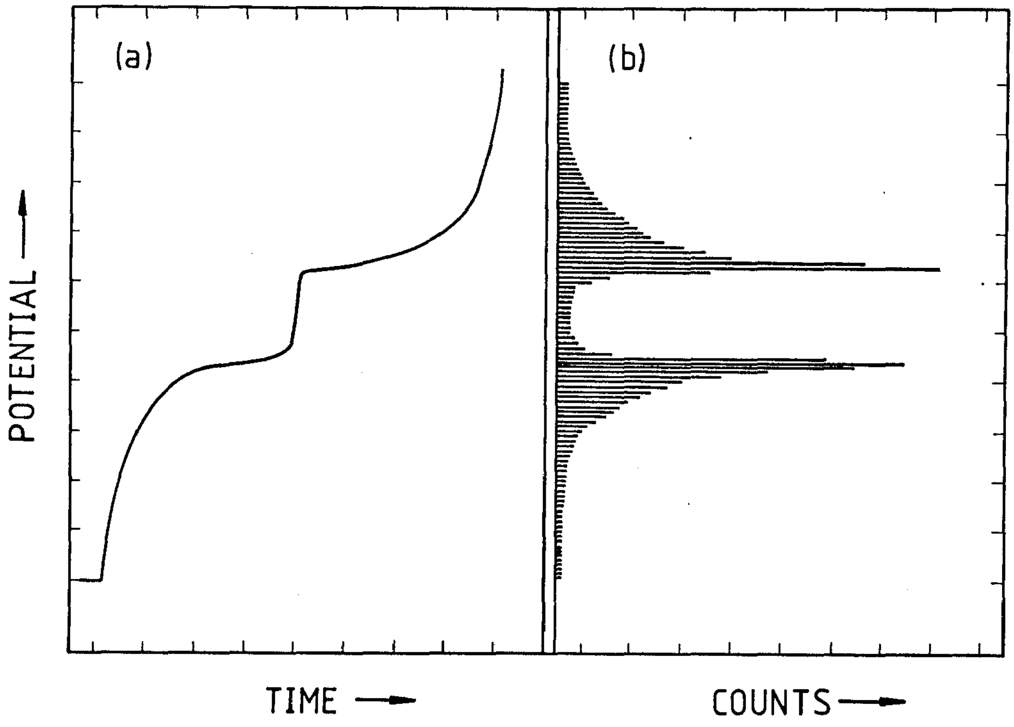

FIGURE 3.5 The presentation of data as (a) $E = f(\text{counts})$ can show dissymmetry more clearly than (b) the $E = f(t)$ curve.

PROGRAM STRPOL: (Appendix E) This program performs an ASV experiment for the number of times, and at the potentials, selected by the user (normally about 10-15). The data collected from each ASV experiment is saved on the disk, and can be used at the end of the SP experiment to construct a stripping polarogram. A disk will normally hold up to 40 ASV data files.

Data Processing Programs. Data processing programs can be written for a particular analysis as the need arises. Below are described two general-use programs developed specifically for our purposes.

PROGRAMS PLOTR AND PLOTRQ: (Appendix F) These are curve smoothing programs, which will take data from a disk file and by proper convolution with given sets of integers [103] will smooth the data according to a best fit linear or quadratic line segment. The resulting smoothed curve is then output to a recorder. The results of smoothing a "noisy" curve are shown in Figure 3.6a. The process is especially effective for eliminating higher frequency noises. In Figure 3.6b the data is not only smoothed, but also expanded for better visual observation.

PROGRAM BLINE: (Appendix G) This program will take two disk files and subtract the data of one from the other. This process can be useful in regards to ASV peaks which may have very steep or complicated baselines. Figure 3.7 shows some of the advantages of this procedure.

3.2 MEDIUM EXCHANGE FLOW-THROUGH CELL

There are three very important features of a flow-through system. First, in respect to ASV, is that stripping can be performed in a solution which has a different composition from that used in the deposition step. This allows one to select an

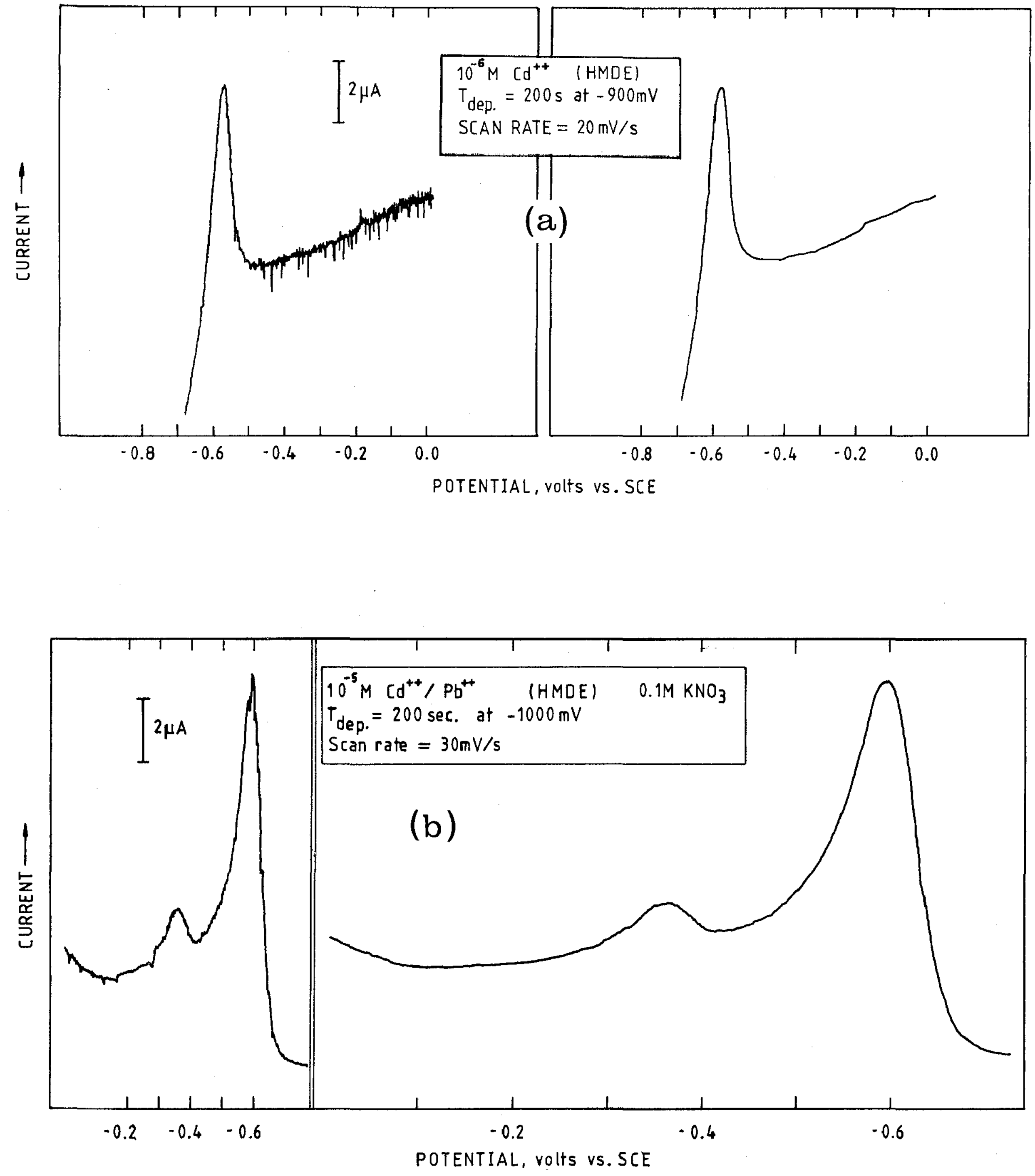

FIGURE 3.6 (a) The result of using smoothing on data which originally contained significant noise. (b) The data here is not only smoothed, but also expanded for better observation.

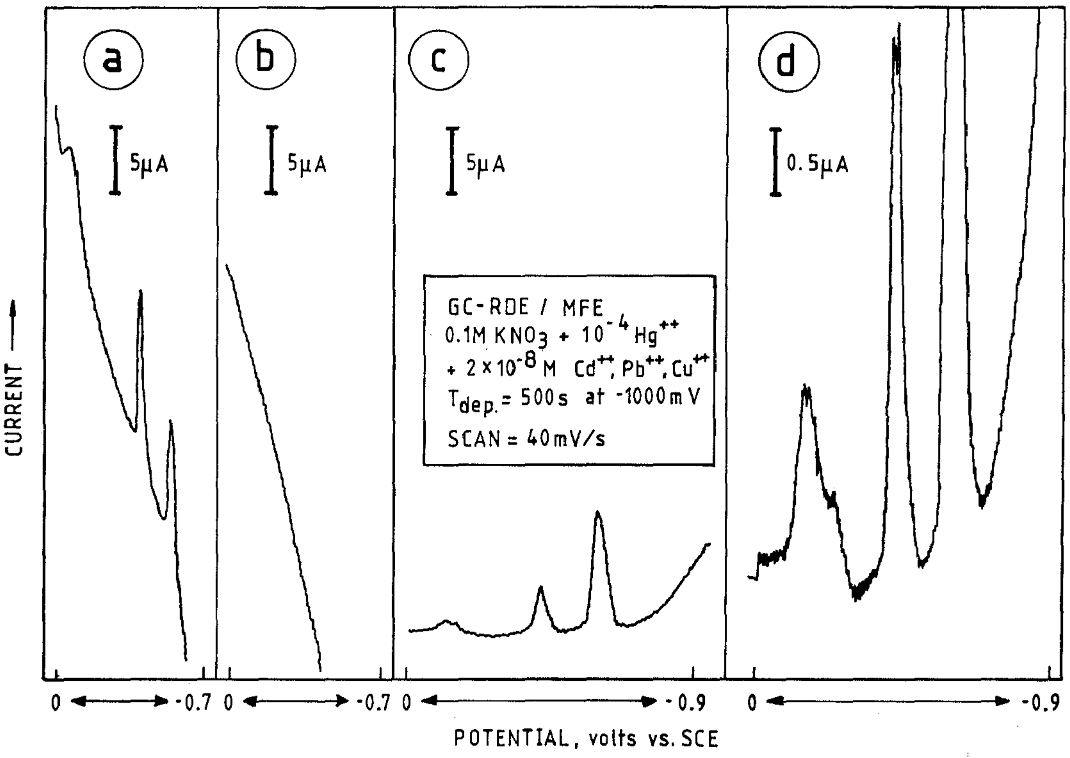

FIGURE 3.7 This set of curves shows, (a) the original data, (b) the baseline, (c) the result of subtracting b from a, and (d) digital "magnification" of the processed data.

optimum electrolyte in each case. Second, is the ability to always maintain an applied potential at the electrode. This is important with mercury films, where changes in the electrode surface electric field can alter the surface tension of the mercury and cause distortion or even loss of the mercury film. Third, is the ability to change solutions without exposing the electrode to air. This is also very important in forming a mercury film, since contact of the mercury with air, even for a brief moment, will cause the formation of a monolayer oxide film on the surface of the mercury. Flow-through systems for ASV, and other techniques, have been described by Koster and Ariel [104], Siegenthaler and Schmidt [105], Anderson et al. [106], and Wang and Green [107].

The flow-through cell system was specially designed and fabricated for use in this research. It is unique in that it combines a rotating disk electrode, a medium exchange capability, and allows in-situ microscopic observation of the electrode surface. The flow-through cell, shown in detail in Figure 3.8, consists of a plexiglas body (#4) containing: a 2mm diameter platinum auxiliary electrode (#9) mounted flush with the cell wall; a solution inlet fitting (#10) (Swagelok No.540-10); and a 3mm i.d., 6mm o.d., outlet through which both the gas and solution are discharged (#5). The cell bottom is a 2mm x 39mm dia. optical-quality quartz plate (#8) providing a window for in-situ viewing of the electrode surface with a reflecting microscope (#3) (described in Sec.3.4). The cell also has an RIN 14.5/23 opening for a rotating disk electrode (#1) (described in Sec.3.3), and another for a combination, saturated calomel - 0.1M $NaNO_3$ bridge, reference electrode (#2). The main cell chamber requires a minimum of 14 ml, but not more than 20 ml, of solution.

Calibration studies, using a colored dye and spectrophotometric measurements were carried out to determine the amount of solution required in order to completely replace the previous solution. With continuous flow (≈ 30 ml/min) provided by a peristaltic pump (Masterflex Pump No.7016, Cole Parmer Corp.), 8 ml aliquots were sequentially taken and their light transmittance measured with and without the RDE rotating (1000 rpm). The results, shown in Figure 3.9, indicate that without the RDE rotating 99.5% of the original solution is replaced after ≈ 140 ml of flow. However, with the RDE rotating the same value is reached after only ≈ 120 ml has been replaced.

The adsorption of metal ions on the plexiglas was tested with zinc(II) and mercury(II) solutions. In both cases, after filling the cell with 0.01M solutions of the above, letting them stand for 24 hours, and rinsing with deionized water,

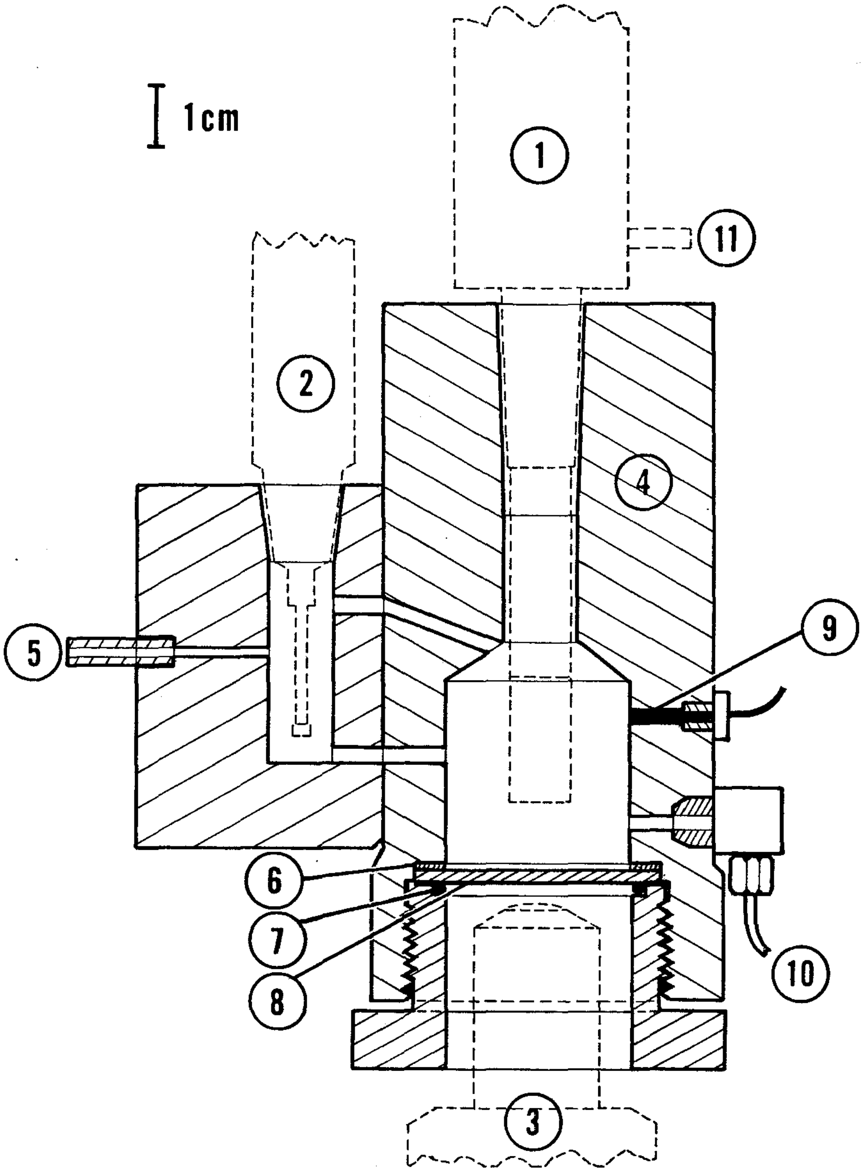

FIGURE 3.8 Detailed view of medium exchange flow-through cell. (1) RDE, (2) reference electrode, (3) reflecting microscope, (4) plexiglas cell body, (5) solution/gas outlet, (6) silicon gasket, (7) rubber o-ring, (8) quartz window, (9) platinum auxiliary electrode, (10) solution inlet, (11) gas inlet.

no detectable (<10^{-8}M) adsorption of either was noted upon filling the cell with 1M HNO_3 for 24 hours and then measuring with ASV. These results are in agreement with previous studies of adsorption on plexiglas [108].

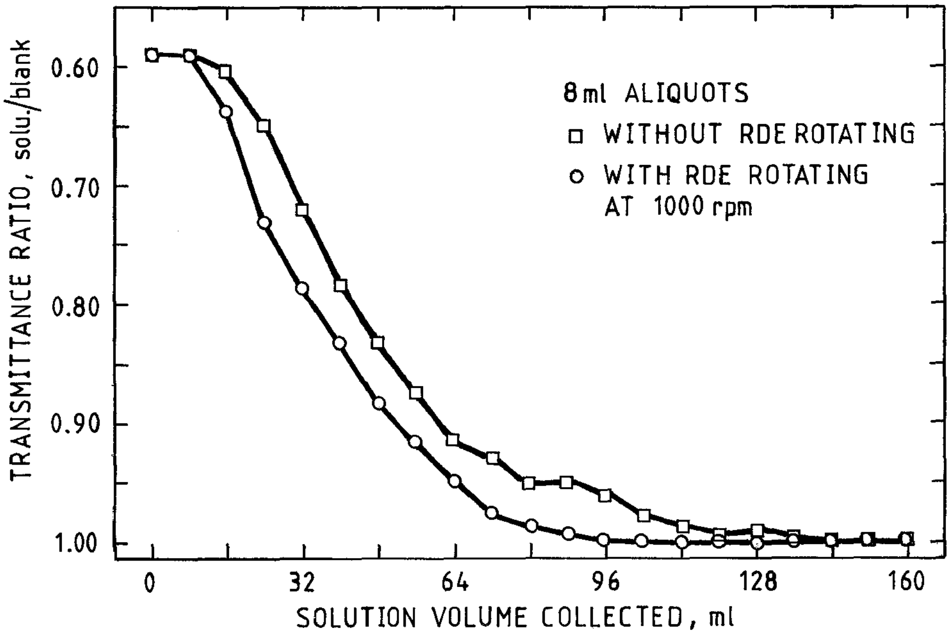

FIGURE 3.9 The amount of new solution required to replace the previous one. (cell volume = 14 ml, flow rate = 30 ml/min.)

3.3 ROTATING DISK ELECTRODE

The rotating disk electrode consists of a mechanical drive assembly, a power supply, and an interchangeable electrode tip.

The main body, which contains the drive motor, centering devices, and contact brushes, is a Tacussel EDI-55442 rotating electrode (SOLEA-Tacussel, Lyon, France).

The power-supply was built in-house, and can provide a variable output voltage of 0 - 12 VDC. The rotation rate of the electrode was calibrated, after approximately each 500 hours of operation, using a stroboscope (General Radio Corp.). For values of 500 to 4000 rpm the rate of rotation was found to be accurate to within 1% of the value set by adjusting the corresponding calibrated output voltage of the power-supply.

The active electrode substrate (2mm dia. x 10mm long) is press-fit into the center of a specially fabricated cylindrically shaped Teflon tip (1cm dia. x 2cm long : see Fig.4.3). The materials used for the electrodes, their fabrication, and the different surface pretreatments, will be discussed in greater detail in Sec.4.2.

3.4 MICROSCOPE SYSTEM

The microscope used for viewing the electrode surfaces is a Leitz EPIVERT reflected-light polarizing microscope (Ernst Leitz GMBH, Wetzlar, West Germany), with available magnifications of 250x and 600x, a binocular eyepiece, and a Pentax-ME 35mm camera for taking photographs (shown in Fig.3.1).

3.5 REAGENTS

All solutions were prepared with deionized water from a Millipore Milli-Q system.

Unless otherwise indicated, all chemicals used were analytical reagent grade (Merck), and all metal-ion solutions, including the mercury(II) used for film formation, were prepared from their respective nitrate salts.

High-purity (99.95%) nitrogen gas (Carbagas) was used for purging oxygen from solutions.

The alloy materials and pure metals used for the electrode substrates are discussed in Chapter 4.

(This page intentionally left blank.)

4. SELECTION OF A MERCURY-FILM SUBSTRATE

Since the necessary effort to test all the possible materials suitable for supporting a mercury film, would be unacceptable in terms of both time and money, certain criteria were established in order to eliminate unlikely prospects. Once the field of choices had been limited to about six different substrate materials, they were further evaluated on the basis of their physical properties, electrochemical reactions in water at the mercury deposition potential, and finally on the formation and stability of a mercury film on their surfaces.

4.1 SELECTION CRITERIA

As was first pointed out in Sec.1.4, an ideal mercury film substrate should: *i)* be insoluble in mercury; *ii)* undergo no chemical reactions with mercury; *iii)* provide the necessary interface forces capable of supporting a stable mercury film.

At first glance it would appear that most materials which support a good mercury film, do so precisely because they are soluble in, and/or form a compound with, mercury. However, long range attractive interactions (≈ 100 molecular diameters) due to London-Van der Walls forces, dipole moments, and coulombic forces can also exist at interfaces. These forces can provide, in the case where no reaction and/or solvation occurs, a means of forming a stable mercury film.

An initial selection of materials was then made based on the low solubility of the substrate in mercury (Sec.4.1.1), and the non-chemical interaction of substrate with mercury as defined by the electrochemical work function (Sec.4.1.2).

It should be remarked at this point, that because of the requirement of having an electrically conducting substrate, we ruled out, beforehand, a substantial number of the elements, leaving mainly the transition metals. However, this still left a rather large number of metals and their intermetallic/alloy compounds to be considered.

4.1.1 Solubility of Substrate Material in Mercury

The data used for the solubility of metals in mercury was mainly taken from Vydra et al. [27], Shunk [109], and updated in some cases by the pre-publication data of Galus and Guminski [110], and is given in APPENDIX H for reference.

By necessity, the definition of solubility is not very rigorous or precise. A metal which shows <u>high</u> solubility, may do so not because it is "soluble", but because it undergoes a chemical reaction to form an intermetallic compound, thus appearing to be solvated. On the other hand, a metal may show <u>low</u> solubility because its rate of solvation is extremely slow or because of some passivation effect occuring at the interface. These and other experimental problems are responsible for many of the differences found between solubility values in the literature [110].

For practical electrochemical purposes we consider metals as being "soluble" if their solubility is $> 10^{-4}$ weight %, and "insoluble" if their solubility is $< 10^{-6}$ weight %.

No general laws have yet been found from which one can predict the solubility of any metal in mercury [27]. In spite of this, two interesting sets of correlations were obtained during our efforts to find some type of property to make such predictions.

Generally, the more periodic properties that two elements have in common (atomic size, electronegativity, valency, etc.), the greater the probability that they will be more soluble in each other. Thus, one type of correlation which might be expected, is between an element's position in the periodic table with respect to mercury and its solubility in mercury. Such a correlation is shown in Figure 4.1a. As can be seen, the metals most soluble in mercury are those nearest to it in the periodic table between groups IB and IVA, and those least soluble lie further away between groups IVB and VIIIB.

Another correlation was conceived on the basis of surface free energy, γ. Very qualitatively, one might expect that any associations in a solution would tend to restrict the motion of the atoms and thus the entropy, S, of the system should decrease, i.e. $S \propto 1/\text{solu}$. At the same time, from the thermodynamic definition of free energy ($G = E-TS$) we have that $\gamma \propto -S$, so we would expect that $\gamma \propto -1/\text{solu}$. A plot of the solubility as a function of surface free energy, shown in Figure 4.1b, gives just such a correlation.

The two sets of data are independent of each other and thus can be used as a cross-check for solubility. This was clearly demonstrated in the case for the solubility of iridium, which was given by Vydra et al. [27,pg.59] as 0.001 weight % at 20°C. In both graphs, the value appeared to be too high by two orders of magnitude. This solubility value is now considered to be incorrect, the accepted upper limit value being 10^{-5} weight % at 500°C [111]. The solubility at 20°C being at least an order of magnitude lower. There are several

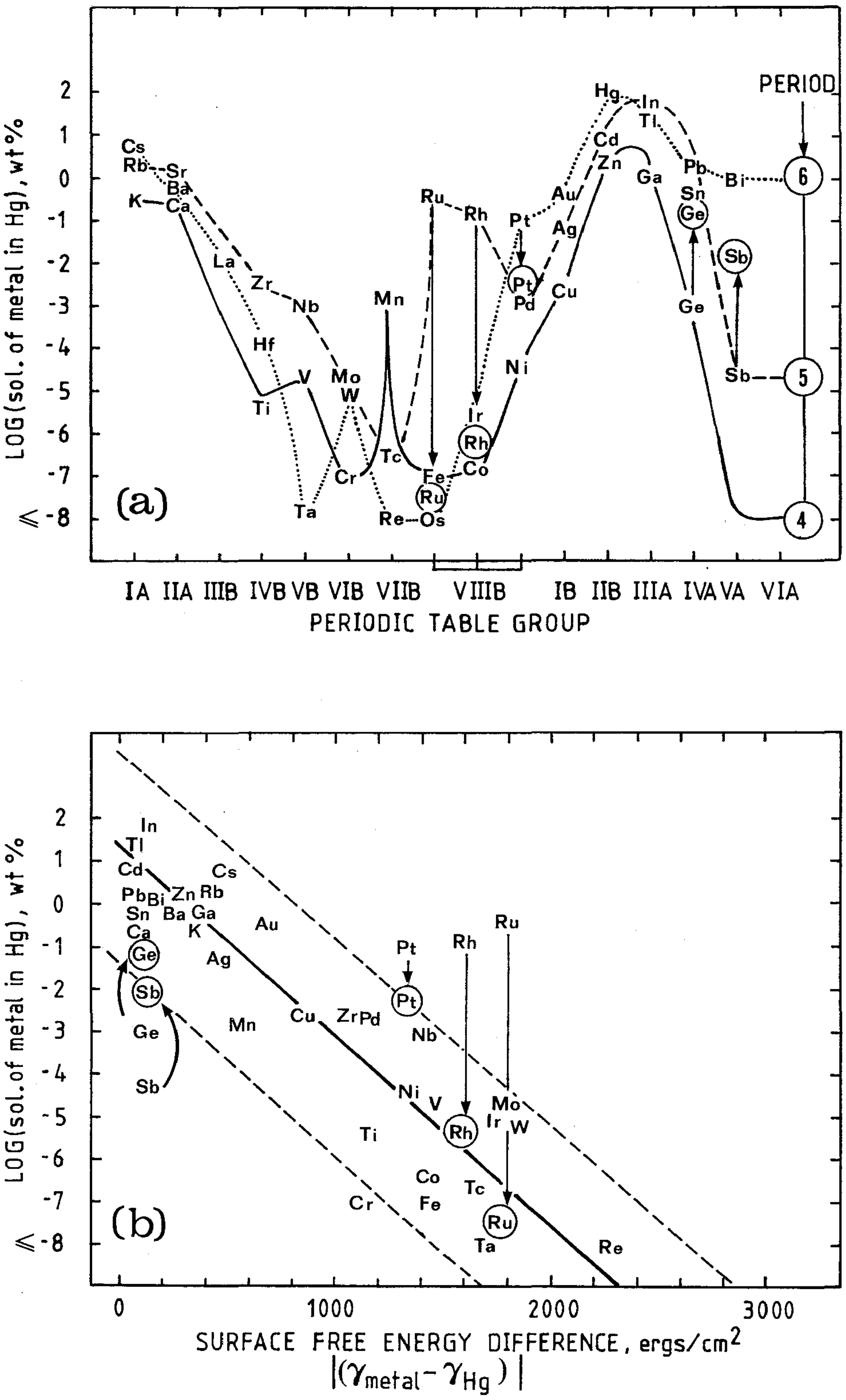

FIGURE 4.1 The solubility of certain metals in mercury as a function of (a) the periodic group, and (b) the surface free energy difference between the metal and mercury [112].

other elements for which the same situation may exist. For example, note that "correcting" the solubilities for Rh, Ru, and Pt in either plot (circled symbol), also "corrects" it in the other. However, we did not pursue the problem any further, since it did not directly affect this research.

In terms of solubility, we were then left with about fifteen pure metals as possible substrates.

In addition to the pure metal substrates selected above, we also decided to consider binary alloy substrates. Higher order alloys were not considered due to lack of data.

Primarily, one may distinguish between three types of alloys:

(1) If the atoms are completely indifferent to each other, they become mixed together so thoroughly that the alloy is homogeneous down to the atomic level. This type of structure is referred to as a random solid solution alloy.

(2) When formed from two unlike metals which slightly attract each other, the two metals often become arranged in some regular alternating pattern. This type of structure is known as an ordered solid solution alloy.

(3) If the metals differ electrochemically, the bond between them becomes partly ionic and the structure is then termed an intermetallic compound.

For a solid solution alloy, each constituent metal can separately dissolve and undergo its own reactions with mercury. An intermetallic compound, however, will remain as a single molecule with its own unique set of properties.

Based on the above facts, only intermetallic compounds were considered as substrate choices. The concept here was that mainly because of its size, a larger intermetallic molecule would be substantially less soluble in mercury than any of its individual components. Of even greater interest was that one of the components could be selected because it formed some type of "bond" with mercury, and the other because it was completely insoluble in mercury. Thus, hopefully, the resulting substrate would be able to support a mercury film without dissolving in, or chemically reacting with, the mercury.

A number of intermetallic compounds were found to fit the above requirements in terms of composition but had to be eliminated as possible choices due to major problems in respect to their: *i)* fabrication, *ii)* electrical conductivity, or *iii)* mechanical properties. A list of the above compounds and the reasons for their elimination can be found in APPENDIX I.

Finally, four intermetallic compound substrates were selected for fabrication; NiAl, NiSb, PtSi, and Pt_2Si_2Co. The Co was added to the PtSi in order to increase its mechanical strength and is not involved in the Pt-Si bonding.

4.1.2 Interactions Between Substrate and Mercury

The interaction between the mercury and the substrate is defined electrochemically as the underpotential of deposition. This deposition underpotential, E_u, can exist either due to a chemical reaction between the first layer of mercury and the substrate, or due to the earlier mentioned attractive forces. It has been shown [113] that when chemical interactions between substrate and mercury can be discounted, E_u is related directly to the electrochemical work function, Φ, (ie. the energy arising from a partial or total charge transfer between the metals). The greater the difference in Φ, the greater will be the polarity and thus the attractive-force bonding of the mercury and substrate. In other words, due to this stronger bonding of substrate and mercury, a large $\Delta\Phi$ favors film formation over three-dimensional nucleation.

Figure 4.2 shows a plot of the solubility data as a function of $\Delta\Phi$ (taken from Trasatti [114]). The most important item to note is that the metals at the bottom right-hand corner are especially suitable in terms of non-solubility and maximum attractive-force bonding.

At that point, using the above data, we had then limited our choices to Ir, Ni, Co, Re, and Fe.

4.1.3 Final Selection of Substrates

Before proceeding with the fabrication and tests, four last eliminations were made. Even though we had already rejected all but five of the metals, we found it also necessary to eliminate Re, Ni, Co and Fe, since, according to their electrochemical equilibrium diagrams [115], they all undergo dissolution at the

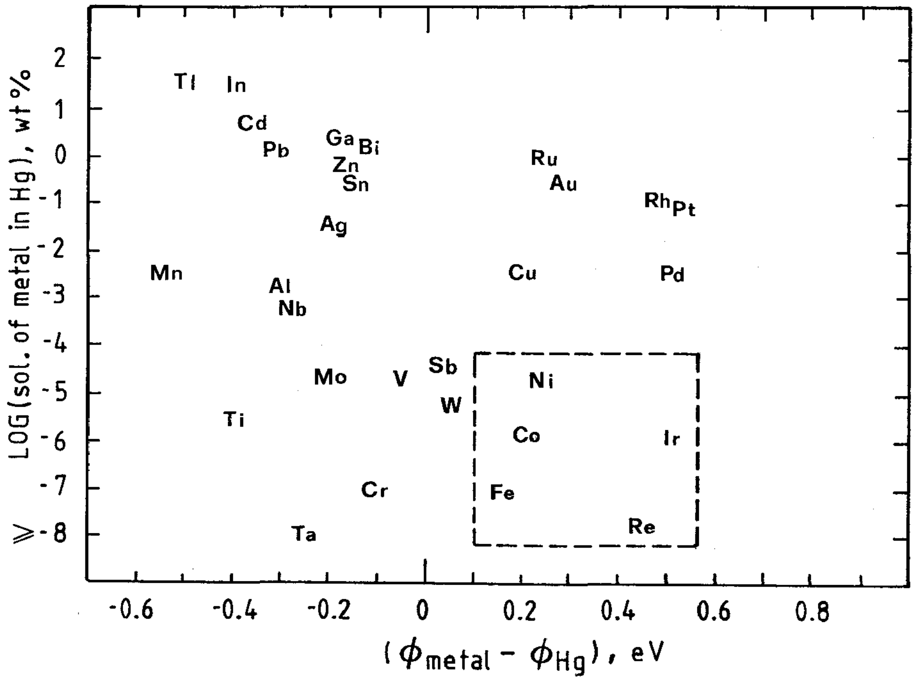

FIGURE 4.2 The solubility of certain metals in mercury as a function of the difference in the work functions $\Delta\Phi$ of the metal and mercury.

pH's and potentials where mercury deposition would take place.

This left iridium as the sole choice of the pure metal substrates, the alloy substrates still being NiAl, NiSb, PtSi, and Pt_2Si_2Co.

4.2 PREPARATION OF ELECTRODES

4.2.1 Fabrication

The metal alloy substrates were made with the aid of a high temperature RF-furnace (Univ.of Geneva, Physics Dept. Dr.Jorda) by melting together appropriate amounts [109] of each component metal (Goodfellow Metals, Cambridge England, 99.9% purity) in a cylindrical tungsten crucible (2-3mm dia. x 20mm length).

The iridium metal (99.9% purity) was obtained in wire form 2mm dia. x 5cm (Heraeus GmbH, Hanau W.Germany).

Since the electrodes were to be used with the rotating disk assembly shown in Figure 1.3 (see also Sec.2.1), each substrate material was machined or ground into a cylindrical form (2-3mm dia. x 10mm) which was then press-fitted into a changeable Teflon tip shown below in Figure 4.3.

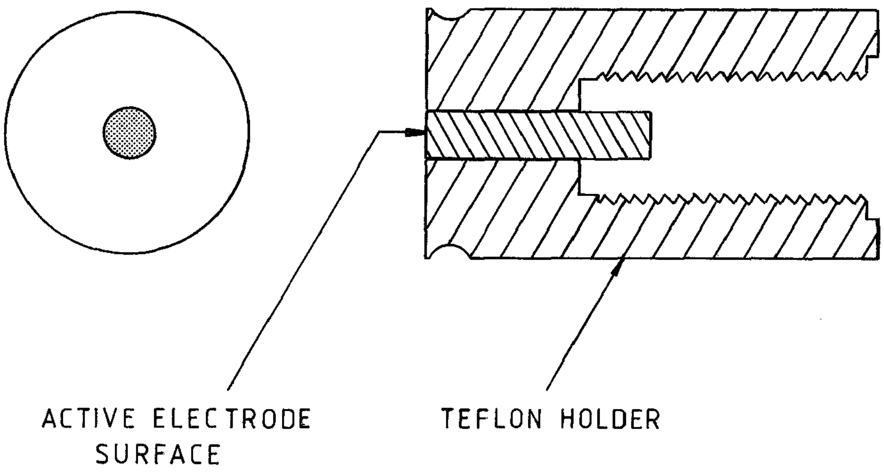

FIGURE 4.3 Diagram of the changeable Teflon rotating disk tip with the press-fitted electrode substrate.

4.2.2 Pre-treatments

As was earlier shown in Section 1.3, it is difficult to find a method for the pre-treatment of electrode surfaces that will give reproducible results. For these initial tests we took what one may call a "qualitative average" of the most common methods found in the literature.

Polishing. Each electrode was initially given a rough polishing by hand (while the disk assembly was rotated at 1000rpm), successively, with 400 and 600 grit silicon carbide paper (Union Carbide Co.) for a period of about five minutes. This was then followed by polishing, for another five minutes, with SURFEX 3µm diamond paste sprayed onto a MARCON-F200mm polishing cloth (Metzger & Co, Lotzwil Switzerland). The electrode was then well rinsed with diamond paste solvent, acetone and deionized water.

This procedure worked well with all substrates except Pt_2Si_2Co and Ir. In both of these cases, the substrates were found to be extremely hard, taking about 30-40 minutes for each polishing step before a surface of the same smoothness as that of the others was obtained.

Chemical and Electrical Pre-treatments. Before deposition of the mercury-film, each electrode was placed in concentrated nitric acid for 5 minutes (while rotating at 1000rpm), rinsed with deionized water, and then electrochemically cleaned by polarizing it at a potential of -1.5 VDC vs.SCE in a solution of 0.1M $HClO_4$. The electrode was left in this solution, under a N_2 blanket, until the mercury deposition step was about to start.

4.2.3 Mercury-film Deposition

So as not to expose the electrode surface to oxygen, the cleaning solution used above was replaced by the deposition solution using the medium exchange system (see Sec.3.2). The electrode was then plated with mercury using an electrolyte, which had been de-oxygenated with N_2, and containing 0.1M $HClO_4$ and 0.001M Hg^{++}. A wide range of deposition potentials (+500 to -1500 mV vs.SCE) and times (30 seconds to 5 hours) were used in order to find the optimum value for each electrode substrate material.

4.3 RESULTS

For each substrate, we determined: (1) the hydrogen overpotential (ie. the potential where hydrogen-gas evolution from reduction of water commences), as an indication of the cathodic limit for the quantitative deposition of mercury; (2) the most anodic potential at which mercury could be reduced; and (3) whether or not a mercury film could be formed and maintained.

In each of the above cases, the parameters were determined both by recording the current-potential curves, and simultaneously observing the surface with the microscope.

The results for each substrate are described below and summarized in Table 4.1.

It should be noted at this point, that in order to facilitate the description of the mercury films obtained here and in the following sections, the physical form of the mercury on the surface has been charcterized into four types of partial surface coverage: spheres, semi-spheres, domed patches, flat patches; and two types of complete coverage: a semi-spherical film, and a true film. All of these six types are shown in Figure 4.4.

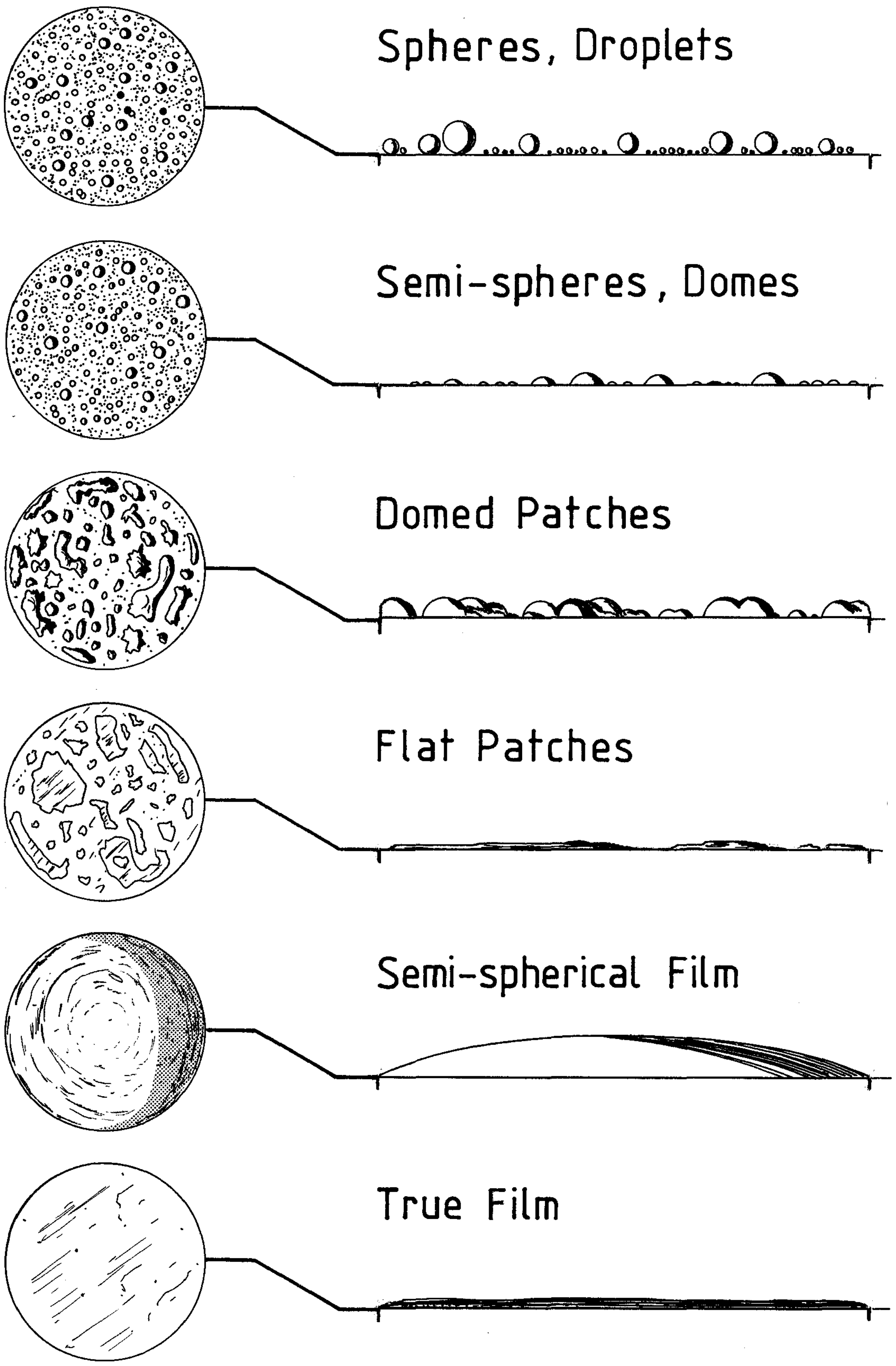

FIGURE 4.4 The six types of surface coverages by mercury.

TABLE 4.1 Experimental results for the five different substrates tested.

SUBSTRATE MATERIAL	HYDROGEN OVERPOTENTIAL (mV)	MERCURY REDUCTION POTENTIAL (mV)	TRUE FILM
Ni-Al	-800	*	NO
Ni-Sb	-650	-350	NO
Pt-Si	-350	+100	NO
Pt_2Si_2Co	-350	+100	NO
Ir	-650	+300	YES

* Could not be determined because of interference caused by surface reaction.

The NiAl substrate had the most cathodic hydrogen overpotential at -800 mV, but unfortunately showed one of the most rapidly deteriorating surfaces with the application of any potential more positive than -750 mV. This made it very difficult to deposit mercury without interference from hydrogen gas formation. The mercury itself was deposited in flat patches, most likely due to the rapid surface oxidation and deterioration occuring during the initial few seconds after application of the deposition potential.

The NiSb substrate showed a slightly more anodic hydrogen overpotential at -650 mV and the oxidation of the surface did not occur unless the deposition potential was set more anodic than -300 mV. The deposition of mercury at -350mV resulted in domed patches, but after several cycles of depositions and cleaning, the surface showed signs of cracking and pitting. Polishing the surface revealed both the cracks, and especially the pits, to be significantly deep, only removable by abrading the surface with 600 grit silicon carbide paper for 5 minutes.

The two silicon alloy substrates showed no major differences between themselves, except for the PtSi substrate being more susceptible to surface scratching and more brittle, making it harder to obtain and maintain a smooth surface on it. In both cases the hydrogen overpotential was at -350 mV and the deposition of mercury started at +100 mV. Further tests were carried out only on the Pt_2Si_2Co substrate. The mercury deposited at -100 mV for 600 seconds, formed a homogeneous coverage composed of spheres, which, with longer deposition times coalesced into a large semi-sphere covering the entire surface. Thus, the overall behavior of this substrate seems to be very similar to that of glassy-carbon (see Sec.1.3). Its properties seem to lie between those of elemental platinum and silicon: its surface can be polished to a glassy luster (Si), it appears to be inert under normally used conditions (Pt), it has good conductivity (Pt), and is slightly brittle (Si).

The most promising electrode substrate studied was iridium. The hydrogen overpotential was found to be about -650 mV and the anodic limit for the deposition of mercury at about +300 mV. The deposition of mercury at +100 mV for 600 seconds produced a true film about 50% of the time. The other 50% of the time, semi-spheres were produced, which, with increased deposition time resulted in complete coverage of the surface by a semi-spherically shaped film. The iridium surface, which initially took longer to polish, was found to be exceptionally hard and inert, and maintained its luster for the entire month of testing. In these initial tests the iridium substrate seemed to behave similarly to the platinum substrate (see Sec.1.3) but with the difference, as expected, of not being soluble in, or reacting with, the mercury.

4.4 CONCLUSION

The literature contains a large amount of information relative to the electrochemical properties of the more common alloys, containing such metals as Cu, Zn, Fe, Cr, Ni, Al, etc., but almost nothing about the type of intermetallic compounds we had selected to synthesize. Thus, we did not have any way of predicting their electrochemical properties or behavior under the conditions at which mercury deposition takes place.

In view of the above, it is not surprising then that none of the four substrates behaved as we had hoped. They all seemed to possess the desirable properties of being insoluble in, and chemically unreactive with, mercury, but unfortunately, they also showed no tendency to form any type of film-promoting bonds. In the case of the two nickel alloys, they also underwent an undesirable electrochemical reaction causing oxidation and/or deterioration of their surfaces.

We concluded that, although there may exist intermetallic compounds which may behave as we would like, unless more information could be found to better predict their electrochemical behavior, it would be too expensive and time consuming to pursue the "make-and-test" procedure any further.

The preliminary results obtained for the iridium substrate were very promising and indicated that it might well possess, simultaneously, the two properties described in Sec.4.1, of insolubility in, and bonding with, mercury.

Iridium also possesses many other properties desirable in an electrode substrate: it is quite hard and can be polished to a flat mirror-like surface, it is immune to attack by any of the acids, and it has good electrical conductivity.

Therefore, we decided to conduct further experiments in order to optimize the conditions for forming a mercury film, and to better understand the iridium as an electrode substrate.

5. CHARACTERIZATION OF IRIDIUM AS A MERCURY-FILM SUBSTRATE

The deposition of mercury-films on substrates such as platinum, silver, gold, nickel, and carbon (Sec.1.3) is well documented in the literature. Unfortunately, the same cannot be said for iridium. A literature search going back 30 years managed to turn up only 4 papers dealing with mercury deposition on iridium, and these were mainly concerned with the behavior of mercury as a poison for hydrogen and oxygen adsorption on its surface.

There are several reasons for this lack of past research with an "iridium electrode". Even though it possesses several of the same desirable properties as the other precious metals, it is substantially harder, more inert, and was more expensive, thus making it difficult to mount, make electrical connections with, and purchase, respectively. These problems do not exist to the same extent today, thanks to the rotating disk assembly (Sec.3.3) which permits easy and reliable mounting of the electrode material, and the "relative" low cost and availability of the iridium.

The purpose of the research, described in this chapter, was to quantify the parameters which would be necessary in order to characterize and optimize the iridium-MFE.

5.1 SURFACE PROPERTIES OF IRIDIUM

The few surface reaction investigations of pure metallic iridium have mainly dealt with hydrogen and oxygen adsorption and anodic potential-cycling surface modifications.

The oxygen/surface reactions are of interest to us, both in avoiding any oxidation of the surface, and because of the possibility of using this surface oxide/hydroxide-film to help promote mercury-film formation (Sec.2.2). The adsorption of hydrogen is also of interest to us since its surface coverage and overpotential are useful as indicators of the amount of mercury surface coverage.

5.1.1 Anodic Surface Modification Reactions

During the anodization of iridium in sulfuric acid, Otten and Visscher [116] found that repeated cycling between -200 mV and +1200 mV "drastically" changed the iridium surface. A layer of modified surface was formed with a thickness depending upon the number of cycles (e.g., ≈ 3 nm after 80 cycles, measured by reflective ellipsometry). At the same time, the recorded peak currents increase steadily and the voltammograms become almost symmetrical about the potential axis. No change is noticed, however, if the anodic limit of the potential scan is less than +1150 mV. Figure 5.1 shows a repeating cyclic voltammogram obtained with our iridium electrode, in 0.1M $HClO_4$, at a scan rate of 100 mV/s.

Rand and Woods [117] have suggested that the large, symmetrical peaks on the voltammogram (peaks II and V: Fig.5.1) are associated with an oxide phase and that the charge corresponding to these peaks arises from changes in stoichiometry of the oxide, similar to those observed for iron in alkaline or chromium in acid solutions. That is, a reaction involving the addition of OH species such as:

$$Ir(OH)_3 + H_2O \longleftrightarrow Ir(OH)_4 + H^+ + e$$

They found that there is a negligible influence on the overall shape of the voltammogram as the scan rate is increased from 40 to 400 mV/s, thus, indicating that the stoichiometry change is very reversible for iridium.

The oxide phase is not removed from the electrode surface during cathodic scans or even after holding the electrode for long periods of time, between cycles, at potentials more negative than -1500 mV. Although the stoichiometric changes in the oxide phase are reversible, the initial formation of the oxide species is highly irreversible. The growth of the peaks during continuous potential cycling is due to the accumulation of the oxide phase formed during each cycle.

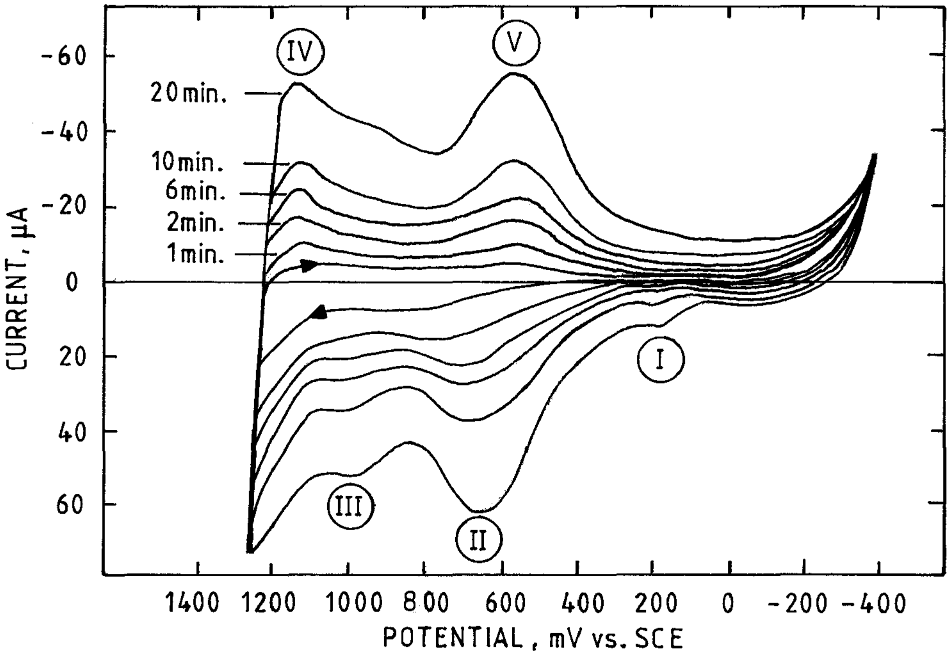

FIGURE 5.1 The potential-current curve for the iridium-RDE. First scan is indicated by arrows. The other curves are recorded at the indicated time, during the repetitive scanning.

The phase oxide layer present on a cycled iridium electrode can be removed and the electrode returned to its original state (i.e., monolayer of IrO_2) if it is placed in either hot chromic acid solution or 5M H_2SO_4.

Formation of a Polymeric Ir-OH Film. X-ray analysis of the surface products formed during the oxidation of iridium in 0.1N H_2SO_4 has shown [118] that the only oxide found in the potential range of 500 to 2200 mV is IrO_2. Zerbino et al. [119] have suggested that in aqueous solutions, where IrO_2 exists as $Ir(OH)_4$ (i.e., as $IrO_2 \cdot 2H_2O$), this layer may undergo the following three reactions:

$$Ir(OH)_4 + H^+ + e \longleftrightarrow Ir(OH)_3 \cdot H_2O$$

$$Ir(OH)_3 + H_2O + H^+ + e \longleftrightarrow Ir(OH)_2 \cdot 2H_2O$$

$$Ir(OH)_2 + 2H_2O + H^+ + e \longleftrightarrow Ir(OH) \cdot 3H_2O$$

These reactions explain the relatively reversible redox couples appearing in the +100 mV to +1200 mV region. It has been shown [120] that this behavior is related to the anodic formation of a polymeric-type hydrated iridium hydroxide film involving $Ir(OH)_4$ units, and occurs not only in H_2SO_4, but also in $HClO_4$ solutions. The electrode/solution interface will then consist of three planes: *i*) a solid iridium substrate, *ii*) a hydrated-oxi-hydroxi-iridium layer, and *iii*) the solution.

5.1.2 Influence of Mercury on Hydrogen Adsorption

Some work in this area has been carried out by the Russian groups of Semenova et al. [121], Maximov et al. [122], and Chemeris et al.[123].

Hydrogen adsorption on iridium has been shown to be very sensitive to the monolayer coverage of adsorbed mercury. It has been claimed, that with coverages of $< 0.1\%$ (in 0.1N H_2SO_4), one atom of mercury will displace ≈ 70 atoms of hydrogen from the surface [121]. With increasing mercury coverage, the number of hydrogen atoms displaced decreases, along with both the extent of surface coverage by hydrogen, and to a lesser degree, the iridium-hydrogen bonding energy. The effects of mercury and hydrogen on the iridium electrode are in good agreement with those observed for the other platinum group metals [122].

A very important observation, noted by two of the research groups [122,123], was that mercury-contaminated iridium electrodes cannot be completely cleared of adsorbed mercury, except by a very anodic polarization. Figure 5.2 below shows the adsorbed mercury monolayer coverage as measured by anodic oxidation and/or the hydrogen evolution charge. As can be seen, zero surface coverage is not approached until a potential of at least +1000 mV is attained.

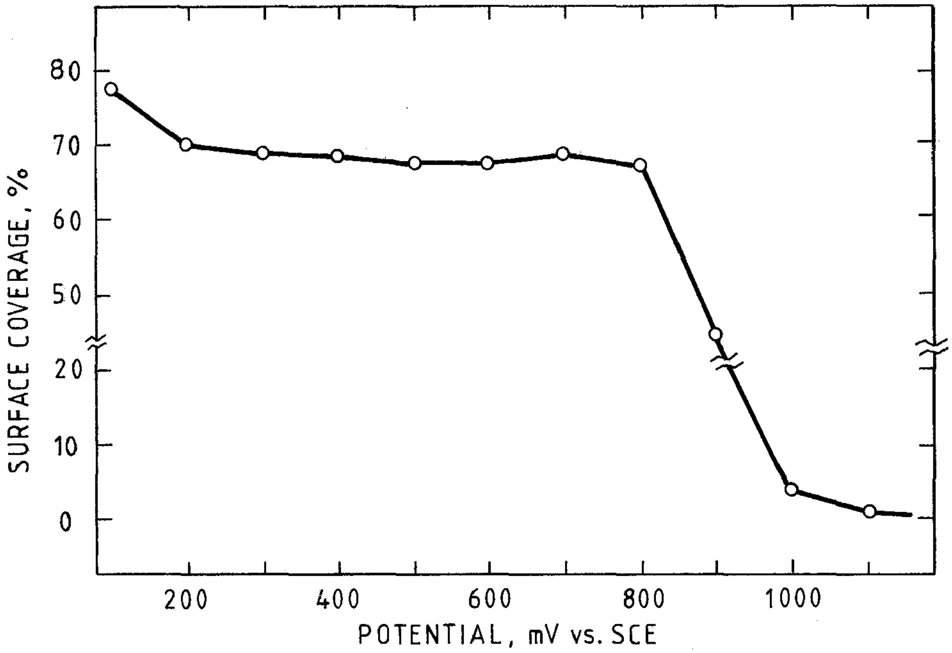

FIGURE 5.2 The mercury surface coverage on an iridium electrode as a function of adsorption potential [taken from 123].

($1N\ H_2SO_4 + 10^{-4}M\ Hg^{++}$)

5.2 SELECTION OF SURFACE PRETREATMENTS

Although a pretreatment procedure was adopted for use in Sec.4.2.2, its main purpose was to expedite the initial substrate selection process, and was not necessarily an optimal method for any single substrate. Hence it is most sensible to attempt optimizing the procedure specifically for iridium.

5.2.1 Nature of Pretreatments Tested

The pretreatments to which the iridium was subjected, either passively or actively, can be separated into three main categories:

Physical. This mainly includes: *i*) the treatments during the fabrication process which result in the formation of its crystal structure and mechanical properties and, *ii*) the degree to which the surface is polished before its actual use. The fabrication effects were beyond our control, since the iridium was purchased rather than made in-house (Sec.4.2.1). The polishing, however, could easily be done by using a diamond paste spray and polishing cloth (Sec.4.2.2). Since for a thin flat mercury-film it is desirable to have the smoothest possible surface, before all other pretreatments, the surface was polished using, as the final abrasive, a 1μm diamond spray. The polishing was continued for as long as required to obtain a mirror-like finish (under microscopic observation at x250).

Chemical. Once the electrode is polished, the immediate de facto chemical "treatments" are those caused by contact with: air, water, and the final organic polishing solvants. At this point we most likely had a surface which was slightly oxidized and might have had some adsorbed organics on it.

It seemed wise then to simply complete the oxidation of the surface, as was done for the original (Sec.4.2.2) selection tests, by using a strong acid, in this case concentrated HNO_3.

Electrochemical. The choice for the electrical treatment, if any, amounted to what potential the electrode should be subjected to as a final step prior to mercury deposition. Many of the studies reported in the literature for metals other than iridium [38,40,45,68] use equally either cathodization or anodization (sometimes neither). Since none of them refer specifically to iridium, we tested both types of electrical treatments.

Taking all of this into consideration, we established six electrode pretreatments to be tested. (NOTE: All pretreatments included the polishing procedure, described above, as their initial step.) The pretreatments tested were as follows:

(1) The electrode was washed only with deionized water. Thus, we had at most a partial air/water oxidized monolayer.

(2) In addition to treatment #1, the surface was washed with concentrated HNO_3 for five minutes, and then rinsed with deionized water. This gave us a chemically-oxidized surface.

(3) Same as #2, except that the electrode was washed for 30 minutes in concentrated HNO_3.

(4) Same as #1, but with the addition of anodization at +1.5 V for 5 minutes in 1.0M HNO_3. This resulted in an electrically-oxidized surface.

(5) Same as #1, but with the addition of cathodization at -2.0 V for 5 minutes in 1.0M HNO_3. This resulted in an electrically-reduced surface.

(6) Same as #4, but after the anodization the surface was cathodized at -2.0 V for an additional 5 minutes. This gave an electrically-oxidized-then-reduced surface.

To measure the efficacy of the pretreatment, we followed two parameters: the contact angle, and the reduction potential of mercury on the iridium substrate.

5.2.2 Pretreatment Effects on Mercury-Iridium Contact Angle

As was earlier mentioned (Sec.2.2), the contact angle θ depends on the relative values of the mercury/iridium, iridium/solution, and mercury/solution, interface surface energies. In this case we wanted to find a pretreatment with the smallest possible value of θ, corresponding to a maximum wetting of the iridium surface by mercury (i.e., the pretreatment which would most likely promote formation of a thin mercury film).

The contact angle for each pretreatment was obtained by placing a mercury drop on the iridium disk of the inverted RDE, and photographing it (x250) sideways through the microscope. The mercury drop was extruded from a micrometer-controlled hanging mercury drop electrode (Metrohm EA-290). The radius of the mercury drops (for turning one division on the micrometer) was estimated, by weighing 20 drops and taking the average, to be 0.025 ± 0.002cm. The photograph was enlarged, and θ determined by two methods. Figure 5.3 shows an actual photo for pretreatment #1, and the methods of determining the angle θ.

In the first method (Fig.5.3a), θ is determined geometrically, by drawing two tangents perpendicular to the substrate surface (A,B), and from the center of the line connecting them (C), drawing a radial line (D) to the interface intersection, and measuring θ between the radial tangent (E), and the surface/drop interface (F).

The second method, based on the Winterbottom Theory [124], (Fig.5.3b) defines θ mathematically as:

$$\theta = 180 - \arccos(x/r) \qquad (5.1)$$

where x is the distance from the substrate surface to the maximum diameter parallel to the substrate, and *r* is the radius. Since implicit in this second method is that the shape of the drop is spherical, a different value of θ for the two methods indicates that the drop is distorted. For all our measurements, the two methods gave the same value of $\theta \pm 0.25^\circ$.

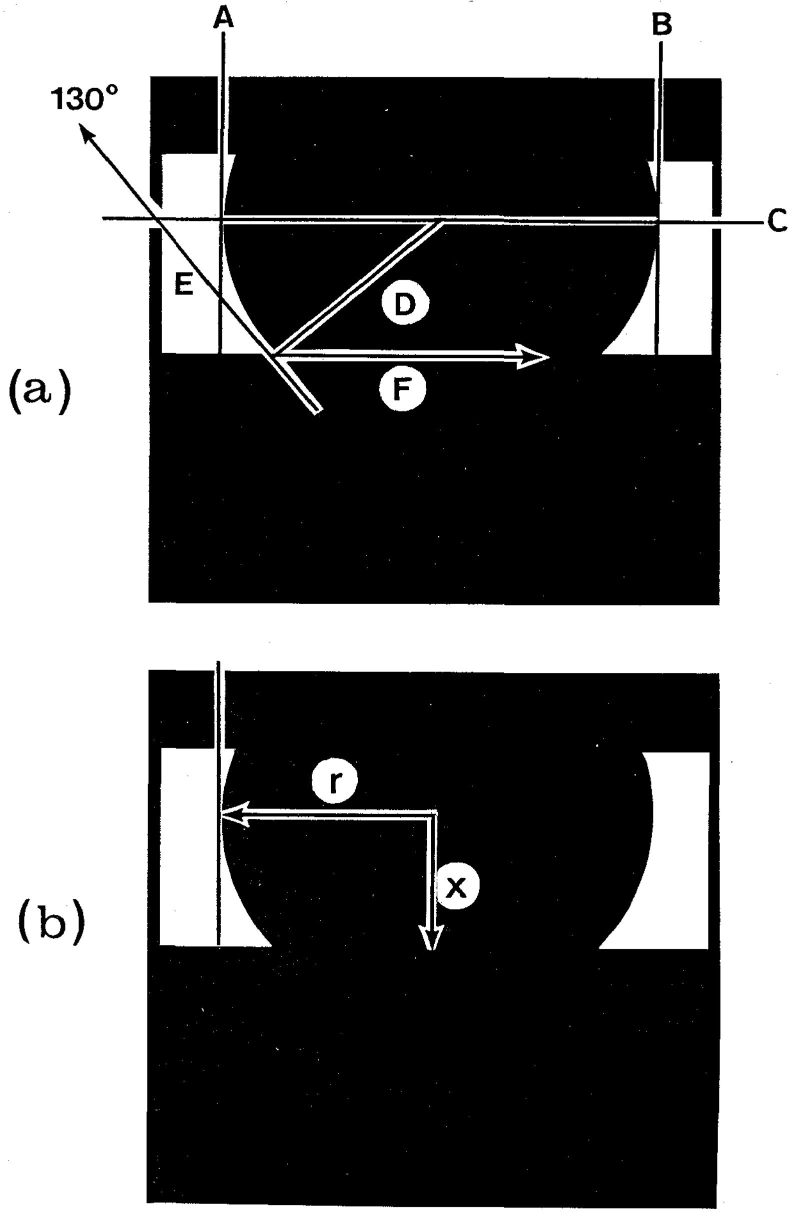

FIGURE 5.3 Determination of the mercury-iridium contact angle (a) geometrically and (b) by Eq.(5.1).

The results for the determination of the contact angle are summarized in Table 5.1. The value given in each case is the average of two measurements.

It is interesting to note that, as expected, θ was the largest ($\approx 130^\circ$) for the electrode with the least pretreatment (#1). The concentrated HNO_3 by itself or with anodization did not seem to make too much of a difference in pretreatments #2, #3 and #4, giving practically the same value for θ of 129°, 128° and 129°, respectively.

The smallest value of $\theta = 121^\circ$ was found for the cathodization (#5). However, the pretreatment that preceded cathodization by anodization (#6) gave a slightly higher value of $\theta = 125^\circ$.

From the above data, we concluded that cathodic polarization was much more effective than either concentrated HNO_3 or anodization at reducing the contact angle. At this point it seemed to indicate that either an acid-oxidized surface is the same as an anodized surface, or that the surface was not oxidized by any of the preceding treatments, and that the cathodization may be reducing some type of surface impurity originating in the polishing step.

No literature data could be found for the contact angle of mercury on iridium, therefore, we have no way of evaluating whether the contact angle obtained ($\approx 121^\circ$) should be thought of as an absolute value for mercury on iridium (in air), or whether to consider it only as a relative value for use in judging the efficacy of the pretreatment. For platinum [70] and paladium [125] the contact angles are given as 38 and 40°, respectively. Considering the much higher solubility of these metals in mercury (APPENDIX H) as compared to that of iridium, the value of $\theta = 121^\circ$ for iridium appears reasonable.

TABLE 5.1 Pretreatment effects on contact angle and reduction potential for mercury at the iridium electrode.

#	PRETREATMENT *	CONTACT ANGLE (degrees)**	REDUCTION POTENTIAL (mV vs. SCE)***
1	rinsed with water (air oxidized ?)	130	+230
2	5 min/con.HNO_3 (chem.oxidized)	129	+210
3	30 min/con.HNO_3 (chem.oxidized)	128	+190
4	same as #1 plus 5 min/1M HNO_3 +1.5V (elec.oxid)	129	+180
5	same as #1 plus 5 min/1M HNO_3 -2.0V (elec.red.)	121	+170
6	same as #4 plus 5 min/-2.0V (elec.oxid.+red.)	125	+190

* All pretreatments include initial polishing step.

** ± 0.5°

*** ± 5 mV

5.2.3 Pretreatment Effects on Mercury Reduction Potential

Complementary to the contact angle measurements, we also recorded a cyclic voltammogram for each pretreatment, paying special attention that the reduction curve was taken on the first cathodic scan. The electrodes were prepared using exactly the same pretreatments as those used for the contact angle measurements.

The solutions used contained 0.1M $HClO_4$ + 10^{-4}M Hg^{++} in deionized water, and were purged with N_2 for 30 min. before starting. The cyclic voltammograms were all recorded at 20 mV/s starting at +700 mV to a vertex of -200 mV, and using the RDE with ω = 1000 rpm.

Figure 5.4 shows, as an example, a cyclic voltammogram made after pretreatment #1. The half-wave potential, $E_{1/2}$, for the

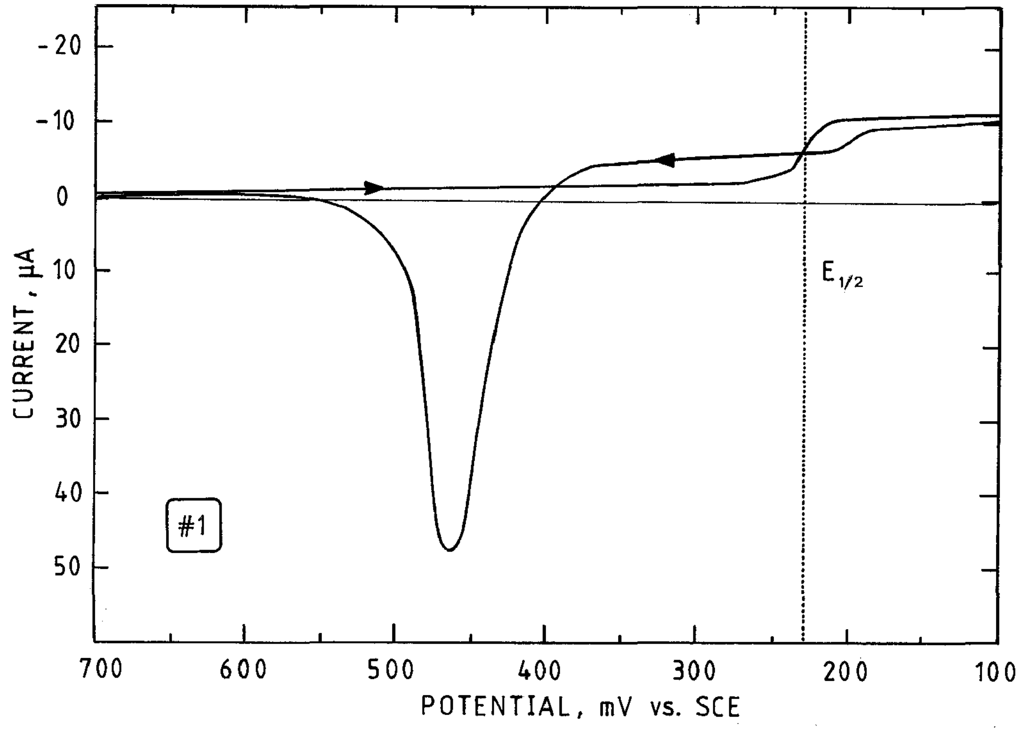

FIGURE 5.4 Cyclic voltammogram of mercury on the iridium substrate electrode with conditions given in text.

reduction of mercury(II) is at 230 mV. The anodic peak at 460 mV is due to the bulk oxidation of mercury.

There are three features of this cyclic voltammogram which should be briefly noted at this point. In the cathodic direction scan there is a small peak on the plateau of the Hg(II) reduction wave. In the returning anodic scan *i)* there is a sudden decrease in the reduction current at approx. 200 mV, which as will be shown later, may be due to the formation and adsorption of Hg_2Cl_2 on the iridium surface, and *ii)* the the reduction continues until approx. 410 mV, which is due to reduction of mercury(II) on the bulk mercury which now exists on the iridium surface, and will not be oxidized until the potential is > 410 mV. These features will be considered more thoroughly in Sec.5.3.

The results for the determination of the half-wave reduction potential of mercury(II), $E_{1/2}$, corresponding to each pretreatment, are summarized in Table 5.1.

5.2.4 Selection of a Pretreatment

Figure 5.5 shows the relationship between the contact angle, θ, and the reduction potential, $E_{1/2}$, for each pretreatment (#1-#6 in Table 5.1). The oxidation and reduction pretreatments both affect the surface similarly in terms of $E_{1/2}$, but somewhat differently in terms of θ.

For both types of <u>oxidation</u> pretreatments, acid and electrical (#2,#3,#4), there is a substantial decrease of $E_{1/2}$ ($\approx$ 50 mV), especially with increasing oxidation strength, but only a small decrease of θ ($\approx 2^\circ$). On the other hand, the cathodization pretreatment (#5) shows the largest decrease of all for both $E_{1/2}$ and θ ($\approx$ 60 mV and 9°).

The above behavior suggests that both, the chemical and electrochemical pretreatments, produce an oxide layer on

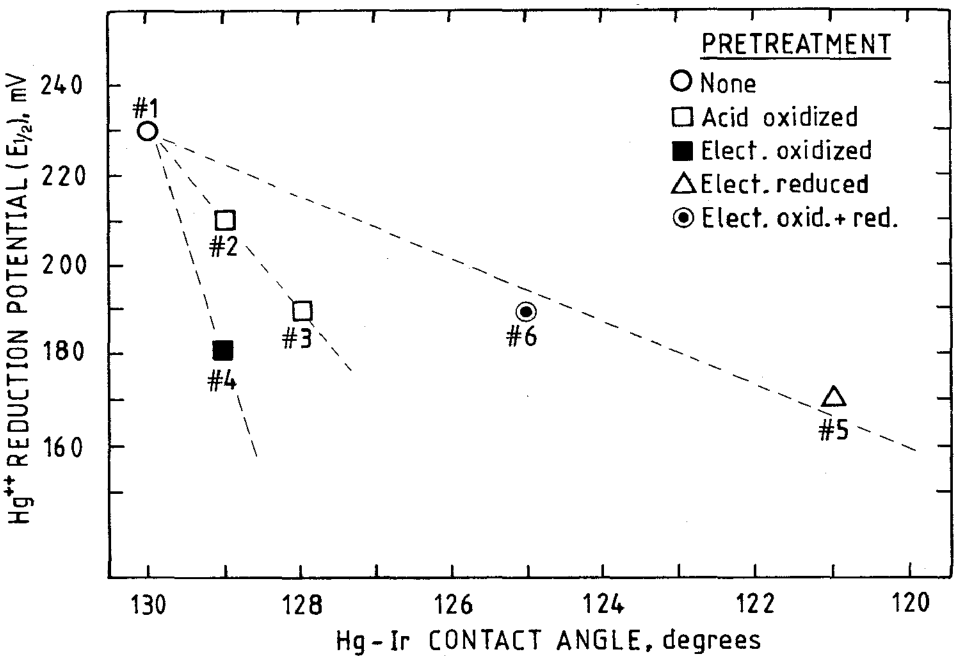

FIGURE 5.5 The relationship between the contact angle θ and the mercury reduction potential $E_{1/2}$ for each pretreatment (#1-#6) as described in Table 5.1.

the iridium surface. This layer makes it more difficult (i.e., requires more energy) for the reduction of mercury(II), but makes no difference in the ability of mercury to spread on the surface (no decrease in θ). This means that eventually, when some nuclei are formed, the reduction of mercury(II) will continue on these nuclei in preference to the oxide coated surface ($Hg^{++} \rightarrow Hg^{0}$: +400 mV). This situation is not favorable for the formation of a homogeneous mercury film.

The cathodization (#5) reduces the oxide layer, making it easier for mercury to spread, but making it just as difficult for the reduction of mercury (II), as did the oxide layer.

For the combined anodization-cathodization (#6), we have probably only partially reduced the anodized surface, hence, it exhibits a midway behavior.

Thus, from the above results, a cathodized surface seems to provide a better substrate on which to form a mercury film.

5.3 INTERACTIONS OF MERCURY ON IRIDIUM

It is essential for the preparation of a well-controlled mercury-film electrode, and its eventual application to metal analysis and speciation in natural waters, that we understand the interactions which may or may not occur between the mercury film and the iridium surface. In the following sections we will look at several parameters with the aim of better understanding these interactions.

5.3.1 Reduction of Mercury on Iridium

One of the more simple and direct methods for determining the interactions of mercury and the iridium surface is to make a cyclic voltammogram, using a mercury(II) solution and a "defined" iridium surface (pretreatment #5). Such a curve is shown in Figure 5.6a with 20 consecutive repeating cycles.

For the cathodic scan, the most prominent features are the "shift" of the reduction wave-A from ≈ +160 mV to +275 mV, and peak-B which appears on top of wave-A at ≈ +70 mV. As can be seen, the reduction wave is not a clean sigmoidal shape as would be expected for the diffusion controlled reduction of Hg(II). It is complicated by a small bend (shown by the arrow) at the foot of the wave and a "split" reduction wave.

The interpretation of the curves in Figure 5.6 requires that we take into account certain facts. The bulk of the solution contains Hg(II), but as soon as some Hg(0) droplets are formed at the electrode surface, Hg(I) is formed as a result of the disproportionation reaction:

$$Hg^{2+} + Hg^{0} \xleftrightarrow{K} Hg_2^{2+} \qquad (5.2)$$

The equilibrium constant K can be computed from the Nernst relationship, using the two couples Hg^{2+}/Hg_2^{2+} : (E_o'), and Hg_2^{2+}/Hg^{0} : (E_o'') to give:

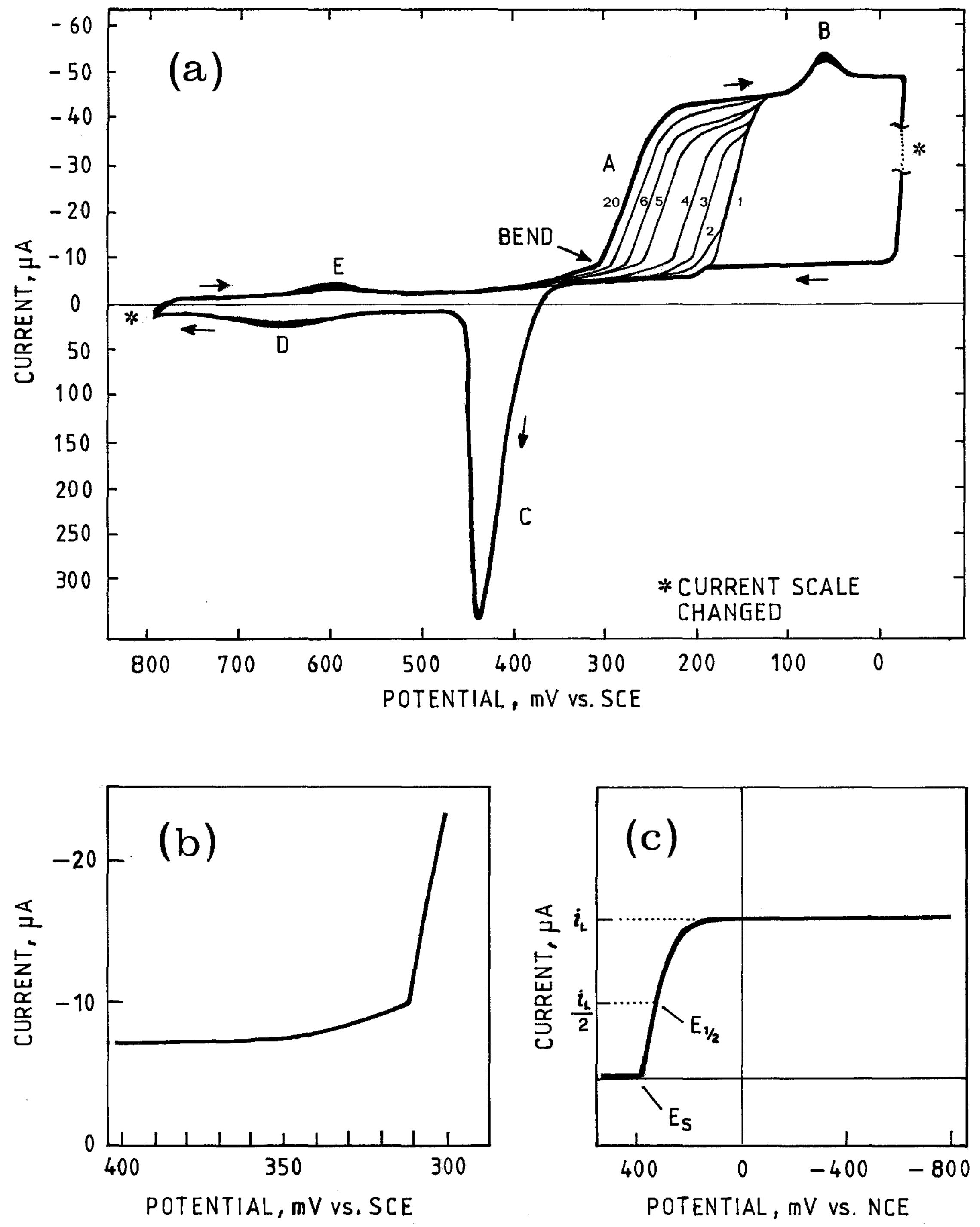

FIGURE 5.6 (a) Consecutive cyclic voltammograms for reduction and oxidation of mercury on an iridium substrate: 10^{-3}M Hg^{++}, 0.1M $HClO_4$, ν = 20mV/s, and ω = 1500rpm, (b) enlargement of the "bend" at the foot of wave-A, (c) reduction wave for Hg(I) or Hg(II) at the mercury drop electrode [From:128,pg.167]

$$E = E_o' + (RT/nF)\ln[Hg^{2+}]^2/[Hg_2^{2+}] \qquad (5.3)$$

$$E = E_o'' + (RT/nF)\ln[Hg_2^{2+}] \qquad (5.4)$$

At any potential, subtraction of Eq.(5.3) from Eq.(5.4) gives:

$$\ln([Hg_2^{2+}]/[Hg^{2+}]) = (E_o''-E_o')F/RT$$

The value of K is $\approx 1.3\times10^2$ at 25°C [126], so that at equilibrium, in a non-complexing medium such as $HClO_4$, the the concentration of Hg_2^{2+} will be about 120 times greater than that of Hg^{2+}. Thus, after the formation of this Hg^o, wave-A will proceed by a two step reduction:

$$Hg^{2+} + Hg^o \longleftrightarrow Hg_2^{2+} \qquad (5.5)$$

$$Hg_2^{2+} + 2e^- \longleftrightarrow 2Hg^o \qquad (5.6)$$

However, instead of two waves corresponding to each of the above reactions, we observe only one wave (Fig.5.6a), since the potentials of these reactions are not sufficiently separated in the acid medium used [127].

For solutions containing Hg(I), the reduction wave usually starts very abruptly, as shown in Figure 5.6c [see 128,Ch.10]. This is not the case for the iridium substrate, since Hg(I) must be formed at the surface by reaction (5.5). However, it is very likely that the bend observed in Figure 5.6a,b, is the equivalent to the point seen at E_s (Fig.5.6c) for the mercury drop electrode.

Shift of Reduction Wave-A. The Hg(II) initially deposited during the cathodic scan (at $E < 200$ mV), is mostly reoxidized during the anodic portion of the scan. However, the scan is probably neither sufficiently anodic nor slow enough to oxidize all of the Hg(0) so that some, in the form of a monolayer, still remains on the surface at the start of the next cathodic scan. On both platinum [45] and gold [129] this has been explained as being a result of intermetallic compound formation between mercury and substrate material. It will be shown later that iridium does not form soluble intermetallic compounds with mercury (there are no amalgam oxidation-peaks as there are for gold and platinum), but that a Hg(0) monolayer is formed between 600 and 400 mV. Apparently, this monolayer coverage is only partial at first, but increases with the number of scans, becoming almost complete, as evidenced by the $E_{1/2}$ potential, which approaches that for the reduction of Hg(I/II) on Hg(0) (410 mV).

The reduction wave can be made to return to its original position, either by applying a potential > 1000mV or by repeating pretreatment #5 (Table 5.1). Both of these treatments destroy the mercury monolayer formed between 600 and 400 mV.

Behavior of Peak-B. This peak at +70 mV is seen on the limiting current plateau during the cathodic scan and appears to grow slightly during the scanning. However, it was discovered that peak-B disappeared when we changed to a freshly prepared solution of $HClO_4$ + Hg^{++}, and that it increased with the use of the solution for cyclic voltammetry. Furthermore, changing to a different iridium substrate (an exact duplicate and pretreated the same as the first) the peak appeared unchanged, with the same height and shape.

In a further study, 200 µl additions of 10^{-1}M Hg^{++} were made, increasing the concentration from 10^{-3}M to $8x10^{-3}$M Hg^{++}. While the diffusion limited plateau at 250 mV increased from 60 µA to 270 µA, peak-B did not change noticeably. This led us to believe that this peak: *i*) was not directly dependent on the concentration of either the mercury (II) or acid, and *ii*) was a surface-limited phenomenon.

Point (*ii*) was further confirmed by running the same voltammogram without the RDE rotating. The reduction wave-A changed into a peak (Fig.5.7), with a shape corresponding to that for a diffusion controlled process. Peak-B maintained the same shape, indicating that it is a result of a surface-limited process.

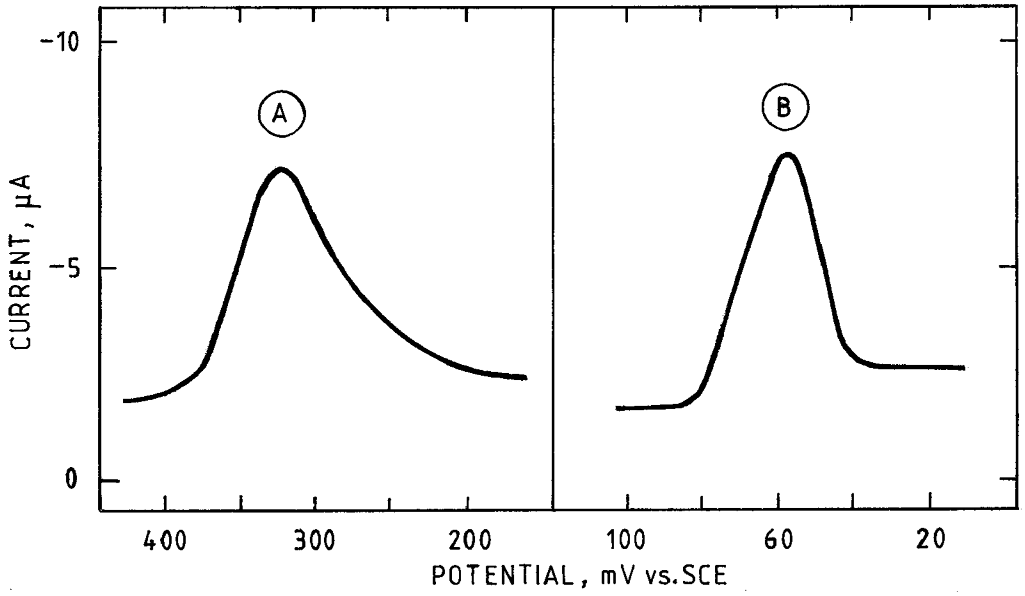

FIGURE 5.7 Linear scan voltammogram showing that peak-A and peak-B correspond to diffusion and surface-limited processes. (same conditions as Fig.5.6, except ω = 0 rpm)

<u>Interpretation of Peak-B</u>. It is well known that Hg(I) easily forms insoluble salts with anions, X, adsorbable on mercury electrodes. This was shown in partcular [128] for Cl^-, Br^-, I^-, OH^-. The formation of adsorbed Hg_2X_2, in d.c. polarography with the DME, results in the production of a so called <u>adsorption prewave</u> for the oxidation of mercury according to:

$$2Hg^{o} + 2X \xleftrightarrow{2e} Hg_2X_2 \qquad (5.7)$$

and <u>postwave</u> for the reduction according to:

$$Hg_2X_2 \longleftrightarrow Hg_2^{++} + 2X^- \xleftrightarrow{2e} 2Hg^{o} \qquad (5.8)$$

With the RDE, the latter is transformed into an adsorption peak (as is the case for peak-B) but a prewave must also be observed for the oxidation.

In our system there are only two possibilities for X, either OH^- or Cl^-. The OH^- is at a very low concentration (10^{-13}M), but the concentration of Hg(I) or Hg(II) may be as high as 10^{-1}M at the electrode surface. Using the solubility products for the Hg(I) and Hg(II) hydroxides, and the stability constants for $HgOH^+$, $Hg(OH)_2^0$, $HgOH_3^-$, $Hg_2(OH)^{3+}$ and $Hg_2(OH)_2^{++}$ indicates that formation of the solids is unlikely and that only $HgOH^+$ and $Hg_2(OH)^{3+}$ could possibly form at the surface. But these species are unlikely to be adsorbed. The most probable reason for the appearance of peak-B is the formation of Hg_2Cl_2 at the surface, the Cl^- being slowly released by diffusion through the fritted glass of the SCE. This would explain the slow increase of peak-B and its disappearance when changing the test solution. In such a case, the limiting current of the pre-oxidation wave is controlled by the diffusion of the Cl^- at the surface during reaction (5.7) [128]. The same SCE-bridge combination was placed in the cell with 25ml of 0.1M $HCLO_4$, and the concentration of Cl^- measured every hour using DPP with the DME. After 16 hours the concentration of Cl^- in the cell was found to be $\approx 3x10^{-5}M$, confirming the contamination.

Although peak-B resulted from unforeseen Cl^- contamination, the situation turned out to be useful for confirming that the reduction mechanism is linked to the reaction of Hg(II) with the monolayer of Hg(0), formed between 600 and 400 mV, to produce Hg(I).

Various initial potentials of between 1000 and 100 mV were applied to the electrode for 30 seconds, after which a single cyclic voltammogram was recorded. The value of 30 seconds was chosen, since the height of peak-B was found to be dependent on time for periods of less than 30 seconds. In Figure 5.8 we can see that peak-B does in fact <u>increase</u> as a function of the initial potential for $E < 600$ mV, as a result of reaction (5.7), and abruptly decreases at $E < 100$ mV, since at that potential Hg_2Cl_2 is directly reduced.

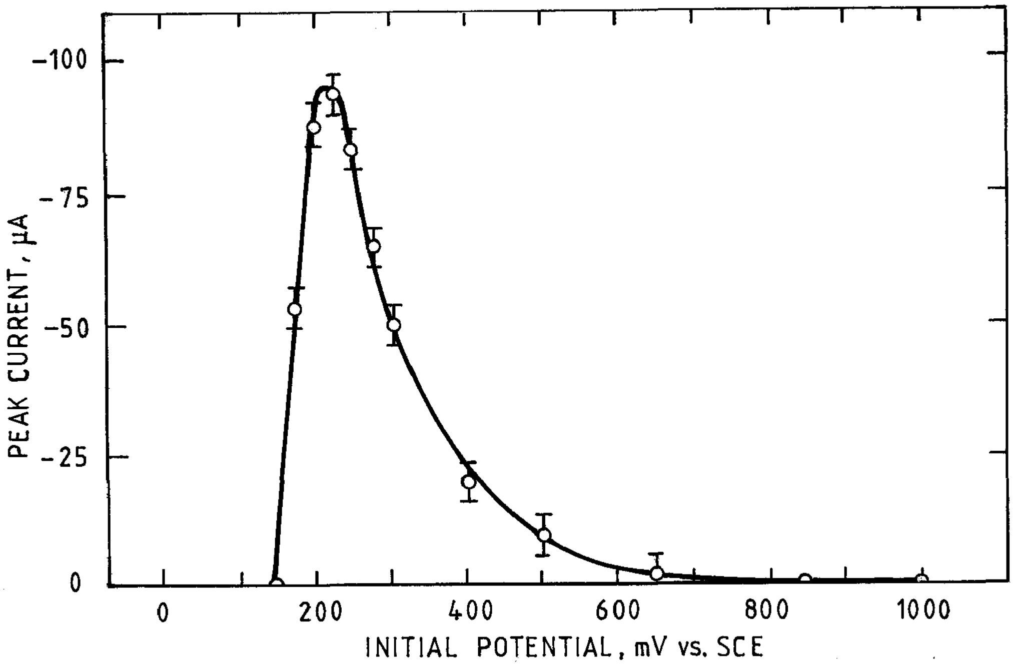

FIGURE 5.8 The dependence of peak-B height on the starting scan potential. (same conditions as Fig.5.6)

A final closer examination of peak-B, shows that the limiting current on the cathodic side of peak-B is larger than on the anodic side. This is consistant with the existence of an adsorbed Hg_2Cl_2 layer, since once it is reduced to Hg(O), this new mercury surface is available for further reduction of mercury (II).

Determination of $E_{1/2}$ for Hg(II) → Hg(O). In view of the above difficulties with the pre-reduction of Hg(II), and the adsorption of Hg_2Cl_2, a more accurate value for $E_{1/2}$ could be obtained by measuring the stripping current as a function of deposition potential. The iridium was given pretreatment #5 before each measurement, and conditions as indicated on Figure 5.9. From the reduction curve we obtain a half-wave potential, $E_{1/2}$, of 162 mV, slope = 30.9 mV and n = 1.88.

As a comparison, the mercury (II) reduction potentials for several other substrates, and their respective solubilities in mercury, are given in Table 5.2.

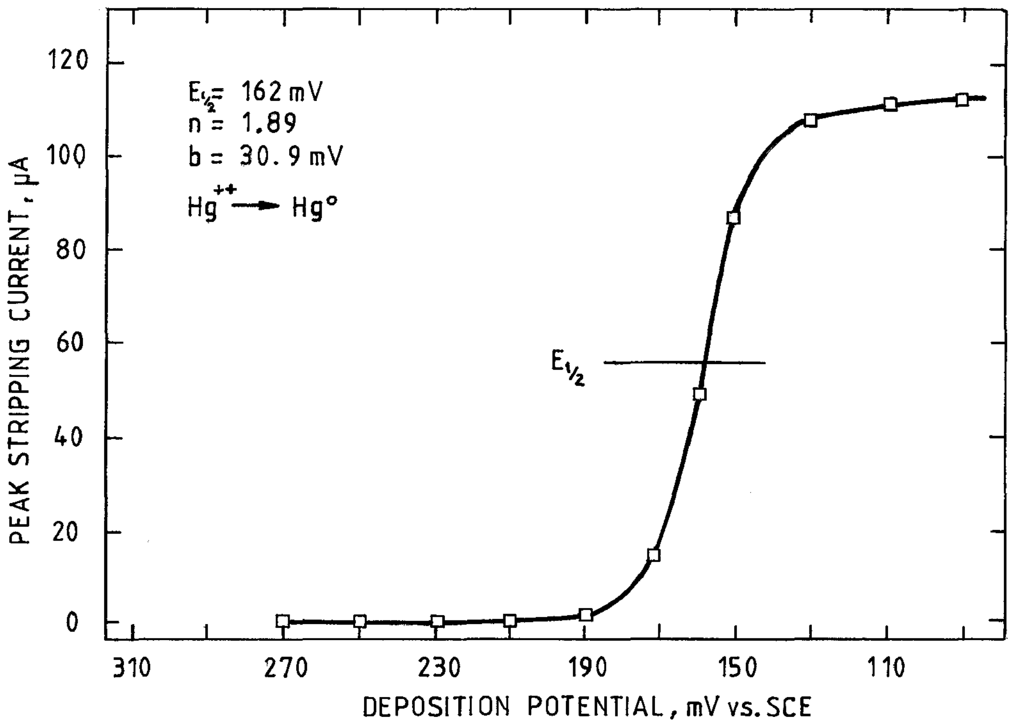

FIGURE 5.9 Current-potential curve for the reduction of mercury (II) on iridium. (10^{-4} Hg^{++}, 0.1M $HClO^{4}$, 10 second depositions, ω = 1500 rpm, each point is the average of three separate measurements).

TABLE 5.2 Comparison of the Half-wave Potential for the Reduction Wave of Mercury(II) on Various Electrode Substrates with Iridium

ELECTRODE MATERIAL	SOLUBILITY IN MERCURY, wt%	$E_{1/2}$ mV	REFERENCES
GC	0	60	[55]
Ir	10^{-5}	162	THIS WORK
Pt	0.09	220	[55]
Au	0.14	395	[55]
Hg	100	410	[55]

5.3.2 Oxidation of Mercury on Iridium

Of the two stripping peaks that appear in Figure 5.6a, peak-C (+430 mV) is easily explained in terms of the oxidation of Hg(O) to Hg(I), which in a non-complexing medium, occurs at about +420 mV (vs.SCE) [128]. The second, smaller oxidation peak-D at ≈ +650 mV is of special interest however. As previously mentioned, in the cases of platinum [45] and gold [129] this area is sometimes occupied by several larger peaks. In these metals the peaks are due to the oxidation of Au-Hg or Pt-Hg intermetallic compounds.

In order to identify peak-D, a second set of CV curves were made with the same conditions as in Fig.5.6a, except that the concentration of mercury was 10^{-4}M and a higher sensitivity was used. In addition, the potential was held at +100 mV for an increasing amount of time so as to deposit more mercury between each scan. The results are shown in Figure 5.10. Peak-D increases slightly at first with the increased mercury deposition but eventually reaches a limit, while peak-C continues to increase with time at 100 mV. One can also notice that there is a reduction peak (E), whose evolution is parallel to that of peak-D. We thus conclude that peak-D is due to the oxidation of a layer of mercury possesing different properties in relation to the iridium surface, since it is oxidized at an underpotential of stripping (UPS), and reduced at a corresponding underpotential of deposition (UPD) (peak-E). This result supports our assumption of attractive force bonding, as was shown by the mercury-iridium work function difference (Sec.4.1.2).

<u>Quantity of Mercury Corresponding to Peak-D</u>. For all square lattice metals, such as platinum, gold and paladium, it has been shown [45] that mercury is also deposited in a square lattice and that its atomic radius is equal to 1.57×10^{-8}cm.

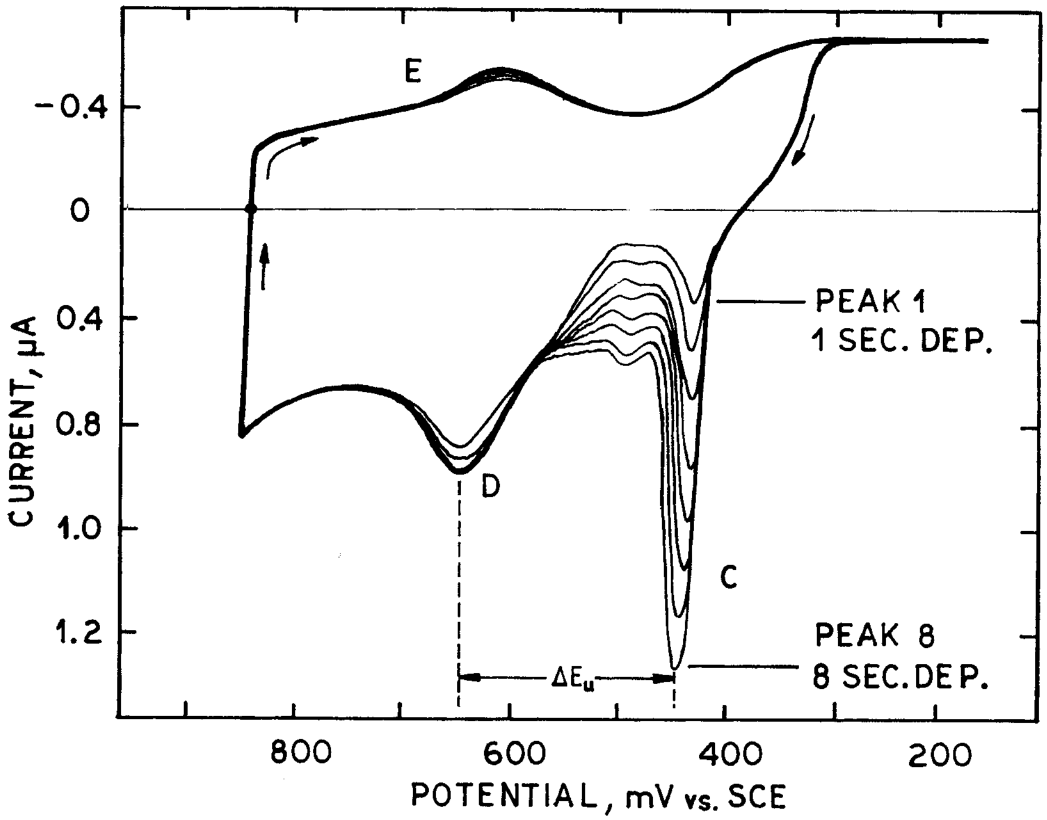

FIGURE 5.10 Consecutive cyclic voltammograms of the mercury oxidation peaks for the iridium substrate.

Therefore, since iridium is also a square lattice metal , it is assumed here that this value is correct for the radius of UPD of mercury on iridium. Thus, a monolayer of mercury contains $1.74x10^{-9}$g.at/cm^2. In this case, the charge necessary for stripping one monolayer of mercury from iridium should be 330μC/cm^2.

The area of peak-D, determined by the cutting and weighing method, was found to correspond to a total charge of $5.63x10^{-6}$C, or 179μC/cm^2. With the roughness factor, estimated to be ≈ 1.3 [45] for an iridium substrate polished to a mirror-finish with 1.0μm diamond paste, this charge corresponds to an estimated mercury surface coverage of 0.42. This value is very reasonable, since only a portion of the iridium surface would be available for UPD. This value can also be compared to that given by Lindstrom and Johnson [130] of 0.33, found for the cluster model of an UDP layer on gold, with mercury(I) and mercury(0) in the ratio of 1:2.

It is interesting to note that this result above, along with a similar value obtained for the monolayer reduction peak-E (0.38 coverage), indicates that remarkably, this partial monolayer of mercury on iridium behaves as if it were bulk mercury.

5.3.3 The Underpotential Shift

As long as no chemical interaction exists between the layer and substrate, which we assume true for iridium, Kolb et.al [113] have derived an expression predicting the monolayer-bulk underpotential shift, ΔE_u, from the work-function difference, $\Delta\Phi$, of the substrate and monolayer material:

$$\Delta E_u = \alpha\Delta\Phi \quad \text{with } \alpha = 0.5 \text{ V/eV} \tag{5.9}$$

The value for iridium has never been calculated or empirically determined. Using the work-function values for iridium and mercury, given by Trasatti [114], of 4.97 and 4.50 eV, respectively, the calculated value of $\Delta\Phi$(Ir-Hg) = <u>235 mV</u>. Using the peak potentials (Fig.5.10) of 430 mV and 640 mV for the bulk and monolayer stripping, the difference of which is indedendent of the mercury(II) concentration, we find ΔE_u = <u>207 mV</u>. Considering the uncertainties in the values of Φ, this value is in good agreement with theory. It has been shown [113] that the relationship between $\Delta\Phi$ and the half-width, b, of the monolayer peak can be described by a Temkin-type isotherm, and from their data (Fig.7 in [113]) we can predict that b should fall between 100 mV and 150 mV. Our result of b = 130 mV is also in agreement with this value.

A very interesting point can be made in terms of showing the type of interaction responsible for the mercury/iridium bond. Given below in Figure 5.11 is a plot of the theoretical

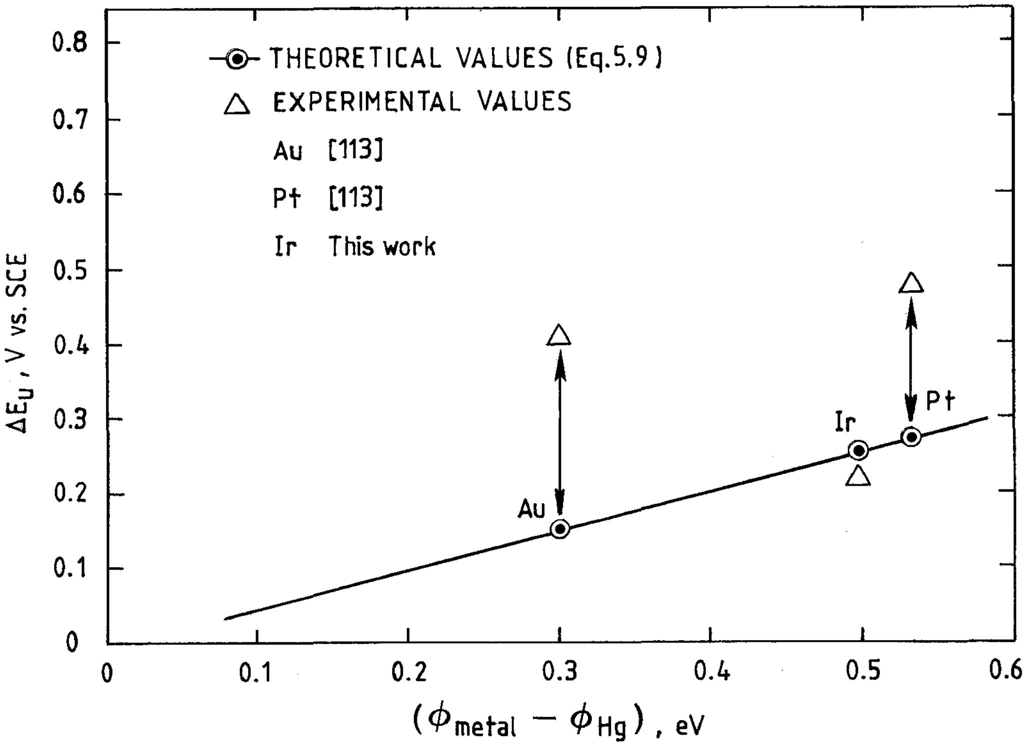

FIGURE 5.11 Underpotential shift ΔE_u as a function of the difference in work-functions $\Delta\Phi$ of substrate and mercury.

values of ΔE_u and $\Delta\Phi$ (according to Eq.(5.9)) for gold, platinum and iridium, and the experimentally determined values for gold and platinum from reference [113], and for iridium from this work. The results support the conclusion that iridium does not undergo any chemical reactions with mercury. Both platinum and gold form intermetallic compounds with mercury (gold especially more than platinum), thus their underpotential shift predicted from Eq.(5.9) includes a contribution from the chemical bonding, whereas iridium evidently undergoes no such reactions. This is a very important consideration, in terms of the analytical applications, for a mercury-film formed on an iridium substrate.

5.4 EFFECTS OF VARIOUS DEPOSITION CONDITIONS

A very large number of variables may affect the formation of a mercury film on the iridium surface. Among these we have, for example, electrolyte composition, temperature, stirring rate, degassing, as well as potential, current, and deposition time, to mention but a few. Due to the unfeasibility of rigorously studying all of them, only electrolyte composition and deposition potential were investigated, since these two are known to have a pronounced effect on mercury film formation and structure.

5.4.1 Electrolyte

The effect of the electrolytes was studied in two main areas. We first looked at the usable potential range of the iridium, in terms of the oxidation and reduction of water, with different acid and neutral electrolytes. We then looked at several types of electrolyte compositions such as neutral, basic, acid, and complexing, in terms of the formation of a mercury film.

<u>Usable Potential Range of Iridium</u>. The potential range of the iridium substrate was tested mainly to define the cathodic limit for the quantitative deposition of mercury, and to gain some knowledge as to the anodic limit for possible future use.

Potential limits for redox waves of water are difficult to define precisely, since no limiting currents or peaks are normally obtained. For this research, the potential limits were arbitrarily defined as the point where the oxidation or reduction yielded a current in excess of 1 µA.

Two points should be mentioned in connection with the redox limits of water:

1) The most readily reduced or oxidized species present must be H^+ and H_2O. Care must be taken that no electrolyte component, or the surface of the substrate, be reduced or oxidized. Both of these points were taken into account in this study.

2) Theoretical curves exist for the redox of water [115] independent of the electrode material. These curves do not, however, indicate the actual potential for the material. An overpotential exists for many materials and may vary with the electrolyte composition.

The curves in Figure 5.12 show the experimental limits for the iridium substrate in several different electrolytes. The curves were taken with the following conditions: a potential scan of 4 mV/s, the RDE rotating at 1000 rpm, and the reference electrode was a SCE with a $NaNO_3$ bridge for the perchlorate containing solutions. The theoretical [115] cathodic and anodic

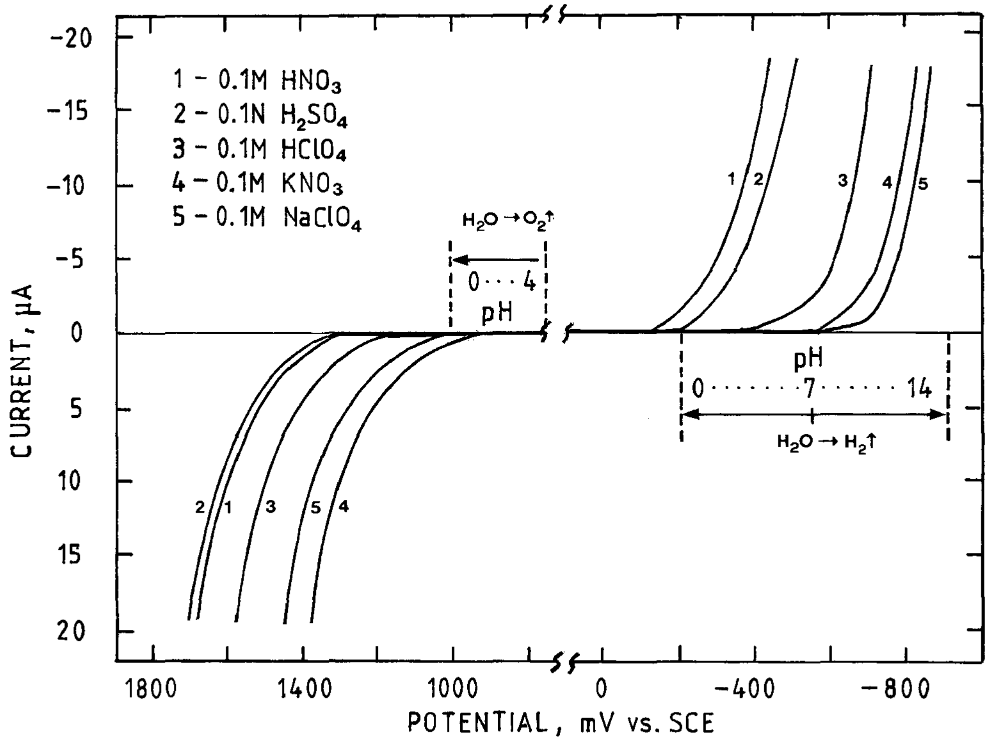

FIGURE 5.12 The anodic and cathodic potential limits for the iridium substrate in various electrolytes. Scan rate 4 mV/s.

values, as a function of pH, are shown above and below the respective curves.

As can be seen, the actual anodic limits exceed the theoretical values but the cathodic limits are generally within them. As expected, the acids have a more anodic limit while the neutral salts have more cathodic limits. The limits exhibited by all the electrolytes tested on iridium do not present any major problems, and any of them would fulfill our requirements on the basis of the potential range for mercury(II) reduction.

Electrolyte Effects on Mercury-film Formation. The five electrolytes tested and the results for the formation of a mercury film are summarized in Table 5.2 and described below.

For both KNO_3 and HNO_3 the deposition of mercury(II), with the RDE (ω = 1000 rpm) in the potential range -200 mV to -1500 mV for 10 minutes, always gave deposits composed of small droplets uniformly distributed over the surface. With longer deposition times (60-90 minutes), the droplets coalesced to form domed patches and eventually a single large semi-sphere covering the entire surface (but never a true film).

For the solutions containing EDTA, en, and NTA, the deposition of mercury occurred very slowly. After 90 minutes the entire surface was covered with a thin deposit of mercury, which however was neither uniform nor smooth and consisted of flat patches. Prolonged deposition for up to 5 hours caused degradation of the surface and a solid black film to form over the surface.

The $HClO_4$ was the only electrolyte with which a true mercury film could be formed, even if only 50% of the time. The reason a true film can form with $HClO_4$ may have something to do with the fact that it is known to be a non-adsorbing and non-complexing anion.

TABLE 5.3 Effect of electrolytes on the formation of a mercury film. (Hg^{++} = 0.001M, ω = 1000 rpm)

ELECTROLYTE	DEPOSITION TIME	POTENTIALS mV vs. SCE	RESULT *
0.1M KNO_3	10 min. 90 min.	-1000 -1000	droplets 2400/mm^2 semi-spheres 80/mm^2
0.1M KNO_3 + EDTA 0.05M	90 min. 5 hours	-200/-1500 -1000	flat patches blackish film
0.1M KNO_3 + 0.0001M NTA	90 min.	-1500	100µ domed patches 10/mm^2
0.1M KNO_3 + 0.05M en	30 min	-1600	50µ domes 8/mm^2
0.1M HNO_3	10-90 min.	-200/-1500	droplets only 200-2500/mm^2
0.1M $HClO_4$	10-30 min.	-200/-400	Hg film 50% of the time, rest droplets
0.5M NH_4OH 0.05M EDTA	30 min. - 5 hours	-200/-1500	flat patches - with black crust

* : See Fig.4.4 for definition of form terminology.
en : ethylenediamine
NTA : nitrilotriacetic acid
EDTA : ethylenediaminetetraacetic acid

5.4.2 Pulsating Deposition Potential

During the preceding studies, the use of d.c. deposition potentials from -100 mV up to -1600 mV, in a variety of electrolytes, led us to the conclusion that there was no distinct advantage in the use of any one specific reduction potential over another. The sole difference noted was that for a potential range from -100 to -400 mV, an increase in the potential sometimes caused an increase in the rate of mercury deposition.

In order to improve the uniformity of the mercury film on iridium, we investigated the use of pulsating or square-wave deposition potentials. This type of technique is currently used in metallurgy to give smooth solid depositions [131], but to our knowledge has never been applied to deposition of mercury.

Effect of pulsating potential on depositions. A computer model [131] of a diffusion layer generated under the action of a d.c. potential is shown in Figure 5.13a. Due to the thinner diffusion layer, the flux of mercury(II) ions is greater on any raised surface feature, such as deformations or mercury nuclei, resulting in faster deposition of mercury at these points. At the same time the increase in flux causes an increase in current, which in turn alters the potential field, creating an electrically "shielded" region around what is now a growing mercury droplet. This type of effect is thus responsible for an "amplification" of surface roughness.

It has been shown [131] that a pulsating potential will give a much thinner diffusion layer, whose thickness depends on the frequency, and is constant over the entire surface. With higher frequencies the diffusion layer can be thin enough to follow the micro-profile to such an extent, that no surface deformation is amplified. Figure 5.13b shows the concentration profile obtained with a pulsating potential.

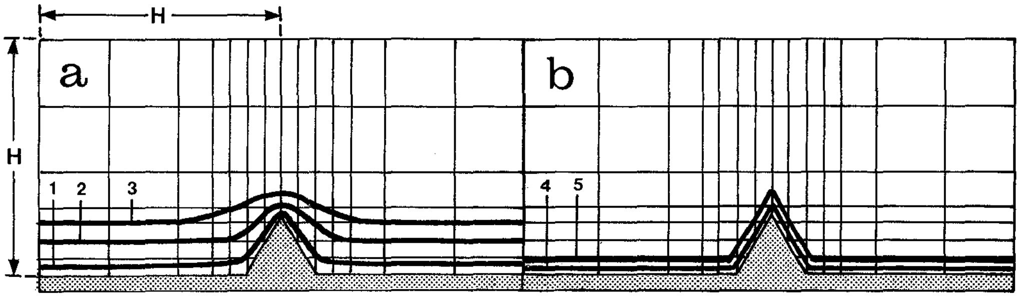

FIGURE 5.13 (a) Computer calculation of the iso-concentration lines for which *C*(t) = 0.5*C*(t=0), made by application of the method of finite differences to solve Fick's second law for a model diffusion field (Hx2H)cm in which there is a triangular protrusion. Lines 1-3 are for periods of $0.1H^2/D$, $5H^2/D$, and $10H^2/D$ seconds respectively. (b) Iso-concentration lines for the same system, but with the applied potential pulsating at a frequency of $100(D/H^2)$ Hz. Line 4 pertains to the time interval of $0.1H^2/D$ sec. and line 5 to times > $5H^2/D$ sec.

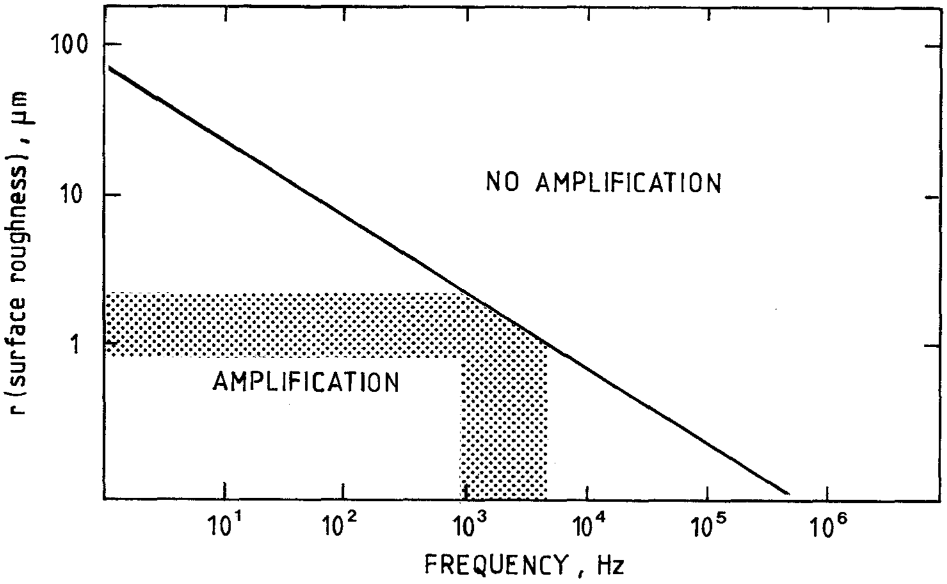

FIGURE 5.14 Surface deformity amplification as a function of the surface roughness curvature radius, *r*.

The diffusion layer becomes constant when its thickness reaches the same order of magnitude as the radius of curvature of the protruding and receding surface features. For a frequency of ν Hz, the diffusion layer thickness is given by [131]:

$$\delta = (D\pi/0.367\nu)^{1/2} \tag{5.10}$$

where D is the diffusion coefficient (cm^2/sec). Thus, one can define a minimum, above which there is no amplification of the surface features (Figure 5.14). Since most of the surface will bear the markings of the final diamond polishings (3 and 1μm), and the initial mercury nuclei will be < 1 μ (see Eq.2.10), we should be able to obtain a minimum of surface feature amplification using frequencies greater than 1000 Hz.

<u>Conditions</u>. A square-wave potential was applied using a GSTP Signal Generator (Tacussel, Lyon, France). The solutions containing 0.1M $HClO_4$ + 0.01M Hg^{++}, were purged with N_2 for 30 min., and deposition was made for 5 minutes with the RDE at ω = 1500 rpm. The square-wave potential used had an amplitude of 700 mV and an anodic base of +410 mV. This latter limit was chosen so as to cause a slight oxidation of the mercury (see Fig.5.6a), thus destroying part of the diffusion layer. The amplitude was chosen to provide a sufficiently cathodic pulse to re-nucleate any available surface sites.

<u>Results</u>. The results for the application of different frequencies are shown in Figure 5.15. A definite change in the deposition was noticed starting at about 50 Hz. As expected, the mercury became more and more spread out in the form of flat patches, and the first signs of a film were evident at about 500 Hz. A true film was deposited at 2000 Hz. No change was noticed again until approx. 10000 Hz, at which point the surface was still covered by a film, but seemed to be thinner and had more deformities. This condition remained unchanged up

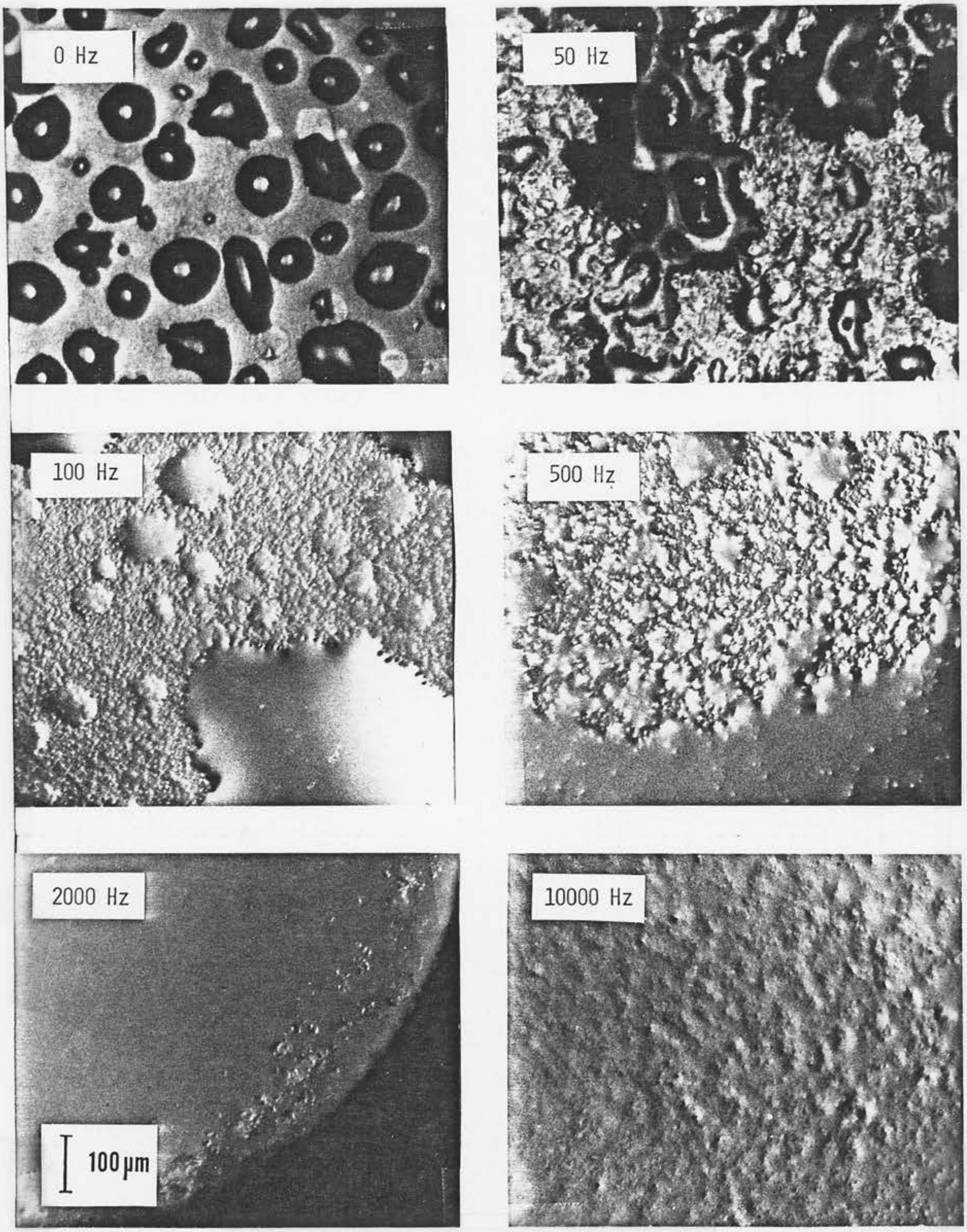

FIGURE 5.15 Photomicrographs of the iridium surface coverage by mercury, deposited at the indicated frequency and conditions described in text.

to the last value of 20000 Hz that we tested, where the film reverted back to the same condition as at 500 Hz. We attribute this behavior to the possibility that for frequencies above 5000 Hz, the electrical components which make up the cell may not be capable of responding to such high frequencies and thus the actual applied potential at the surface of the iridium may be decreased and distorted.

5.5 DEPOSITION PROCEDURE FOR A MERCURY-FILM ON IRIDIUM

Unlike mercury films on platinum and gold, which are formed by an amalgamation process, the mercury film on iridium depends on weaker forces to maintain it in place. For this reason, the preparation and use of the iridium mercury-film electrode (Ir-MFE) requires a bit more time and care. This is nowhere near being a problem, however, when the end result is a mercury-film electrode, which is just that, and not a Pt-Hg alloy-film electrode. Furthermore, with the computer controlled system, the flow and exchange of solutions, the application of potentials and the experimental sequence in general, are easy to control, requiring a minumum of operator effort.

Keeping in mind the results and conclusions arrived at in Sections 5.2 and 5.4, we give here a basic procedure which has, 8 out of 10 times, resulted in a stable long-term mercury film.

It should be noted at this point, that in our experience with mercury-films, we surmise that a true flat film probably cannot exist at thicknesses of more than 1µm. A film of about 20µm may look very flat to the naked eye, but when viewed under a polarizing microscope, it becomes evident that the surface is slightly convex. This seems reasonable, since rough calculations show that for a 1µm mercury-film, we already have ≈ 4000 layers of mercury atoms. Considering the high surface tension of mercury, it seems unlikely, that 4000 layers of mercury atoms could be kept from pulling together into a configuration of least surface tension, i.e., a semi-sphere.

In preparing the mercury film then, we must be aware that at some thickness, it will cross over from a true flat film, to a semi-spherical film. This situation is further discussed in Sec.6.1.4.

The procedure and results given below are for a thin flat mercury film ($< 10\mu m$), since it is more difficult to prepare than a thicker, semi-spherical film ($> 20\mu m$). The latter can be prepared using the same procedure, but once it is formed it will tend to act more like a mercury drop.

The procedure consists of three basic parts: (1) pretreatment of the iridium substrate surface, (2) deposition of the mercury, (3) medium exchange and electrode storage.

Pretreatment. Most of the work for the research described here was done with iridium substrates, which had been subjected to pretreatment #5 (see Table 5.1). However, we later made some changes (included below) which appear to improve the film formation. (NOTE: When the term electrode is used, it refers to the active area of the iridium substrate (see Fig.4.3), but when the abbreviation RDE is used, it refers to the entire electro-mechanical assembly, with the iridium substrate mounted into the Teflon tip, and the tip attached to the RDE body.)

The electrode pretreatment procedure, which is carried out each time a film is to be made, is as follows:

- polish the surface for one minute with the $1\mu m$ diamond spray, with the RDE rotating at about 1000 rpm,
- rinse with the special "blue diamond solvent", followed by acetone and deionized water,
- place in concentrated HNO_3, for five minutes, while rotating at ≈1000 rpm (we later started using chromic acid in place of nitric acid, because it appears to clean the

surface better, especially in terms of organics),

- rinse with deionized water and place quickly and directly into a de-oxygenated deposition electrolyte, containing only 0.1M $HClO_4$, and <u>no</u> mercury,
- apply -2.0 volts (vs.SCE) for 5 minutes, with the RDE rotating at 3000 rpm or more (this is useful in keeping the surface as free as possible of bubbles) while simultaneously applying a stream of N_2 gas bubbles in such a way as to "scrub" the evolving H_2 bubbles off the active electrode surface,
- after the cathodization is finished, the potental should be maintained at 0.0 volts (vs.SCE) until the deposition step.

<u>Deposition of Mercury</u>. The deposition steps should be carried out as soon as possible after the pretreatment. One should then proceed as follows:

- disconnect the electrode circuit, and either make an addition, or exchange the solution, to give a mercury concentration of 0.01M (still in 0.1M $HClO_4$). The exchanged solution should be de-oxygenated prior to coming in contact with the electrode.
- with the RDE rotating at 1500rpm, apply a 2000 Hz square-wave potential with a 50 mV baseline and an amplitude of ± 350 mV (see Sec.5.3.2). The deposition time should be selected for the film thickness desired (e.g., 30 minutes will give a 10µm film). (NOTE: calibration studies indicated that the effective d.c. current recorded during a deposition was always in agreement with the charge used for the deposition, and can thus be used to calculate the film thickness).
- once the deposition is finished, the electrode circuit is opened, and as quickly as possible, the deposition solution is replaced (using flow-through) by a pre-deoxygenated

0.1M $HClO_4$ solution, and a d.c.potential of 0.0 volts (vs.SCE) is applied.

- at this point, if a mercury film exists, one may use the medium exchange method and proceed with the sample analysis, bearing in mind to always maintain 0.0 V (vs.SCE) on the electrode at all times. If a partial or no film exists, the potential is increased gradually to about -900 mV, while observing the electrode surface through the microscope. The semi-film can be made to spread out, and by "playing" with the potential between -100 to -900mV, the film can usually be made to take form within 10 or 20 minutes. If a film is not formed at this point, the entire procedure should be reapeated starting with the pretreatment.

Electrode Storage. Mercury films made during this research have been kept for as long as two weeks without showing any signs of deterioration, by keeping them in a solution of 0.1M $HClO_4$ with an applied potential of about -50 mV (vs.SCE) and under a slow N_2 gas bubbling (about six bubbles/min.). If the electrode circuit is left open for more than 10 hours, a surface oxide starts to form. This oxide is usually only visible by microscopic observation. Electrodes have been left in air for several days without showing visual deterioration of the film, but once placed back in solution the film invariably reverts to droplet form and cannot be made to re-form a film again under any condition.

6. APPLICATIONS OF THE IRIDIUM MERCURY FILM ELECTRODE

In the previous chapter we have shown that the preparation of an iridium mercury-film electrode (Ir-MFE) is possible and that it is sufficiently stable to be used under normal experimental conditions.

The primary objective of the work described in this part was to provide quantitative evaluation of the Ir-MFE, while showing its possible applications. These studies were made keeping in mind the eventual application of the electrode for, *i*) the quantitative analysis of trace metals using ASV, and *ii*) their speciation using anodic stripping techniques, and in particular, stripping polarography.

The first part of this chapter is concerned with the characterization of the Ir-MFE in terms of the experimental ASV current-potential parameters. A comparison is then made with the theoretical predictions of De Vries and Van Dalen [64] (see Sec.2.3), for mercury-film electrodes. With the results from our work and from the literature, we will show that the above MFE theory does not, and cannot, apply to real MFE's with thicknesses greater than about 1µm.

The second part deals with the application of the Ir-MFE for: *i*) quantitative analysis of trace metals, and *ii*) testing the validity of Eq.(2.26) in describing the behavior of stripping polarograms with MFE's (Sec.2.4).

The metals selected were cadmium(II) and lead(II), whose behavior in aqueous solutions and with MFE's has been previously investigated [1,132,133], and zinc(II), the study of which is known to be difficult with mercury films formed on platinum and gold substrates [36].

6.1 EVALUATION OF THE MERCURY-FILM ELECTRODE THEORY

There are several parameters which play a significant role in the analytical use of a mercury-film electrode. These include the physical parameters of the mercury-film, such as film thickness or concentration of the reduced metal in the film, and the ASV parameters, such as scan rate, deposition time, peak stripping current, and deposition potential.

6.1.1 Film Thickness

In an ASV experiment, the thickness of the mercury film (ℓ) can have a direct effect on three experimental parameters (see Fig.2.7), the peak current (i_p), peak potential (E_p), and half-width ($b_{1/2}$), of the stripping peak.

The experiments to test these effects were carried out using mercury films of several thicknesses (0.1 to 52μm) prepared according to the procedure in Sec.5.5, and using as test ions, lead(II), cadmium(II), and zinc(II). The electrolyte used in all cases was 0.1M KNO_3. All potentials are in reference to a SCE with a $NaNO_3$-bridge. The peak potential is given as the difference of E_p-$E_{1/2}$, where the values of $E_{1/2}$ used for cadmium(II), lead(II), and zinc(II) are -580mV, -382mV, and -1000mV, respectively.

The results are detailed below in Tables 6.1, 6.2, 6.3, and Figure 6.1a,b,c. They will be discussed and compared with theory in Sec.6.1.4.

TABLE 6.1 The effect of mercury film thickness on the peak current (i_p), peak potential (E_p), and half-width ($b_{1/2}$), of ASV peaks with several metal ions (0.1M KNO_3, ω = 2000 rpm).

SCAN RATE = 20 mV/s

Mercury Film Thickness (µm)*	CONDITIONS			PEAK PARAMETERS ***		
	Test Ion	Conc. (M)	t (sec)	$b_{1/2}$ (mV)	E_p-$E_{1/2}$ (mV)**	i_p (µA)
0.1	Cd^{++}	10^{-7}	600	36	-92	2.2
0.5	Cd^{++}	10^{-7}	600	46	-61	1.0
2.0	Cd^{++}	10^{-6}	200	42	-20	5.4
6.5	Pb^{++}	10^{-6}	120	43	-21	0.85
8.0	Pb^{++}	10^{-6}	120	44	-18	0.95
12.0	Cd^{++}	10^{-6}	200	44	-17	2.3
14.0	Pb^{++}	10^{-6}	120	48	-2	1.8
24.0	Pb^{++}	10^{-6}	120	49	0	1.7
26.0	Cd^{++}	10^{-6}	100	50	18	1.7
32.0	Zn^{++}	10^{-5}	100	75	5	1.6
48.0	Zn^{++}	10^{-5}	100	93	40	0.7
52.0	Cd^{++}	10^{-6}	100	90	37	1.7

* film thickness is ± 1%

** $E_{1/2}$ = -580mV (Cd^{++}); -382mV (Pb^{++}); -1000mV (Zn^{++})

*** potentials are ± 2mV (vs.SCE)

TABLE 6.2 The effect of mercury film thickness on the peak current (i_p), peak potential (E_p), and half-width ($b_{1/2}$), of ASV peaks with several metal ions (0.1M KNO_3, ω = 2000 rpm).

<u>SCAN RATE = 40 mV/s</u>

Mercury Film Thickness (μm)*	CONDITIONS			PEAK PARAMETERS ***		
	Test Ion	Conc. (M)	t (sec)	$b_{1/2}$ (mV)	$E_p - E_{1/2}$ (mV)**	i_p (μA)
0.1	Cd^{++}	10^{-7}	600	43	-72	3.9
0.5	Cd^{++}	10^{-7}	600	56	-36	1.9
2.0	Cd^{++}	10^{-6}	200	45	-5	10.0
6.5	Pb^{++}	10^{-6}	120	57	-1	1.5
8.0	Pb^{++}	10^{-6}	120	56	2	1.5
12.0	Cd^{++}	10^{-6}	200	58	6	2.2
14.0	Pb^{++}	10^{-6}	120	61	24	2.7
24.0	Pb^{++}	10^{-6}	120	63	20	2.7
26.0	Cd^{++}	10^{-6}	100	68	38	3.2
32.0	Zn^{++}	10^{-5}	100	87	40	3.2
48.0	Zn^{++}	10^{-5}	100	104	59	2.5
52.0	Cd^{++}	10^{-6}	100	104	60	2.6

* film thickness is ± 1%

** $E_{1/2}$ = -580mV (Cd^{++}); -382mV (Pb^{++}); -1000mV (Zn^{++})

*** potentials are ± 2mV (vs.SCE)

TABLE 6.3 The effect of mercury film thickness on the peak current (i_p), peak potential (E_p), and half-width ($b_{1/2}$), of ASV peaks with several metal ions (0.1M KNO_3, ω = 2000 rpm).

SCAN RATE = 100 mV/s

Mercury Film Thickness (µm)*	CONDITIONS			PEAK PARAMETERS ***		
	Test Ion	Conc. (M)	t (sec)	$b_{1/2}$ (mV)	$E_p-E_{1/2}$ (mV)**	i_p (µA)
0.1	Cd^{++}	10^{-7}	600	64	-52	5.3
0.5	Cd^{++}	10^{-7}	600	78	9	3.4
2.0	Cd^{++}	10^{-6}	200	55	35	21.2
6.5	Pb^{++}	10^{-6}	120	83	42	1.85
8.0	Pb^{++}	10^{-6}	120	92	50	2.15
12.0	Cd^{++}	10^{-6}	200	100	55	4.25
14.0	Pb^{++}	10^{-6}	120	96	77	4.2
24.0	Pb^{++}	10^{-6}	120	104	60	3.7
26.0	Cd^{++}	10^{-6}	100	105	72	4.3
32.0	Zn^{++}	10^{-5}	100	108	63	4.9
48.0	Zn^{++}	10^{-5}	100	112	80	4.8
52.0	Cd^{++}	10^{-6}	100	110	78	5.2

* film thickness is ± 1%

** $E_{1/2}$ = -580mV (Cd^{++}); -382mV (Pb^{++}); -1000mV (Zn^{++})

*** potentials are ± 2mV (vs.SCE)

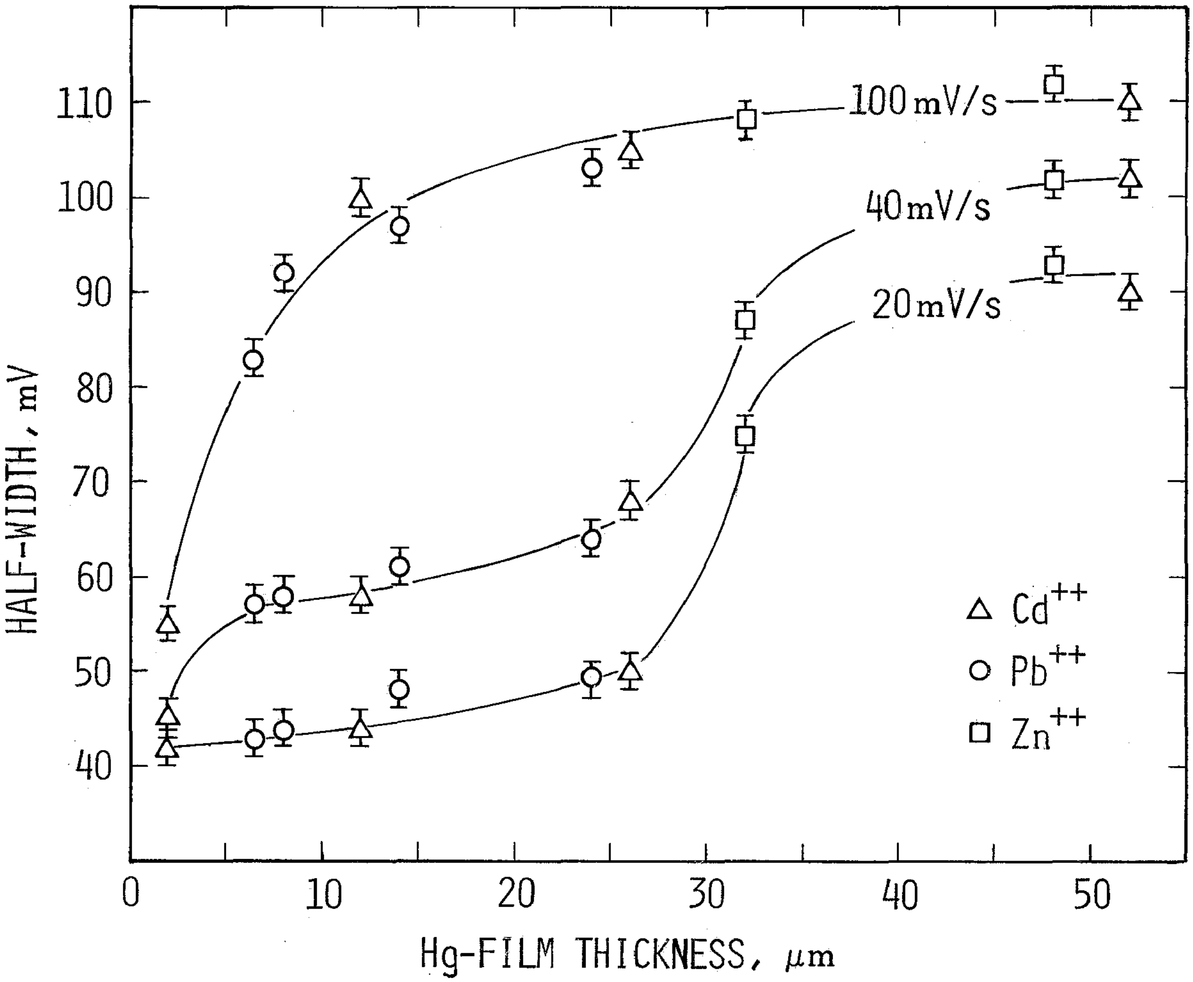

FIGURE 6.1a Effect of mercury film thickness on the stripping peak half-width for different scan rates and with different test ions. Most points are an average of at least three consecutive repetitions. Conditions are indicated in Tables 6.1-6.3.

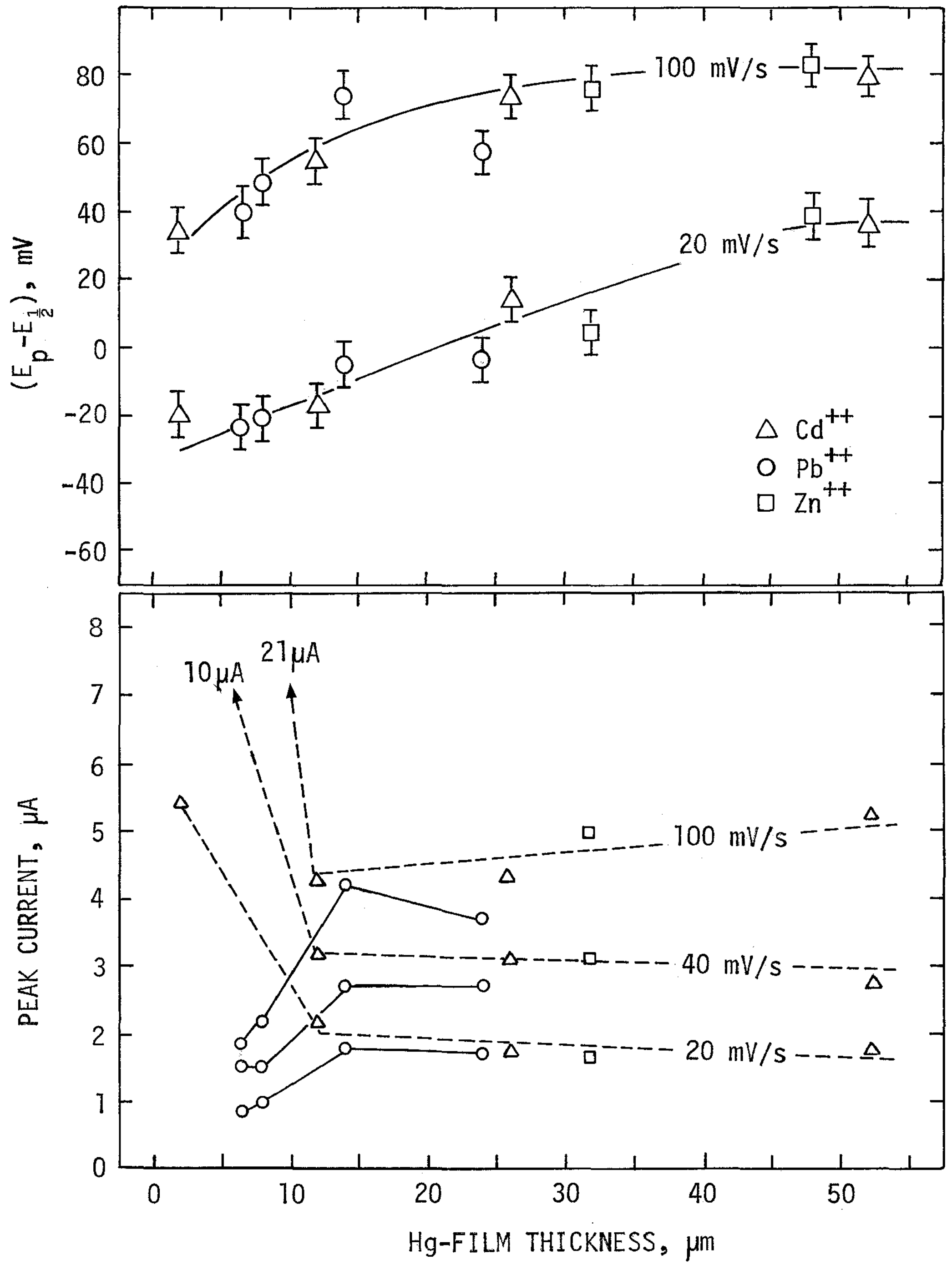

FIGURE 6.1b,1c Effect of mercury film thickness on stripping peak potential and peak current for different scan rates and with different test ions. For comparative purposes the peak potential (E_p) is plotted as the difference with the polarographic half-wave potential ($E_{1/2}$) for the respective ion in the same solution. Conditions given in Tables 6.1-6.3. ($E_{1/2}$ for Cd^{++} = -580 mV, Pb^{++} = -382 mV, Zn^{++} = -1000 mV)

6.1.2. Deposition Time

One of the more important conditions in an ASV analysis is that the peak current should be directly proportional to the concentration of reduced metal in the mercury film. This was tested by measuring the peak current as a function of deposition time using:

i) $4x10^{-6}$M cadmium(II), with a deposition potential of -900 mV vs.SCE, and a mercury film of 1µm, and

ii) $2x10^{-6}$M zinc(II), with a deposition potential of -1300 mV vs.SCE, and a mercury film of 32µm.

In both cases the electrolyte was 0.1M KNO_3, ω = 2000rpm, with the scan rate = 40 mV/s. The results are shown in Figures 6.2 and 6.3.

The linear plots with an intercept at 0,0 confirm the theoretical dependence of peak current on the concentration of the reduced metal in the film, and also confirm that the saturation point for neither cadmium nor zinc is attained under these conditions (see Appendix H).

6.1.3 Scan Rate

For bulk mercury electrodes, such as the HMDE, the peak stripping current is proportional to the square-root of the scan rate, $v^{1/2}$. For mercury film electrodes the theory of De Vries and Van Dalen [64,65] predicts that i_p is a function of v^{α}, where α is nearly 0.5 for a thickness of $\ell \geq$ 100µm and approaches a limiting value of 1 at $\ell \leq$ 10µm (Fig.2.7).

Figure 6.4 shows a log-log plot of the peak current as a function of scan rate, taken from the data in Tables 6.1-6.3, using test ions of lead(II), zinc(II), and cadmium(II),and for several mercury-film thicknesses.

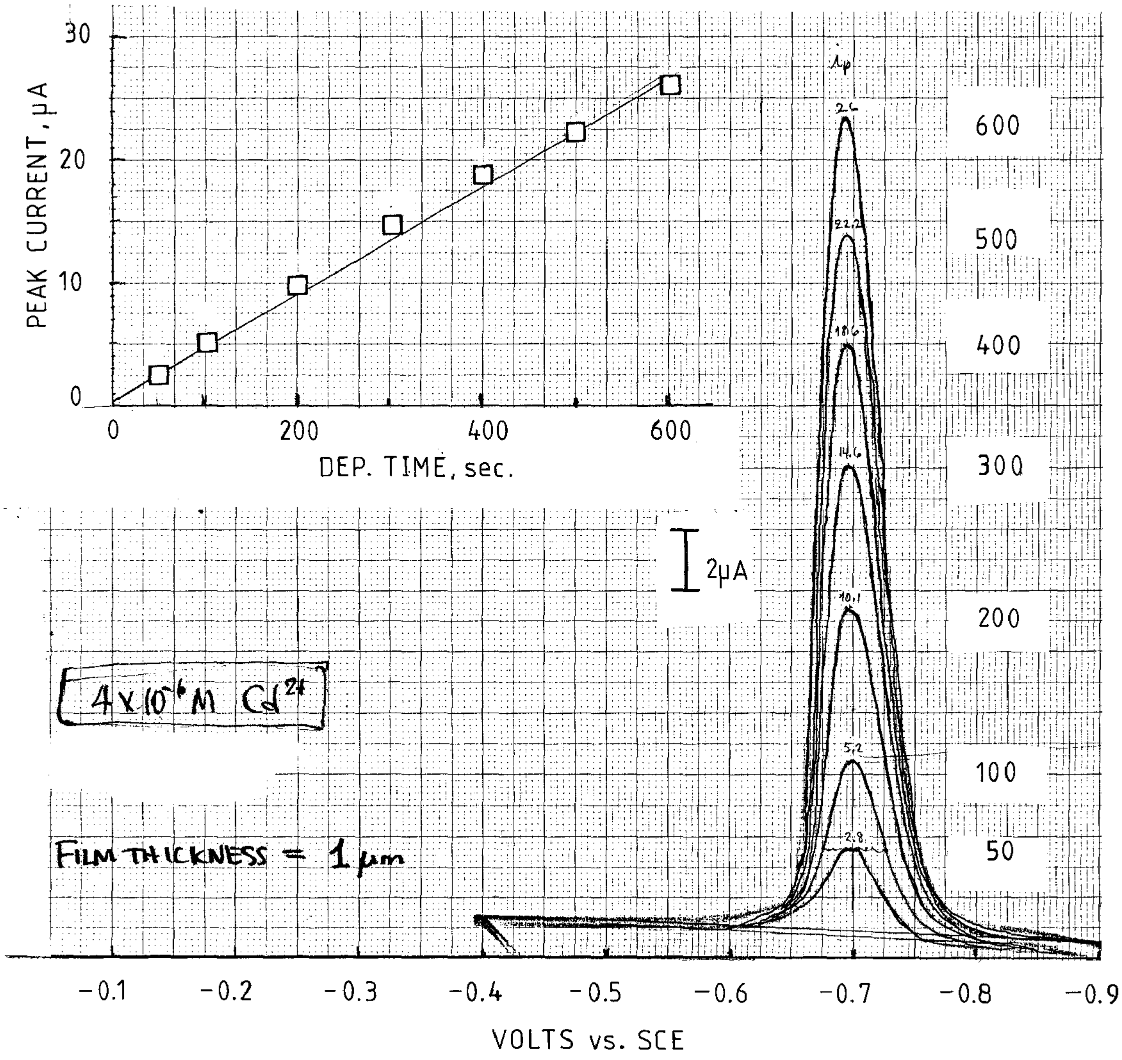

FIGURE 6.2 Effect of deposition time on the anodic peak stripping currents (conditions in text)

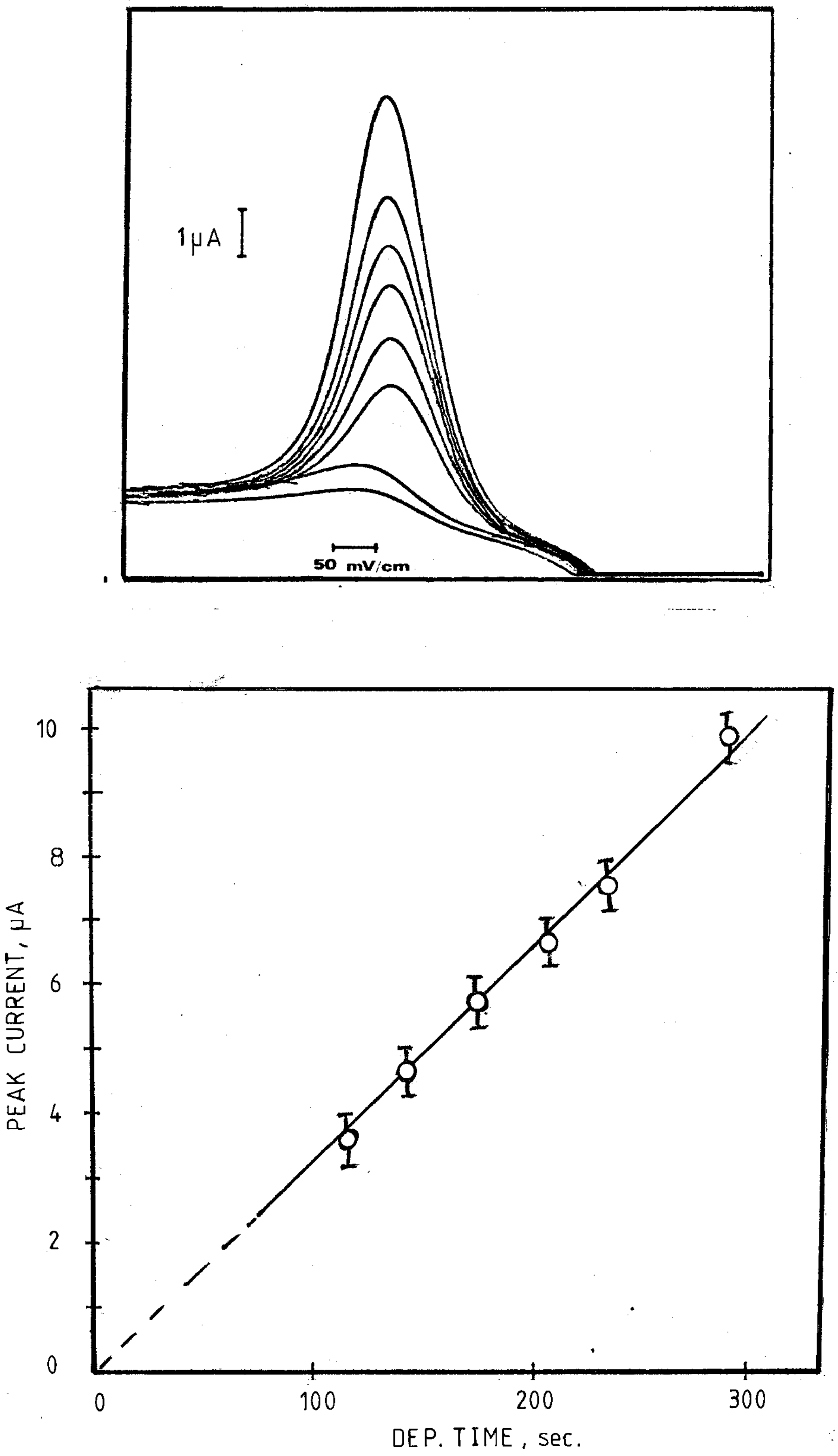

FIGURE 6.3 Effect of deposition time on peak current, with a 32µm mercury film, 2×10^{-6}M Zn^{++}, and 40mV/s scan rate [134].

FILM THICKNESS µm	PEAK CURRENT , µA		
	10mV/s	20mV/s	40mV/s
2	2.63 ± 0.04	5.39 ± 0.04	10.2 ± 0.05
8	0.43± 0.02	0.92± 0.02	1.91 ± 0.04
52	0.79± 0.02	1.62± 0.04	3.20±0.04

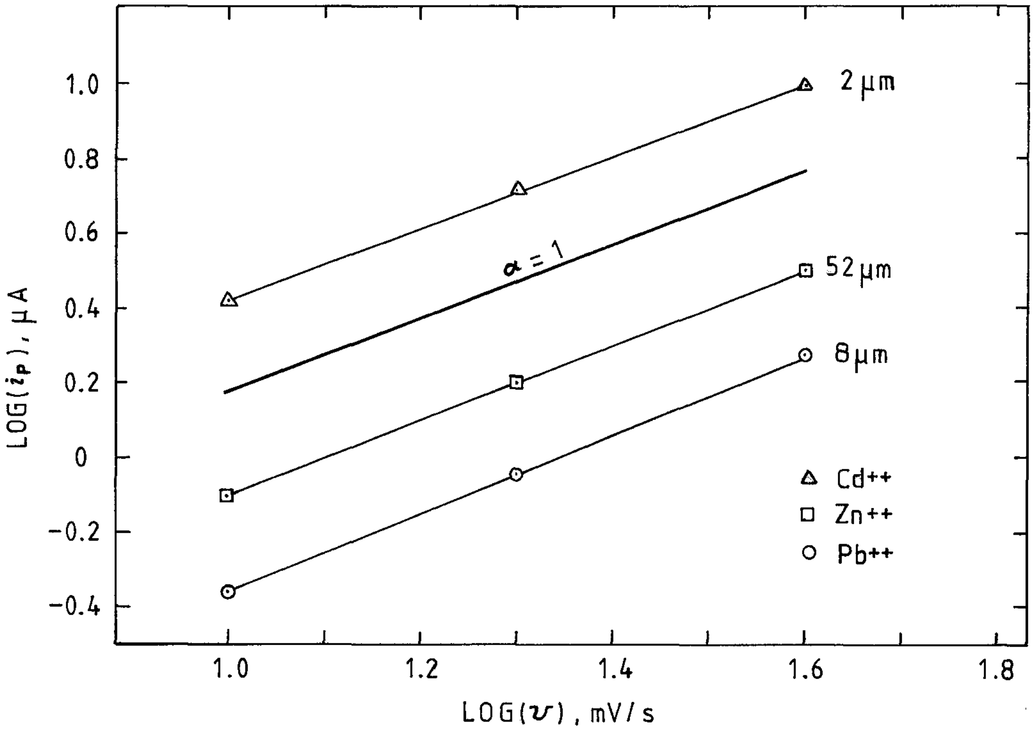

FIGURE 6.4 The dependence of peak current (i_p) on the scan rate (v), with different metal ions and film thicknesses.

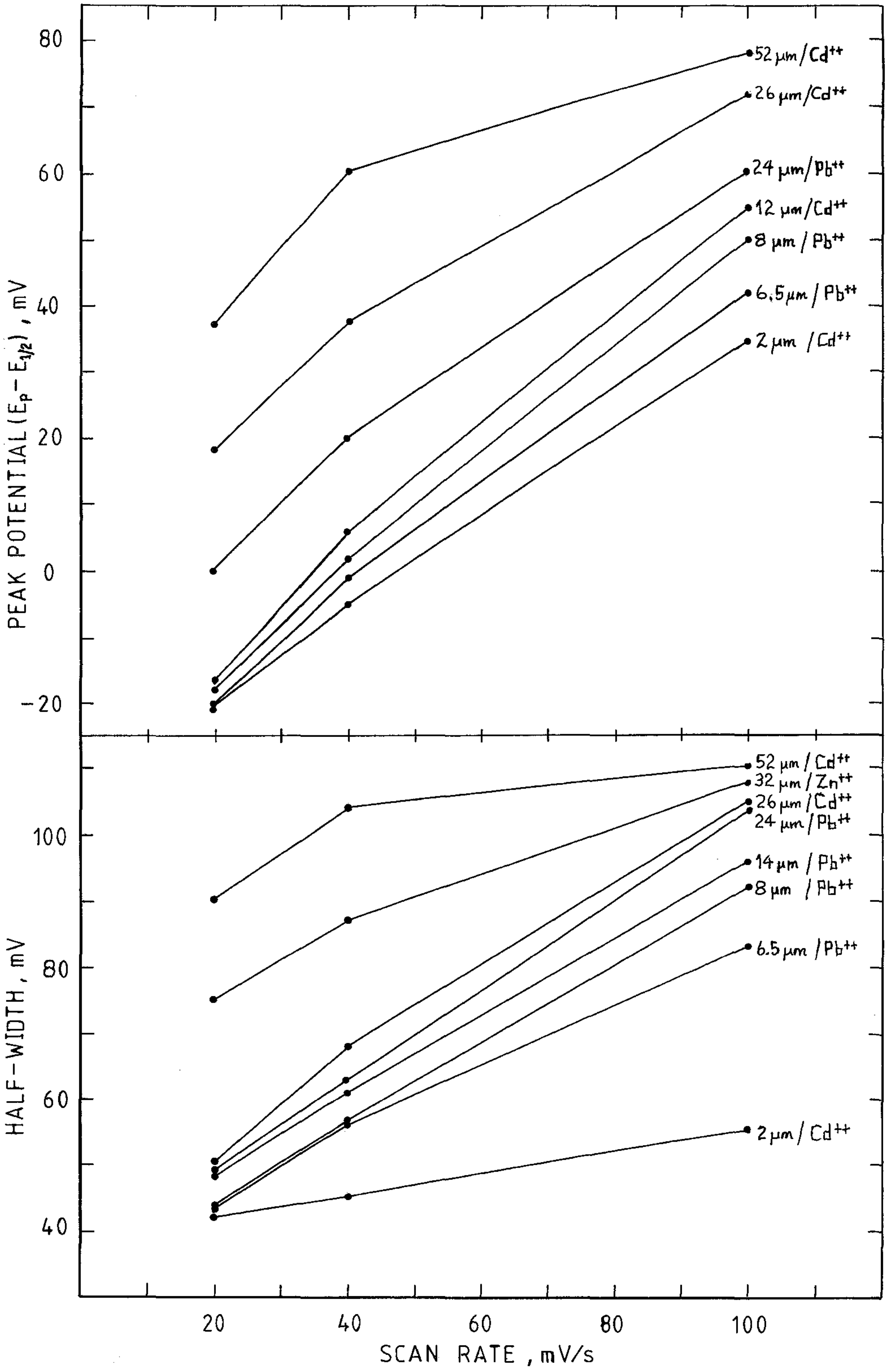

FIGURE 6.5 Scan rate effects on peak potential and half-width for Cd(II), Pb(II), Zn(II), and for various film thicknesses.

The data for the 2, 8, and 48 μm films is used, since these experiments included a scan at 10 mV/s, and thus allow a better comparison.

Evaluating the slope of the log(i_p) vs. log(v) plot, the exponent of the scan rate, α was found to be 0.98±0.04. This value is in excellent agreement with the theory [65] for thin mercury films. It is interesting to note however that this value was obtained even though the other peak parameters (see Figure 6.1) are those normally found with bulk mercury. The variation of the peak potential and half-width with scan rate, is shown in Figure 6.5. The half-width increased with scan rate as expected, but the increase occurred with thinner films and slower scan rates than predicted by theory (see the theoretical comparisons in Section 6.1.4). It appears that the mercury films behave as though they are 2-3 times thicker in terms of these parameters, even though in terms of others, such as for i_p vs. v, they behave as expected.

6.1.4 Thin Mercury Film Behavior: Theory vs Reality

The basic theoretical equations of ASV current-potential curves for thin mercury film electrodes (i.e., < 200μm) were derived by De Vries and Van Dalen in 1964-65 [64,65] (see also Sec.2.3), with some contributions made by Roe and Toni [47] a year later. During these last 20 years the theory has been tested only for certain special conditions and electrodes and, as we will attempt to show, may not apply to "real world" mercury film electrodes.

The only two investigations which attempted to specifically verify the theory were those of Roe and Toni [47] and Perone and Brumfield [66]. Many later studies compared their results with theory, but usually as an evaluation of the usefulness of their mercury films for total concentration analysis, i.e. for applications where exact correspondence between theory and practice is not necessary.

Table 6.4 shows a compilation of the results found in the literature for the values of stripping peak current, peak potential, and peak half-width, along with the electrolytes, ions, and mercury film thicknesses used. Even though it was difficult, we have attempted to find data which is of the same nature for each study, to allow an approximate comparison. The data from Table 6.4, along with that from this work, is shown graphically in Figure 6.6.

The studies can be divided into two groups: those using mercury films $\leq$ 1µ with carbon substrates; and those using mercury films $\geq$ 1µ with metal substrates.

There are two important differences that should be noted between these two groups:

- for all carbon substrates, the authors claim to have had mercury films of 0.002 to 1µm, and that the characterizing parameters (i.e., half-width, peak current and potential) were generally as predicted by theory.
- for all metal substrates, mercury film thicknesses of 1 to 52µm were used, and the characterizing parameters generally acted as though the films were much thicker than they really were.

This second point is especially evident for the values of the half-width, $b_{1/2}$. For example, the data from Cox [39] for films of 1-7µm, give values of $b_{1/2}$ of 45-58 mV, which correspond to mercury films of 5 to 20µm according to the theory of De Vries and Van Dalen. In fact, Cox [39, page 58] stated that "...it appears that the mercury film electrode behaves as though the film is considerably thicker than calculated, the 7.2µm behaves as the 25µm should ...". However, he made no comments or interpretations as to the reasons.

TABLE 6.4 Compilation of experimental results found in the literature for various Hg-film thicknesses and on different substrates.

Hg-film Thickness (μm)	CONDITIONS						PEAK PARAMETERS			Ref.
	Elect. Subst.	Test Ion	Conc. (M)	Electrolyte	t_{dep} (sec)	υ (mV/s)	$b_{\frac{1}{2}}$ (mV)	$E_p-E_{\frac{1}{2}}$ (mV)	i_p (% Theor.)	
0.6	Pt	Pb^{++}	$1.2x10^{-5}$	0.1 M KCl	50	20	42	-40	-	39
1.8	Pt	Pb^{++}	$1.2x10^{-5}$	0.1 M KCl	50	20	43	-28	-	39
2.8	Ni	Cd^{++}	$5.0x10^{-5}$	1.0 M KCl	120	17.2	48	-25	93	47
4.8	Pt	Pb^{++}	$1.2x10^{-5}$	0.1 M KCl	50	20	45	-14	-	39
7.2	Pt	Pb^{++}	$1.2x10^{-5}$	0.1 M KCl	50	20	47	-8	-	39
0.002	gr	Cd^{++}	$2.5x10^{-7}$	0.1 M KCl*	180	12.5	39	-139	84	63
0.002	gr	Pb^{++}	$2.5x10^{-8}$	0.1 M KCl*	180	12.5	38	-134	84	63
0.01	GC	Pb^{++}	$2.0x10^{-7}$	0.1 M KNO_3	300	20	36	-100	-	53
1.0	gr	Cd^{++}	$5.0x10^{-5}$	0.1 M KCl	600	18.6	40**	-110	58	66
0.004	gr	Cd^{++}	$1.0x10^{-4}$	0.2 M KCl*	600	12.5	38	-134	83	63
0.01	gr	Pb^{++}	$5.0x10^{-5}$	0.2 M KCl*	600	12.5	35	-123	83	63

* pH4

** Estimated

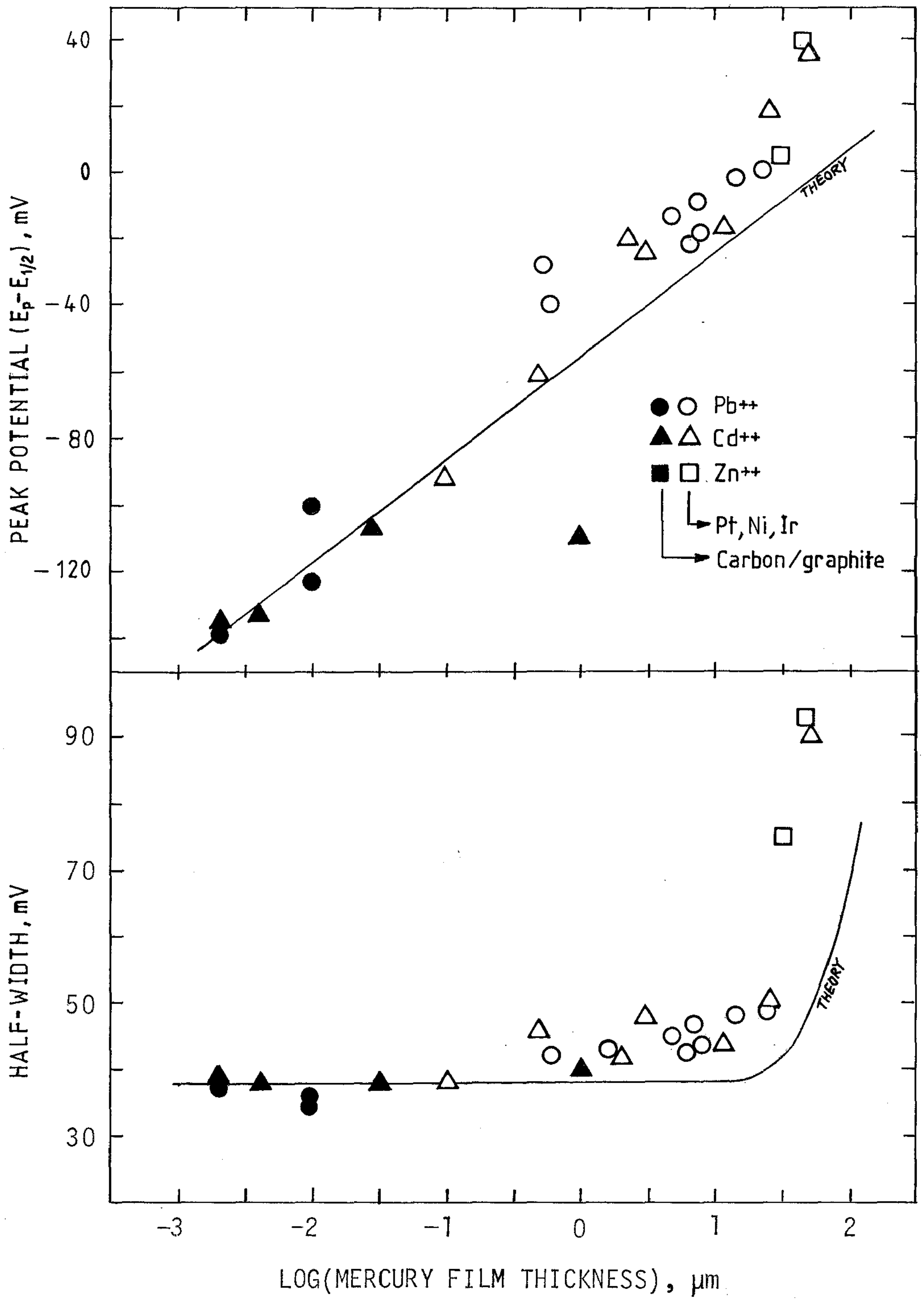

FIGURE 6.6 Comparison of data from both the literature and this work with the theoretical predictions of De Vries and Van Dalen [64,65] for the effect of mercury film thickness on peak potential and half-width.

The True Form of a Mercury Film. We believe that the reason for the above deviation of experimental values from theoretical values is, as we briefly mentioned in Sec.5.5, that no such thing as a true mercury film with constant thickness can exist for deposition of more than ≈ 1μm layer of mercury.

Direct substrate-mercury interactions can bind a monolayer of mercury atoms to the surface (Sec.5.3.3), and long-range attractive forces (Sec.4.1) can keep another ≈ 100 layers stable on the surface. However, mercury having very low viscosity (0.156 dyne·sec/cm^2, 20°C) and very high surface tension (480 ergs/cm^2) will, when left on its own, tend to a spherical shape. Taking the radius of the mercury atoms to be 1.57×10^{-8} cm [45], we can roughly estimate that a monolayer is ≈ 0.0003μm, and so we have ≈ 3400 layers for a 1μm film and more than 1×10^5 layers for a 30μm film. It therefore seems evident that the bulk of mercury for films $\geq$ 1μm is free to take on a natural semi-spherical form.

Figure 6.7 shows the relationship between the thickness of a flat film and the maximum thickness of a semi-spherical film, for equal volumes of deposited mercury. As can be seen, the maximum thickness is approximately two times greater than that assumed if we had a flat film. At the same time the curvature of the film results in an area, at the edge of the electrode, where the thickness always approaches zero, regardless of the maximum thickness.

Morevover, if the film is not plane, the theory of Levich [79] in terms of hydrodynamic flow, may not be strictly applicable. We will however assume that, for our films (max. thickness 52μm) and electrode diameter (2000μm), the hydrodynamic flow at the surface approximates that of a flat surface.

These differences, between assumed and real thicknesses, and the shape itself, may be responsible for the discrepancies between theory and experiment.

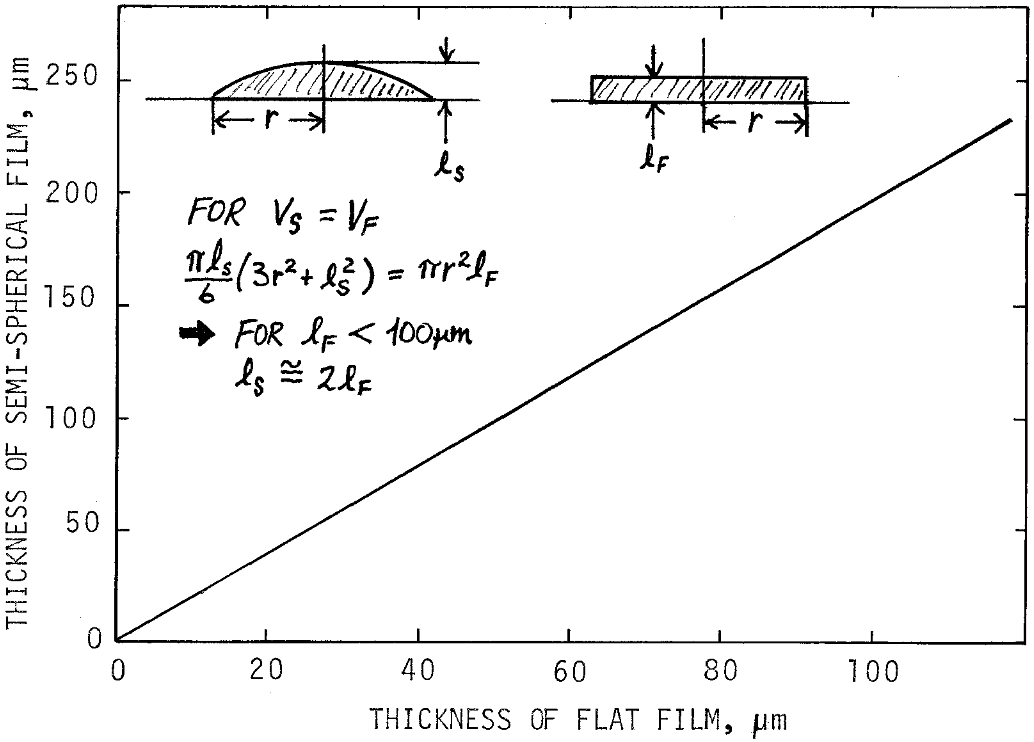

FIGURE 6.7 Relationship between the thickness of a flat film and a semi-spherical film for an electrode with a 1mm radius.

<u>Comparison of Experimental and Theoretical Data</u>. In light of what was said above, the data in Table 6.4 and Figure 6.6 can now be better understood.

For all three parameters, i_p, E_p-$E_{1/2}$, and $b_{1/2}$, the experimental values for films > 1µm behave as though the films are thicker than given, in spite of the fact that the data is taken from different studies and for different electrode materials and metal ions. In some cases the displacement is close to that which would be assumed using the semi-spherical film thicknesses from Figure 6.7. Overall, however, this is not enough to account for the large discrepancies which exist, for example, between experimental and theoretical values for both the peak half-widths and peak potentials.

We must note however that not only will a semi-spherical film behave as a thicker film, but also as a thinner film at or near the edges. We should then expect that the observed behavior of a semi-spherical film of thickness ℓ_s should be a composite of behaviors exhibited by flat films with thicknesses ranging from ℓ_s to $\ell_s \rightarrow 0$.

No theory exists for predicting the ASV parameters for a semi-spherical film, but we may be able to estimate some of the characteristics by assuming the semi-spherical film is composed of many annular flat films. This is shown below in Figure 6.8 along with an example of a rough approximation of the resulting peak half-width. For a flat film of $\ell = 25\mu m$, and using a scan rate = 20 mV/s, theory [65] predicts a half-width of 42 mV. Combining ten peaks with thicknesses of 2ℓ through $2\ell/10$, we obtain a half-width of 59 mV for an equivolume semi-spherical film with $\ell_s \approx 2\ell$.

The picture is even more complicated, however, than is indicated above. Since diffusion can also occur horizontally in the mercury film, the metal oxidized near the edges can be replaced by new metal from the thicker center of the film. During the scan, this process may allow oxidation from the thinner part of the film to continue at potentials more positive than would normally be the case, resulting in a shift of the stripping peak to more positive values.

The actual shape of an ASV stripping peak, made using a semi-spherical film, could be exactly calculated if the appropriate diffusion equations were solved. Such calculations must be done in order to rigorously compare results with theory. The calculations though are no simple matter and have been left for subsequent research. The rough estimates made here, however, do indicate that the peaks obtained with our mercury films can be resonably interpreted if we assume that the film is indeed semi-spherical.

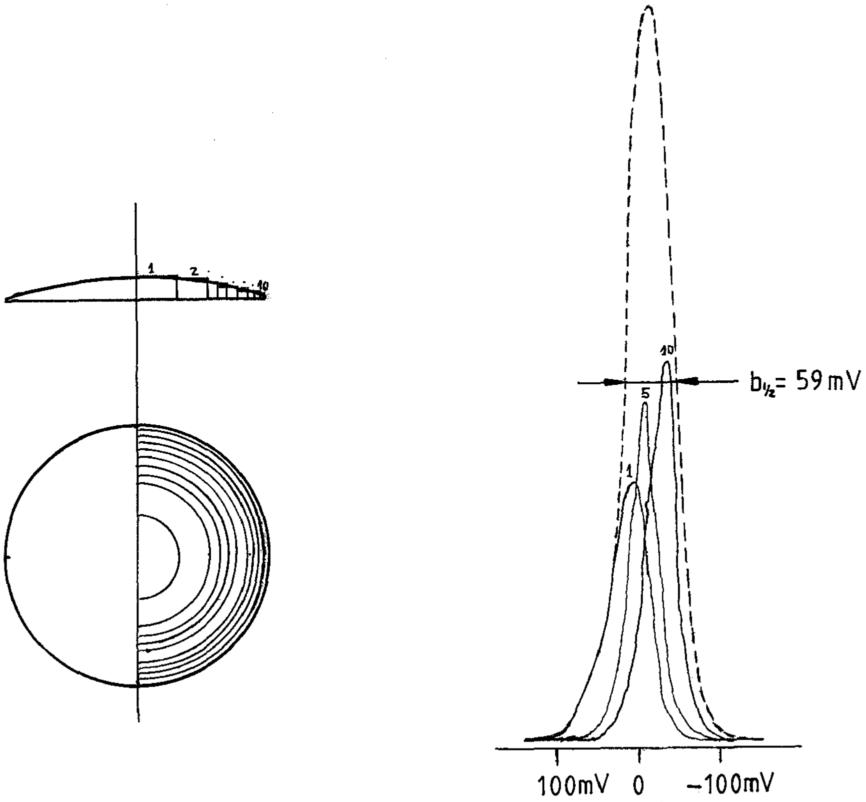

FIGURE 6.8 Approximation of a semi-spherical mercury film stripping peak by combining ASV peaks for flat films.

Mercury Films < 1μm. In contrast to the above results, the behavior of mercury films < 1μm, on both our iridium substrate and the glassy-carbon or graphite substrates used in the studies cited from the literature, was in good agreement with theory [65]. This is to be expected with thinner mercury films on iridium, since we approach the thickness of mercury at which it is easier to maintain a true film due to the interactive forces between the mercury atoms and iridium substrate.

In the case of mercury films on glassy-carbon, we know the surface is covered, not by a true film, but by a very large number of mercury droplets. For the deposition of mercury equivalent to a flat film of $\leq 0.1\mu m$, these droplets are small enough and close enough in comparison with the diffusion layer thickness that they effectively act as a flat surface, and thus agreement with theory [65] is to be expected.

6.2 ANALYSIS OF CADMIUM(II) IN WATER

6.2.1 Variation of Peak Current with Cd(II) Concentration

In any analytical method, it is desirable to know the relationship of the instrumental response to the concentration of the analyte in the sample solution.

The above was tested for the Ir-MFE by measuring the peak current as a function of the concentration of Cd^{++} in the sample solution. Each point is the average of three measurements. The experiment was performed using $1x10^{-6}M$ Cd^{++} in 0.1M KNO_3, with a deposition time of 100 seconds at a potential of -900 mV, a scan rate of 20 mV/s, and ω = 2000 rpm.

The results shown in Figure 6.9 verify that peak current is proportional to the concentration of Cd(II) in solution, and thus allow us to use the Ir-MFE for quantitative analysis.

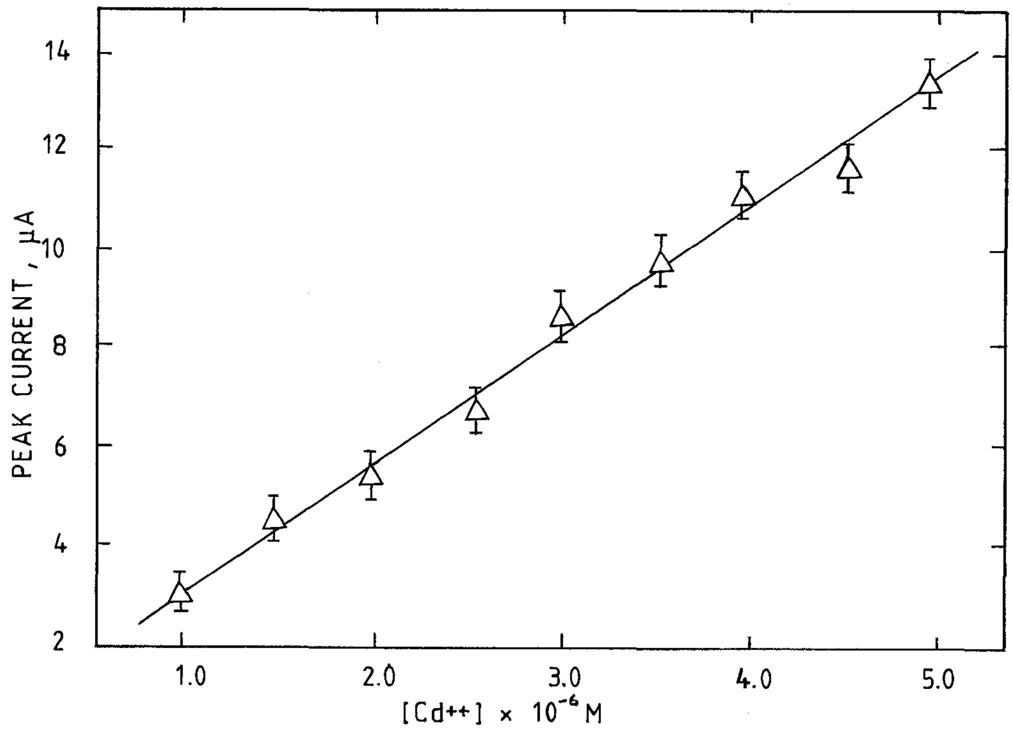

FIGURE 6.9 Variation of peak current with the concentration of Cd(II) in solution.

6.2.2 Stripping Polarography of Cadmium(II)

Several studies have been previously reported which use a glassy-carbon MFE and stripping polarography to perform speciation analysis [94,97,133], but no such studies have been made with "true" mercury film electrodes. Even though some of the studies mentioned above have used very low concentrations of metal ion (e.g. $6x10^{-9}M\ Pb^{++}$, [133]), our main purpose here was to demonstrate the usability of the Ir-MFE, and not to test it at the limits where special precautions would be necessary and/or complications might arise.

The Ir-MFE was used to generate stripping polarograms for $1x10^{-6}M\ Cd^{++}$ in $0.1M\ KNO_3$. The individual ASV runs were performed with a scan rate = 20 mV/S, ω = 2000 rpm both during deposition and stripping, a 1µm flat-film, and at deposition times of 30, 100, 200, and 300 seconds.

Figure 6.10 shows as an example the stripping polarogram for the 100 sec. deposition. Since the electrode was rotating throughout the experiment, and the deposition potential was at different values, we have made a correction to all the peak currents, multiplying them by $100/(100 + t_S)$, where t_S is the time required for the potential to scan from the deposition point to the peak potential. The slopes, half-wave potentials, and number of electrons, were determined from the experimental stripping polarogram by use of a weighted least-squares algorithm [135] (APPENDIX J).

The half-wave potential from the above stripping polarogram, and the three others for 30, 200, and 300 seconds, are plotted in Figure 6.11 as a function of log(deposition time). This data was then used to verify the validity of Eq.(2.26) which was derived in Sec.2.4 for a mercury-film on a RDE.

Using Eq.(2.26) with $D_O = 6.9x10^{-6}cm^2/s$, ℓ = 1µm, $f_O/f_R = 1$, ω = 209 rad/sec, t = 100 sec, and -0.0352 V (vs.NHE)

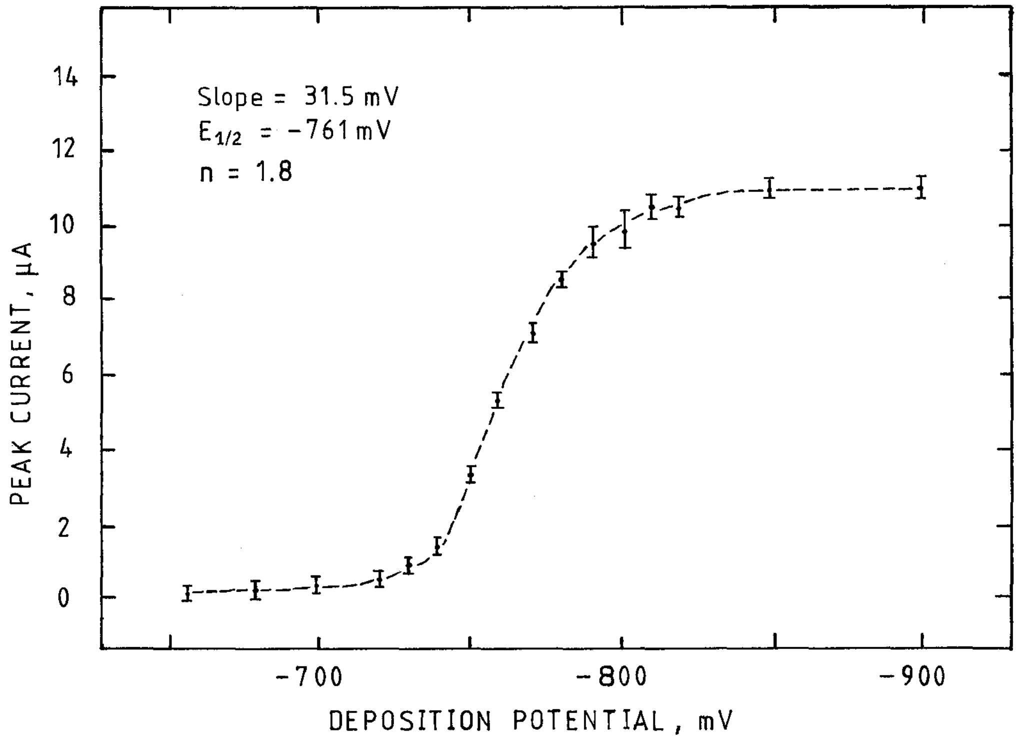

FIGURE 6.10 Sample polarogram for 10^{-6}M Cd(II) in 0.1M KNO_3, with ω = 2000rpm, t_d = 100 sec., and a 1μm film.

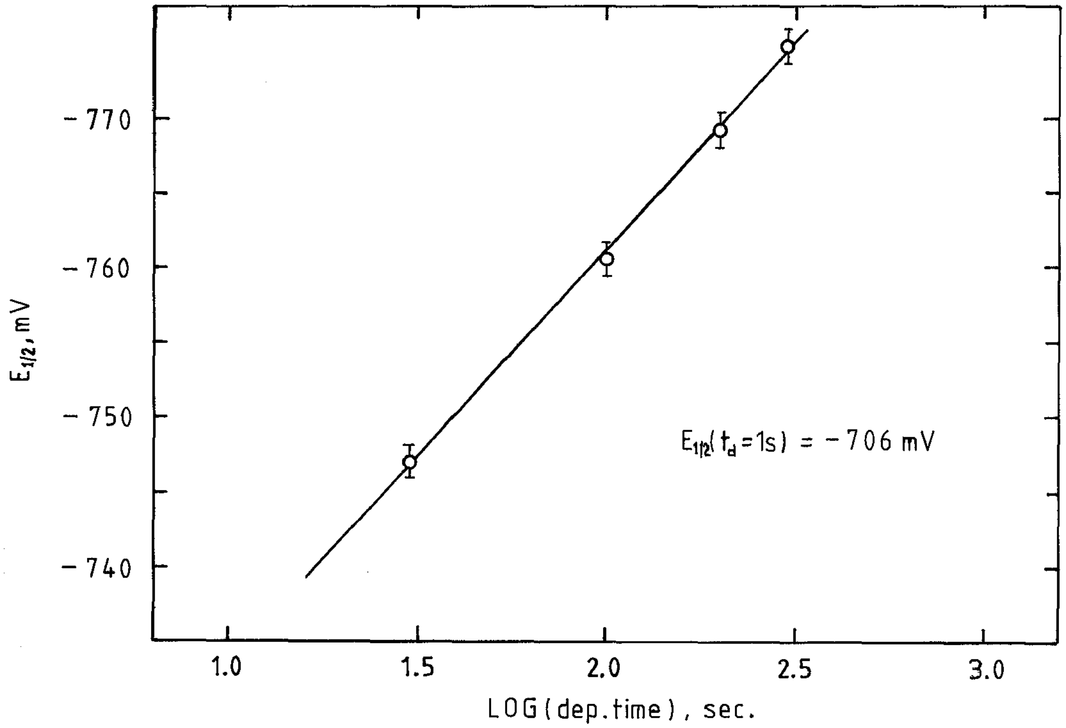

FIGURE 6.11 Plot of the stripping polarogram half-wave potential as a function of the log(dep.time); same solution as above.

for the $Cd^{++} \rightarrow CdHg$ standard reduction potential, we obtain $E_{1/2}$ = -0.747 V (vs.SCE), in contrast to the experimental value of -0.761 V. The difference between these values is not very significant when taking into account the uncertainty of temperature (cell was not thermostated), which may add ± 5 mV, and more importantly the thickness of the mercury film, which was here assumed to be a flat film. If we assume a semi-spherical film, with ℓ = 2µm, the calculated potential is shifted ≈ 15 mV more negative. The experimental slope of the stripping polarogram (31.5mV) is also close to the theoretical value (29.5mV).

The above results show the validity of Eq.(2.26) for describing the behavior of stripping polarograms with mercury films on a RDE, and the ability of the Ir-MFE to obtain such data.

6.3 DETERMINATION OF ZINC(II) IN SEAWATER

As was previously mentioned, the quantitative determination of zinc(II) with Pt or Au based MFE's is difficult due to intermetallic compound formation between the substrate and the reduced Zn in the mercury. Quantitative determinations have been successfully demonstrated using the glassy-carbon MFE. For rigorous speciation studies, however, one may question the definability of the mercury-droplet-covered surface after the vigorous evolution of hydrogen bubbles, occurring during deposition of Zn(II) at potentials $\leq$ -1400 mV (vs.SCE).

The samples were analyzed by making the deposition from the sample itself, and exchanging it for a sodium acetate buffer for the stripping step. This is necessary since in acid solutions, the high hydrogen reduction background current interferes with the zinc stripping peak.

Because of the relatively low concentration of Zn(II) in seawater, special precautions were taken to insure that no contamination occurred. These included using only high purity reagents and washing all containers and pipettes with nitric acid before using.

The seawater samples (Adriatic Sea, Pula, Yugoslavia) were collected in 2 liter PTFE containers and acidified with nitric acid (≈ pH 2). The exchange solution was 0.1M sodium acetate adjusted to pH 5 with acetic acid (Merck "Suprapur"). The depositions were made for 600 seconds at -1300 mV, using a 20μm film, with the electrode rotating at 2000 rpm throughout the analysis.

Figure 6.12 shows the results obtained for successive standard additions of zinc(II) to the sample. The original zinc(II) concentration was found to be 8.2 $\pm$0.4 x 10^{-8}M. This value is in good agreement with other determinations made for the seawater samples from the same or similar areas [136].

In conclusion, we have shown the potential applicability of the Ir-MFE/medium-exchange system for the analysis of zinc(II) in seawater at concentrations similar to those found in many coastal water areas.

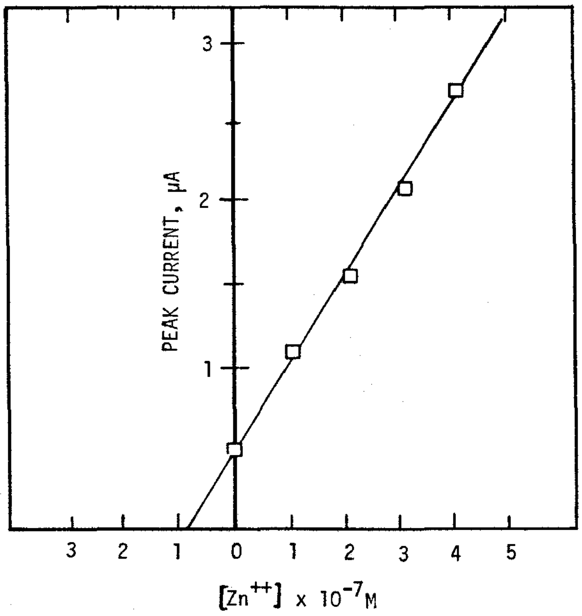

FIGURE 6.12 Determination of the zinc(II) concentration in seawater by standard additions of 1x10^{-7}M increments.

(This page intentionally left blank.)

REFERENCES

1. Florence T. and Batley G., Talanta, 24 (1977) 151-158
2. Buffle J., Trends in Anal.Chem., 1 (1981) 90-95
3. Allen H., Hall R. and Brisbin T., Environ.Sci.Technol., 14 (1980) 441-443
4. Batley G. and Florence T., Mar.Chem., 4 (1976) 347-363
5. Valenta P., in "Trace Metal Speciation in Surface Waters and Ecological Implications", Leppard G. (Ed), Plenum Publ., New York, 1983
6. Van Leeuwen H.P., J.Electroanal.Chem., 99 (1979) 93-102
7. Davison W., J.Electroanal.Chem., 87 (1978) 395-404
8. Ernst R., Allen H.E. and Mancy K.H., Water Res., 9 (1975) 969-979
9. Bilinski H., Huston R. and Stumm W., Anal.Chim.Acta, 84 (1976) 157-164
10. O'Shea T.A. and Mancy K.H., Anal.Chem., 48 (1976) 1603
11. Duinker J.C. and Kramer C.J., Mar.Chem., 5 (1977) 207
12. Shuman M.S. and Woodward G., Anal.Chem., 45 (1973) 2032
13. Chau Y.K. and Lum-Sheu-Chau K., Water Res., 8 (1974) 383
14. Florence T.M. and Batley G.B., J.Electroanal.Chem., 75 (1977) 791-798
15. Kounaves S.P. and Zirino A., Anal.Chim.Acta, 109 (1979) 327-339
16. Bubic S. and Branica M., Thalassia Jugosl., 9 (1973) 47-53
17. Copeland T.R. and Skogerboe R.K. ,Anal.Chem., 46 (1974) 1257A-1268A

18. Ellis W.D., J.Chem.Educ., 50 (1973) A131-A147
19. Buffle J. and Greter F.L., J.Electroanal.Chem. 101 (1979) 231-251
20. Brezonik P.L., Brauner P.A. and Stumm W., Water Res., 10 (1976) 605-612
21. Mota A.M.A., Buffle J., Kounaves S.P. and Goncalves M.L.S. Submitted for publication.
22. Buffle J. J.Electroanal.Chem., 125 (1981) 273-294
23. Buffle J., Tessier A. and Haerdi W. in "Complexation of Trace Metals in Natural Waters", Kramer C.J. and Duinker J.C. (Eds.), Martinus Nijhoff/Dr.W.Junk Publishers, The Hague, 1984
24. Batley G.E. and Florence T.M., J.Electroanal.Chem., 55 (1974) 23-43
25. Brainina K.Z., Talanta, 18 (1971) 513-539
26. Adams R.N., "Electrochemistry at Solid Electrodes" Marcel Dekker Inc., New York, 1969
27. Vydra F., Stulik K. and Julakova E., "Electrochemical Stripping Analysis", Harwood/Wiley, New York, 1976
28. Gardiner K.W. and Rogers L.B., Anal.Chem., 25 (1953) 1393
29. Igolinskii V.A. and Stromberg A.G., Zavodsk.Lab., 30 (1964) 656; CA; 61-8889a
30. Zakharov M.S. and Trushina L.F., Zh.Anal.Khim., 22 (1967) 1219
31. Stojek Z. and Kublik Z., J.Electroanal.Chem., 60 (1975) 349
32. Stojek Z., Ostapczuk P. and Kublik Z., J.Electroanal.Chem., 67 (1976) 301
33. Stojek Z. and Kublik Z., J.Electroanal.Chem., 77 (1977) 205
34. Ostapczuk P. and Kublik Z.,J.Electroanal.Chem., 93 ?? (1978) 195
35. Marple T. and Rogers L., Anal.Chem., 25 (1953) 1351

36. Kemula W., Kublik Z. and Galus Z., _Nature_, 184 (1959) 1795

37. Neeb R., _Z.Anal.Chem._, 180 (1961) 161-168

38. Ramaley L., Brubaker R.L. and Enke C.G., _Anal.Chem._, 35:8 (1963) 1088-1089

39. Cox J.A., Ph.D. Thesis, University of Illinois, 1967

40. Hartley A.M., Hiebert A.G. and Cox J.A., _J.Electroanal.Chem._, 17 (1968) 81-86

41. Van der Leest R., _Anal.Chim.Acta,_ 52 (1970) 151-152

42. Sandoz D.P. et al. _J.Electroanal.Chem._, 24 (1970) 165

43. Robbins G.D. and Enke C.G., _J.Electroanal.Chem._, 23 (1969) 343-349

44. Yoshida Z., _Bull.Chem.Soc.Japan_, 54 (1981) 556-561

45. Hassan M.Z., Untereker D.F. and Bruckenstein S., _J.Electroanal.Chem._, 42 (1973) 161-181

46. Vondrak J. and Balej J., _Electrochim.Acta_, 15 (1970) 1653-1654

47. Roe D.K. and Toni J.E., _Anal.Chem._, 37 (1965) 1503-1506

48. Joyce R.J. and Westcott C.C., National Bureau of Standards Symposium on Trace Characterization, 1966

49. Yoshida Z., _Bull.Chem.Soc.Japan,_ 54 (1981) 562-567

50. Kamenev A.I. and Vinogradova E.N., _Zh.Anal.Khim._, 20 (1965) 1064-1068

51. Mart L., Nurenberg H.W. and Valenta P., _Fresenius Z.Anal.Chem._, 300 (1980) 350-362

52. Matson W., Roe D. and Carritt D., _Anal.Chem._, 37 (1965) 1594-1595

53. Florence T.M., _J.Electroanal.Chem._, 27 (1970) 273-281

54. Miguel A.H. and Jankowski C.M., _Anal.Chem._, 46 (1974) 1832-1834

55. Stulikova M., _J.Electroanal.Chem._, 48 (1973) 33-45

56. Stulikova M. and Vydra F., _J.Electroanal.Chem._, 44 (1973) 117-125

57. Rusling J.F., _Anal.Chem._, 56 (1984) 575-578

58. Sykut K., Cukrowski I. and Cukrowska E., J.Electroanal. Chem., 115 (1980) 137-142

59. Hume D.N. and Carter J.N., Chemia Analityczna, 17 (1972) 747-758

60. Perone S.P. and Davenport K.K., J.Electroanal.Chem., 12 (1966) 269-276

61. Siegerman H. and O'Dom G., Amer.Lab., 4:6 (1972) 59

62. Kauffmann J.M., Laudet A. and Patriarche G.J. Anal.Chim.Acta, 135 (1982) 153-158

63. Stojek Z.,Stepnik B. and Kublik Z., J.Electroanal.Chem., 74 (1976) 277-295

64. De Vries W. and Van Dalen, J.Electroanal.Chem., 8 (1964) 366-377

65. De Vries W., J.Electroanal.Chem., 9 (1965) 448-456

66. Perone S.P. and Brumfield A., J.Electroanal.Chem., 13 (1967) 124-131

67. Heumann T. and Forch K., Z.Metallk., 53 (1962) 122-130

68. Bruckenstein S. and Nagai T., Anal.Chem., 33 (1961) 1201

69. Maslenitskii I. and Zverevich N., Zap.Leningr.Gorn.Inst. 42:3 (1963) 25-34

70. Barlow M. and Planting P., Z.Metallkde., 60 (1969) 817

71. Engstrom R.C. and Stasser V.A., Anal.Chem., 56 (1984) 136-141

72. Janssen L. and Hoogland J., Electrochim.Acta,, 14 (1969) 1097-1099 ; 15 (1970) 339-345

73. Heumann T. and Forch K., Z.Metallk., 54 (1963) 704-709

74. CA 74:P90471j and CA 76:P36804y

75. Van der Linden W.E. and Dieker J.W., Anal.Chem., 119 (1980) 1-24

76. Albery W.J. and Bruckenstein S., J.Electroanal.Chem., 144 (1983) 105-112

78. Pleskov Y.V. and Filinovskii V.Y., "The Rotating Disc Electrode", Consultants Bureau-Plenum Co.,New York, 1976

79. Levich V.G., "Physicochemical Hydrodynamics", Prentice-Hall, Inc., Englewood Cliffs, N.J., 1962

80. Riddiford A.C. in "Advances in Electrochemistry and Electrochemical Engineering", Vol.4, Delahay P. (Ed.), Interscience Publishers, New York, 1964

81. Cochran W.G., Proc.Cambridge Phil.Soc., 30 (1934) 365

82. Clarenbach S. and Grabner E.W., Ber.Bunsen-Ges., 80 (1976) 115-121

83. Blurton K.F. and Riddiford A.C., J.Electroanal.Chem., 38 (1966) 153

84. Newman J.S., "Electrochemical Systems", Prentice-Hall, Englewood Cliffs, N.J., 1973

85. Frenkel Y.I., "Kinetic Theory of Liquids", Vol. III, Izd.Akad.Nank.SSR, Moskva-Leningrad, 1959

86. Kaischew R. and Mutaftchiew B., Electrochim.Acta, 10 (1965) 643

87. Toschev S. and Markov I., Electrochim.Acta, 12 (1967) 281

88. Fleischmann M. and Thirsk H., Electrochim.Acta, 2 (1960) 22

89. Astley D., Harrison J. and Thirsk H., Trans.Faraday Soc., 64 (1968) 92

90. Vetter K.J., "Electrochemical Kinetics", Academic Press, New York, 1967, Chapter 2, Sec.D

91. Morcos I., J.Electroanal.Chem., 50 (1974) 373-377

92. Toschev S. and Mutaftschiew B., Electrochim.Acta, 9 (1964) 1203-1210

93. Zirino A. and Kounaves S.P., Anal.Chem., 49 (1977) 56-59

94. Brown S.and Kowalski B., Anal.Chem., 51 (1979) 2133-2139

95. Shuman M. and Cromer J., Anal Chem., 51 (1979) 1546-1550

96. Zirino A. and Kounaves S.P., Anal.Chim.Acta, 113 (1980) 79-90

97. Huizenga D.L. and Kester D.R., J.Electroanal.Chem., 164 (1984) 229-236

98. Anderson J.E., Bagchi R.N., Bond A.M., et al., Inter.Lab., November (1980) 35-47
99. Kryger L., Anal.Chim.Acta, 133 (1981) 591-602
100. Price J.F., Cooke S.L. and Baldwin R.P., Anal.Chem., 54 (1982) 1011-1014
101. Osteryoung J., Science, 218 (1982) 261-265
102. Graneli A., Jagner D. and Josefson M., Anal.Chem., 52 (1980) 2220-2223
103. Savitzky A. and Golay M.J., Anal.Chem., 36 (1964) 1627
104. Koster G. and Ariel M., J.Electroanal.Chem., 33 (1971) 339-349
105. Siegenthaler H. and Schmidt E., J.Electroanal.Chem., 80 (1977) 129-141
106. Anderson L., Jagner, D. and Josefson, M., Anal.Chem., 54 (1982) 1371-1376
107. Wang J. and Greene, B., Water Res., 17 (1983) 1635-1638
108. Hume, D.N. in "Progress in Analytical Chemistry" Vol.5, Ahuja S. et al. (Eds.), Plenum Press, New York, 1973
109. Shunk R., "Constitution of Binary Alloys", 2nd Supplement, McGraw-Hill, New York, 1969
110. Galus Z. and Guminski C., "Solubility of Metals in Mercury", Report to V.5 Commission of IUPAC, Submitted to Pergamon Press
111. Galus Z., personal communication
112. Murr L.E., "Interfacial Phenomena in Metals and Alloys", Addison-Wesly Co., Reading, Mass., 1975
113. Kolb D.M., Przasnyski M. and Gerischer H., J.Electroanal.Chem., 54 (1974) 25-38
114. Trasatti S., J.Electroanal.Chem., 33 (1971) 351-378
115. Pourbaix M.J., "Atlas of Electrochemical Equilibrium in Aqueous Solutions", Pergamon Press, Oxford, 1966
116. Otten J.M. and Visscher W., J.Electroanal.Chem., 55 (1974) 1-11

117. Rand D.A. and Woods R., J.Electroanal.Chem., 55 (1974) 375-381

118. Schubert C., Page C. and Ralph B., Electrochim.Acta, 18 (1973) 33-38

119. Zerbino J.O., DeTacconi N.R. and Arvia A.J., J.Electrochem.Soc., 125:8 (1978) 1266-1276

120. Zerbino J.O. and Arvia A.J., J.Electrochem.Soc., 126:1 (1979) 93-95

121. Semenova A.D., Fedotova T.G. and Khomchenko G.P., Vestn.Mosk.Univ., Ser.II,Khim., 20:6 (1965) 47-49

122. Maximov Y.M., Kazarinov V.E. and Petrii O.A., Electrokhimiya, 8 (1972) 1254-1259

123. Chemeris M., Stromberg A., Kolpakova N. and Vasil'ev Y., Electrokhimiya, 11 (1975) 1060-1063

124. Winterbottom W.L., Acta Met., 15 (1967) 303

125. Murr L.E., Mat.Sci.Engr., 12 (1973) 277-283

126. Coetzee J.F., in "Treatise on Analytical Chemistry", Part 2, Vol.3, Kolthoff I.M. and Elving P. (Eds.), Interscience, New York, 1961, pg.231

127. Kolthoff I.M. and Miller C.S., J.Am.Chem.Soc., 63 (1941) 2732-2738

128. Heyrovsky J. and Kuta J., "Principles of Polaography", Czechoslovak Academy of Sciences, Prague, 1965

129. Schadewald L.A., et al., J.Electrochem.Soc., 131 (1984) 1583-1587

130. Lindstrom T.R. and Johnson D.C., Anal.Chem., 53 (1981) 1855-1863

131. Despic A.R. and Popov K.I., J.appl.Electrochem., 1 (1971) 275-278

132. Whitfield M. and Turner D.R., in "Lead in the Marine Environment", Proc., Rovinj Yug., Oct.1977, Branica M. and Konrad Z. (Eds.), Pergamon Press, 1979, pp.109-148

133. Sipos L., Valenta P., Nurnberg H.W. and Branica M., ibid, pp.61-76

134. Lorente M.A., Diploma Work, University of Geneva, 1984

135. Oldham K.B., J.Electroanal.Chem., 167 (1984) 107-115

136. Bernard M., Goldberg E.D. and Piro A., in "The Nature of Seawater", Goldberg E.D. (Ed.), Dahlem Conference, Berlin, 1975, pp.43-68

APPENDICIES

APPENDIX A - Specifications for PIA card outputs

OUTPUT VARIABLE	STAND CONTROL FUNCTION
PDRA[0]	Stepper motor pulse train (HMDE)
PDRA[1]	Motor direction (1=up,0=down)
PDRA[2]	Dislodging hammer (HMDE)
PDRA[3]	220VDC outlet (1=on,0=off)
PDRA[4]	Gas valve (1=purge, 0=blanket)
PDRA[5]	Select stand control (1=selected)
PDRA[6]	nc
PDRA[7]	nc

	RELAY CONTROLLED (FUNCTION)
PDRB[0]	A (START SCAN on PRG5)
PDRB[1]	B (PEN DOWN when using CORROVIT)
PDRB[2]	C (STOP SCAN on PRG5)
PDRB[3]	D (GALVANOSTATIC MODE on CORROVIT)
PDRB[4]	E nc
PDRB[5]	F nc
PDRB[6]	G nc
PDRB[7]	H nc

APPENDIX B - Settings of CORROVIT for computer control

Power : ON

Duration : not used

Offset : set to 0000

Function : OPERATION

P/G mode : set to P

Voltmeter range: set to 1000 or 2000 mV range

ΔE/ΔI : not used for potentiometry and set to + for constant current

Current range : Set manually as desired

Depart/Start : not used

APPENDIX C - ASV - anodic stripping voltammetry program for Tacussel-CORROVIT

```
00020 REM ****************************************************************
00030 REM   PROGRAM ASV                                VERSION 14.04.83-A
00040 REM
00050 REM   CONTROL OF TACUSSEL CORROVIT FOR ASV.
00080 REM
00090 REM ****************************************************************
00160 REM   INITIALIZE CONSTANTS
00165 REM
00170 DIM Prg$(1) ADDR $E0A4,Edep$(1) ADDR $E0C9
00180 DIM Tdep$(1) ADDR $E0F4,Tequ$(1) ADDR $E119
00200 DIM Srng$(1) ADDR $E144,Srate$(1) ADDR $E169
00220 DIM Cset$(1) ADDR $E194,Rep$(1) ADDR $E1B9
00250 REM
00251 CLRL$= CHR$($1B)+ CHR$($4B)
00252 INV$= CHR$($1B)+ CHR$($42)
00253 ERA$= CHR$($1B)+ CHR$($45)
00254 UCUR$= CHR$($1B)+ CHR$($55)
00255 DCUR$= CHR$($1B)+ CHR$($56)
00256 HCUR$= CHR$($1B)+ CHR$($4C)
00257 REM
00260 EXT XDOS ADDR $E800
00262 REM
00265 BYTE DRVSEL ADDR $EC08
00270 BYTE CRA ADDR $ED21,CRB ADDR $ED23
00280 BYTE DDRA ADDR $ED20,DDRB ADDR $ED22
00290 BYTE PDRA ADDR $ED20,PDRB ADDR $ED22
00300 BYTE DU1 ADDR Edep$,DU2 ADDR Tdep$
00320 BYTE DU3 ADDR Tequ$,DU4 ADDR Srng$
00340 BYTE DU5 ADDR Srate$,DU6 ADDR Prg$
00360 BYTE DU7 ADDR Cset$,DU8 ADDR Rep$
00363 BYTE KF1(4) ADDR $E0A0,KF5(4) ADDR $E0C5
00364 BYTE KF2(4) ADDR $E0F0,KF6(4) ADDR $E115
00365 BYTE KF3(4) ADDR $E140,KF7(4) ADDR $E165
00366 BYTE KF4(4) ADDR $E190,KF8(4) ADDR $E1B5
00368 REM
00370 INTEGER CHAN ADDR $EC1A,VOLTS ADDR $EC1D
00400 INTEGER POTENTIAL ADDR $EC14,POT,RATE
00410 INTEGER RECORDER ADDR $EC16
00420 INTEGER FS,COUNT,SECS,On,Off
00430 INTEGER DLY,STAT,DELAY,M,I,J,K,L
00440 INTEGER RNGS,RNGE,RNGT,ED,SN,FK,IR
00450 INTEGER CURR(1010),Rate,Rngs,Rnge
00452 REM
00499 RESTORE
00500 DATA 0,0,$FF,$FF,$4,$4,$28,1,0
00510 DATA -1000,1,0,100,20,-1000,0,1000,40,0,1,1
00511 DATA 1
00512 DATA "PURGING","ELECTROLYSIS","EQUILIBRATION"
00514 DATA "SCANNING","READY--MAKE SELECTION"
00520 READ CRA,CRB,DDRA,DDRB,CRA,CRB,PDRA,PDRB,POTENTIAL
00530 READ ED,On,Off,TD,EQ,RNGS,RNGE,RNGT,RATE,PRG,FS,RPT
00531 READ DE
00532 READ PR$,DEP$,EQL$,SCN$,RDY$
00540 REM
00600 DATA $A0,$A0,$A0,$A0,$A0,$A0,$A0,$A0
00602 DATA $C6,$C6,$C6,$C6,$C6,$C6,$C6,$C6
00604 DATA $B1,$B2,$B3,$B4,$B5,$B6,$B7,$B8
00606 DATA $A0,$A0,$A0,$A0,$A0,$A0,$A0,$A0
00660 REM
00665 GOTO 3000
00669 REM ******************************
00670 REM   PROCEDURE: CURSPOS(L)
00672 DEF CURSPOS(L)
00673 PRINT HCUR$;
```

APPENDIX C - (continued)

```
00676  IF L=1 THEN  RETURN
00677  IF L=2 THEN  PRINT
00678  IF L=2 THEN  RETURN
00679  FOR I=1 TO L-2
00680  PRINT DCUR$;
00682  NEXT I
00683  PRINT
00684  RETURN
00690  REM
00691  REM ******************************
00692  REM   PROCEDURE: CANVAS1 & 2
00700  DEF CANVAS1
00710  Prg$= STR$(PRG,"PURGE TIME : [5] secs")
00720  DU6=$20
00730  Edep$= STR$(ED,"DEP.POTENTIAL :      [5] mV")
00740  DU1=$20
00750  Tdep$= STR$(TD,"DEP.TIME   : [5] secs")
00760  DU2=$20
00770  Tequ$= STR$(EQ,"EQUILIBRATION :  [5] secs")
00780  DU3=$20
00790  Srngs$= STR$(RNGS,"SCAN RANGE : [5] TO ")
00800  Srnge$= STR$(RNGE,"[5] mV")
00810  Srng$=Srngs$+Srnge$
00820  DU4=$20
00830  Srate$= STR$(RATE,"SCAN RATE     :[5] mV/sec")
00840  DU5=$20
00850  Cset$= STR$(DE,"STEP E     : [5] mV")
00860  DU7=$20
00870  Rep$= STR$(RPT,"REPETITIONS   : [2]")
00875  DU8=$20
00876  CURSPOS(11)
00877  RETURN
00880  DEF CANVAS2
00882  PRINT HCUR$;
00885  PRINT  USING "[2][X27]PARAMETERS SET[X30][2]",INV$,INV$
00886  REM
00890  FOR I=1 TO 4
00892  READ KF1(I),KF2(I),KF3(I),KF4(I),KF5(I),KF6(I),KF7(I),KF8(I)
00894  NEXT I
00897  REM  ** CANVAS2 ************
00905  CURSPOS(8)
00925  PRINT INV$;" F9 ";INV$;" START     ";INV$;"F10 ";INV$;
00926  PRINT " RESET      ";INV$;" F12 ";INV$;" SAVE DATA       ";
00927  PRINT INV$;" F16 ";INV$;" EXIT"
00930  CURSPOS(14)
00940  PRINT  USING "[2][X27]PRESENT STATUS[X30][2][2]",INV$,INV$
00941  CURSPOS(16)
00945  PRINT  USING "[22,C][20,C][28,C][2]",PR$,DEP$,EQL$
00946  CURSPOS(18)
00950  PRINT  USING "[22,C][2][48,C][2]",SCN$,INV$,RDY$,INV$;
00955  CURSPOS(11)
00960  RETURN
00995  REM
00999  REM ******************************
01000  REM   PROCEDURE:  WAIT
01020  DEF WAIT(SECS)
01030  IF SECS<=0 THEN  RETURN
01040  COUNT=0
01050  COUNT=COUNT+1
01060  FOR K=$1 TO $19F0
01070  NEXT K
01080  IF COUNT#SECS THEN  GOTO 1050
01090  RETURN
01100  REM ******************************
```

APPENDIX C - (continued)

```
01110  REM   PROCEDURE: STIRRER
01130  DEF STIRRER(STAT)
01140  PDRA[3]=STAT
01150  RETURN
01160  REM *******************************
01170  REM   PROCEDURE: CELL
01190  DEF CELL(STAT)
01200  PDRB[2]=STAT
01210  RETURN
01220  REM *******************************
01230  REM   PROCEDURE: PURGE
01250  DEF PURGE(SECS)
01252  IF SECS<1 THEN  RETURN
01254  PDRA[4]=On
01258  WAIT(SECS)
01260  PDRA[4]=Off
01270  RETURN
01280  REM *******************************
01290  REM   PROCEDURE: SCAN
01310  DEF SCAN(Rate,Rngs,Rnge,DE)
01330  DELAY= FIX(DE*6800/Rate)
01332  IDE=DE* SGN(Rnge-Rngs)
01335  PDRB[1]=1
01340  M=9
01350  FOR POT=Rngs TO Rnge STEP IDE
01360  POTENTIAL=POT
01370  FOR K=1 TO DELAY
01380  NEXT K
01390  M=M+1
01400  CHAN=$0100
01410  CURR(M)= FIX(-VOLTS)
01420  RECORDER=CURR(M)
01440  NEXT POT
01441  CURR(8)=M
01442  PDRB[1]=0
01445  RECORDER=0
01450  RETURN
01460  REM *******************************
01470  REM   PROCEDURE: HEADER
01485  DEF HEADER
01490  CURR(1)=PRG
01500  CURR(2)=ED
01510  CURR(3)=TD
01520  CURR(4)=RNGS
01530  CURR(5)=RNGE
01540  CURR(6)=RATE
01550  CURR(7)=FS
01552  CURR(9)=DE
01560  RETURN
01822  REM *******************************
01823  REM   PROCEDURE: NEWDROP
01825  DEF NEWDROP
01826  PDRA[2]=1
01828  PDRA[2]=0
01829  PDRA[1]=0
01830  FOR I=1 TO 40
01831  PDRA[0]=0
01832  FOR K=1 TO 12
01833  NEXT K
01834  PDRA[0]=1
01835  FOR K=1 TO 12
01836  NEXT K
01837  NEXT I
01838  RETURN
```

APPENDIX C - (continued)

```
01940  REM ******************************
01941  REM  PROCEDURE: DISKDRV
01945  DEF DISKDRV(STAT)
01955  IF STAT=On THEN 1970
01960  DRVSEL=$0
01965  DRVSEL=$10
01967  RETURN
01970  DRVSEL=$4
01972  WAIT(1)
01975  RETURN
01980  REM *****************************
01981  REM  PROCEDURE : DISPSTAT
01990  DEF DISPSTAT(SN)
01992  CURSPOS(16)
01995  IF SN>=4 THEN  PRINT  USING 2051,PR$,DEP$,EQL$
01996  IF SN=1 THEN  PRINT  USING 2010,INV$,PR$,INV$,DEP$,EQL$
01997  IF SN=2 THEN  PRINT  USING 2020,PR$,INV$,DEP$,INV$,EQL$
01998  IF SN=3 THEN  PRINT  USING 2030,PR$,DEP$,INV$,EQL$,INV$
01999  IF SN=4 THEN  PRINT  USING 2040,INV$,SCN$,INV$,RDY$
02000  IF SN=5 THEN  PRINT  USING 2050,SCN$,INV$,RDY$,INV$
02001  IF SN<=3 THEN  PRINT  USING 2052,SCN$,RDY$
02010  IMAGE "[2][22,C][2][20,C][28,C][2]"
02020  IMAGE "[22,C][2][20,C][2][28,C][2]"
02030  IMAGE "[22,C][20,C][2][28,C][2][2]"
02040  IMAGE "[2][22,C][2][48,C][2]"
02050  IMAGE "[22,C][2][48,C][2][2]"
02051  IMAGE "[22,C][20,C][28,C][/1]"
02052  IMAGE "[/1][22,C][48,C][2]"
02055  CURSPOS(11)
02060  RETURN
02100  REM *******************************
02102  REM  PROCEDURE : EXIT
02110  DEF EXIT
02112  PRINT ERA$;
02115  DRVSEL=$4
02120  WAIT(1)
02125  CALL XDOS
02130  RETURN
02995  REM ************************************************************
02997  REM        MAIN PROGRAM
02998  REM ************************************************************
02999  REM
03000  DISKDRV(Off)
03005  PRINT ERA$;
03010  CANVAS1
03011  CANVAS2
03012  CURSPOS(11)
03020  ON  KEY 1 THEN  INPUT "PURGE TIME (secs) ",PRG
03025  ON  KEY 2 THEN  INPUT "DEPOSITION TIME (secs) ",TD
03030  ON  KEY 3 THEN  INPUT "SCAN RANGE (START,END) (mV) ",RNGS,RNGE
03035  ON  KEY 4 THEN  INPUT "STEP E (mV) ",DE
03040  ON  KEY 5 THEN  INPUT "DEPOSITION POTENTIAL (mV) ",ED
03045  ON  KEY 6 THEN  INPUT "EQUILIBRATION TIME (secs) ",EQ
03050  ON  KEY 7 THEN  INPUT "SCAN RATE (mV/secs) ",RATE
03055  ON  KEY 8 THEN  INPUT "NUMBER OF REPETITIONS ",RPT
03060  ON  KEY 9 THEN I=0
03065  ON  KEY 10 THEN I=0
03067  ON  KEY 12 THEN I=0
03070  ON  KEY 16 THEN EXIT
03089  REM *****************************
03090  REM  FKEY WAITING LOOP
04000  FK= FKEY
04010  IF FK=0 THEN 4000
04020  IF FK=9 THEN 5000
```

APPENDIX C - (continued)

```
04030   IF FK=10 THEN 170
04032   IF FK=12 THEN 6000 \ Save data in file
04040   CANVAS1
04050   PRINT CLRL$;
04060   GOTO 4000
04990   REM *****************************
04991   REM   ASV EXPERIMENT
05000   DISPSTAT(1)
05005   PURGE(PRG)
05010   FOR IR=1 TO RPT
05020   NEWDROP
05030   POTENTIAL=ED
05040   CELL(On)
05050   DISPSTAT(2)
05060   WAIT(TD)
05070   STIRRER(Off)
05080   DISPSTAT(3)
05090   WAIT(EQ)
05095   DISPSTAT(4)
05100   SCAN(RATE,RNGS,RNGE,DE)
05110   CELL(Off)
05120   POTENTIAL=0
05130   STIRRER(On)
05140   DISPSTAT(5)
05150   NEXT IR
05160   GOTO 4000
05995   REM ******************************
05996   REM   SAVE IN FILE
06000   HEADER
06010   INPUT "FILE NAME ",FNAM$
06020   DISKDRV(On)
06030   OPEN #3,FNAM$,O
06040   RNGT= ABS(RNGS-RNGE)
06050   FOR J=1 TO RNGT+10
06060   PRINT #3 CURR(J)
06070   NEXT J
06080   CLOSE #3
06090   DISKDRV(Off)
06095   CURSPOS(11)
06096   PRINT CLRL$;
06100   GOTO 4000
09000   END
```

APPENDIX C - ASV5 - anodic stripping voltammetry program for Tacussel-PRG5

```
00020  REM ********************************************************************
00030  REM   PROGRAM  ASV5L                                   VERSION 03.09.84
00040  REM
00049  REM   STOPS and STARTS linear scan on PRG5
00050  REM   Manually set PRG5 initial potential to +2500mV
00060  REM   Compiled with:  BASICM ASV5L.SA:1; D=$2000, P=$4000, R=$8000, OS
00062  REM   RUN with     :  BLOAD ASV5L.LO:1;G
00080  REM
00090  REM *********************************************************************
00160  REM   INITIALIZE CONSTANTS
00165  REM
00170  DIM Prg$(1) ADDR $E0A4,Edep$(1) ADDR $E0C9
00180  DIM Tdep$(1) ADDR $E0F4,Tequ$(1) ADDR $E119
00200  DIM Srng$(1) ADDR $E144,Srate$(1) ADDR $E169
00220  DIM Cset$(1) ADDR $E194,Rep$(1) ADDR $E1B9
00250  REM
00251  CLRL$= CHR$($1B)+ CHR$($4B)
00252  INV$= CHR$($1B)+ CHR$($42)
00253  ERA$= CHR$($1B)+ CHR$($45)
00254  UCUR$= CHR$($1B)+ CHR$($55)
00255  DCUR$= CHR$($1B)+ CHR$($56)
00256  HCUR$= CHR$($1B)+ CHR$($4C)
00257  REM
00260  EXT XDOS ADDR $E800
00262  REM
00265  BYTE DRVSEL ADDR $EC08
00270  BYTE CRA ADDR $ED21,CRB ADDR $ED23
00280  BYTE DDRA ADDR $ED20,DDRB ADDR $ED22
00290  BYTE PDRA ADDR $ED20,PDRB ADDR $ED22
00300  BYTE DU1 ADDR Edep$,DU2 ADDR Tdep$
00320  BYTE DU3 ADDR Tequ$,DU4 ADDR Srng$
00340  BYTE DU5 ADDR Srate$,DU6 ADDR Prg$
00360  BYTE DU7 ADDR Cset$,DU8 ADDR Rep$
00363  BYTE KF1(4) ADDR $E0A0,KF5(4) ADDR $E0C5
00364  BYTE KF2(4) ADDR $E0F0,KF6(4) ADDR $E115
00365  BYTE KF3(4) ADDR $E140,KF7(4) ADDR $E165
00366  BYTE KF4(4) ADDR $E190,KF8(4) ADDR $E1B5
00368  REM
00370  INTEGER CHAN ADDR $EC1A,VOLTS ADDR $EC1D
00400  INTEGER POTENTIAL ADDR $EC14,POT,RATE
00420  INTEGER FS,COUNT,SECS,On,Off
00430  INTEGER DLY,STAT,DELAY,M,I,J,K,L
00440  INTEGER RNGS,RNGE,RNGT,ED,SN,FK,IR
00452  REM
00499  RESTORE
00500  DATA 0,0,$FF,$FF,$4,$4,$28,0,0
00510  DATA -1000,1,0,100,30,-1000,0,1000,20,0,1,1
00511  DATA 1
00512  DATA "PURGING","ELECTROLYSIS","EQUILIBRATION"
00514  DATA "SCANNING","READY--MAKE SELECTION"
00520  READ CRA,CRB,DDRA,DDRB,CRA,CRB,PDRA,PDRB,POTENTIAL
00530  READ ED,On,Off,TD,EQ,RNGS,RNGE,RNGT,RATE,PRG,FS,RPT
00531  READ DE
00532  READ PR$,DEP$,EQL$,SCN$,RDY$
00540  REM
00600  DATA $A0,$A0,$A0,$A0,$A0,$A0,$A0,$A0
00602  DATA $C6,$C6,$C6,$C6,$C6,$C6,$C6,$C6
00604  DATA $B1,$B2,$B3,$B4,$B5,$B6,$B7,$B8
00606  DATA $A0,$A0,$A0,$A0,$A0,$A0,$A0,$A0
00660  REM
00665  GOTO 3000
00669  REM *******************************
00670  REM   PROCEDURE: CURSPOS(L)
00672  DEF CURSPOS(L)
```

APPENDIX C - (continued)

```
00673  PRINT HCUR$;
00676  IF L=1 THEN  RETURN
00677  IF L=2 THEN  PRINT
00678  IF L=2 THEN  RETURN
00679  FOR I=1 TO L-2
00680  PRINT DCUR$;
00682  NEXT I
00683  PRINT
00684  RETURN
00690  REM
00691  REM ******************************
00692  REM   PROCEDURE: CANVAS1 & 2
00700  DEF CANVAS1
00710  Prg$= STR$(PRG,"PURGE TIME : [5] secs")
00720  DU6=$20
00730  Edep$= STR$(ED,"DEP.POTENTIAL :     [5] mV")
00740  DU1=$20
00750  Tdep$= STR$(TD,"DEP.TIME    : [5] secs")
00760  DU2=$20
00770  Tequ$= STR$(EQ,"EQUILIBRATION :  [5] secs")
00780  DU3=$20
00790  Srngs$= STR$(RNGS,"SCAN RANGE : [5] TO ")
00800  Srnge$= STR$(RNGE,"[5] mV")
00810  Srng$=Srngs$+Srnge$
00820  DU4=$20
00830  Srate$= STR$(RATE,"PRG5 SCAN RATE:[5] mV/sec")
00840  DU5=$20
00850  Cset$= STR$(DE,"STEP E      : [5] mV")
00860  DU7=$20
00870  Rep$= STR$(RPT,"REPETITIONS   : [2]")
00875  DU8=$20
00876  CURSPOS(11)
00877  RETURN
00880  DEF CANVAS2
00882  PRINT HCUR$;
00885  PRINT  USING "[2][X27]PARAMETERS SET[X30][2]",INV$,INV$
00886  REM
00890  FOR I=1 TO 4
00892  READ KF1(I),KF2(I),KF3(I),KF4(I),KF5(I),KF6(I),KF7(I),KF8(I)
00894  NEXT I
00897  REM  ** CANVAS2 ************
00905  CURSPOS(8)
00925  PRINT INV$;" F9 ";INV$;" START      ";INV$;"F10 ";INV$;
00926  PRINT " RESET       ";
00927  PRINT INV$;" F16 ";INV$;" EXIT"
00930  CURSPOS(14)
00940  PRINT  USING "[2][X27]PRESENT STATUS[X30][2][2]",INV$,INV$
00941  CURSPOS(16)
00945  PRINT  USING "[22,C][20,C][28,C][2]",PR$,DEP$,EQL$
00946  CURSPOS(18)
00950  PRINT  USING "[22,C][2][48,C][2]",SCN$,INV$,RDY$,INV$;
00955  CURSPOS(11)
00960  RETURN
00995  REM
00999  REM ******************************
01000  REM   PROCEDURE:  WAIT
01020  DEF WAIT(SECS)
01030  IF SECS<=0 THEN  RETURN
01040  COUNT=0
01050  COUNT=COUNT+1
01060  FOR K=$1 TO $19F0
01070  NEXT K
01080  IF COUNT#SECS THEN  GOTO 1050
01090  RETURN
```

APPENDIX C - (continued)

```
01100  REM ******************************
01110  REM   PROCEDURE: STIRRER
01130  DEF STIRRER(STAT)
01140  PDRA[3]=STAT
01150  RETURN
01220  REM ******************************
01230  REM   PROCEDURE: PURGE
01250  DEF PURGE(SECS)
01252  IF SECS<1 THEN  RETURN
01254  PDRA[4]=On
01258  WAIT(SECS)
01260  PDRA[4]=Off
01270  RETURN
01280  REM ******************************
01290  REM   PROCEDURE:  STARTSCAN
01310  DEF STARTSCAN
01340  PDRB[0]=1 \ Start scan pulse
01345  WAIT(1)
01350  PDRB[0]=0
01360  RETURN
01370  REM ******************************
01380  REM   PROCEDURE:  STOPSCAN
01390  DEF STOPSCAN
01400  PDRB[2]=1 \ Stop scan pulse
01405  WAIT(1)
01410  PDRB[2]=0
01450  RETURN
01460  REM ******************************
01941  REM  PROCEDURE: DISKDRV
01945  DEF DISKDRV(STAT)
01955  IF STAT=On THEN 1970
01960  DRVSEL=$0
01965  DRVSEL=$10
01967  RETURN
01970  DRVSEL=$4
01972  WAIT(1)
01975  RETURN
01980  REM *****************************
01981  REM  PROCEDURE : DISPSTAT
01990  DEF DISPSTAT(SN)
01992  CURSPOS(16)
01995  IF SN>=4 THEN  PRINT  USING 2051,PR$,DEP$,EQL$
01996  IF SN=1 THEN  PRINT  USING 2010,INV$,PR$,INV$,DEP$,EQL$
01997  IF SN=2 THEN  PRINT  USING 2020,PR$,INV$,DEP$,INV$,EQL$
01998  IF SN=3 THEN  PRINT  USING 2030,PR$,DEP$,INV$,EQL$,INV$
01999  IF SN=4 THEN  PRINT  USING 2040,INV$,SCN$,INV$,RDY$
02000  IF SN=5 THEN  PRINT  USING 2050,SCN$,INV$,RDY$,INV$
02001  IF SN<=3 THEN  PRINT  USING 2052,SCN$,RDY$
02010  IMAGE "[2][22,C][2][20,C][28,C][2]"
02020  IMAGE "[22,C][2][20,C][2][28,C][2]"
02030  IMAGE "[22,C][20,C][2][28,C][2][2]"
02040  IMAGE "[2][22,C][2][48,C][2]"
02050  IMAGE "[22,C][2][48,C][2][2]"
02051  IMAGE "[22,C][20,C][28,C][/1]"
02052  IMAGE "[/1][22,C][48,C][2]"
02055  CURSPOS(11)
02060  RETURN
02100  REM *******************************
02102  REM  PROCEDURE : EXIT
02110  DEF EXIT
02112  PRINT ERA$;
02115  DRVSEL=$4
02120  WAIT(1)
02125  CALL XDOS
```

APPENDIX C - (continued)

```
02130  RETURN
02995  REM ************************************************************
02997  REM        MAIN PROGRAM
02998  REM ************************************************************
02999  REM
03000  DISKDRV(Off)
03005  PRINT ERA$;
03010  CANVAS1
03011  CANVAS2
03012  CURSPOS(11)
03020  ON  KEY 1 THEN  INPUT "PURGE TIME (secs) ",PRG
03025  ON  KEY 2 THEN  INPUT "DEPOSITION TIME (secs) ",TD
03030  ON  KEY 3 THEN  INPUT "SCAN RANGE (START,END) (mV) ",RNGS,RNGE
03035  ON  KEY 4 THEN  INPUT "STEP E (mV) ",DE
03040  ON  KEY 5 THEN  INPUT "DEPOSITION POTENTIAL (mV) ",ED
03045  ON  KEY 6 THEN  INPUT "EQUILIBRATION TIME (secs) ",EQ
03050  ON  KEY 7 THEN  INPUT "SCAN RATE (mV/secs) ",RATE
03055  ON  KEY 8 THEN  INPUT "NUMBER OF REPETITIONS ",RPT
03060  ON  KEY 9 THEN I=0
03065  ON  KEY 10 THEN I=0
03067  ON  KEY 12 THEN I=0
03070  ON  KEY 16 THEN EXIT
03089  REM *****************************
03090  REM  FKEY WAITING LOOP
04000  FK= FKEY
04010  IF FK=0 THEN 4000
04020  IF FK=9 THEN 5000
04030  IF FK=10 THEN 170
04040  CANVAS1
04050  PRINT CLRL$;
04060  GOTO 4000
04990  REM *****************************
04991  REM   ASV EXPERIMENT
05000  DISPSTAT(1)
05005  PURGE(PRG)
05010  FOR IR=1 TO RPT
05030  POTENTIAL=- INT(ED*4135/5000)
05050  DISPSTAT(2)
05060  WAIT(TD)
05070  STIRRER(Off)
05080  DISPSTAT(3)
05090  WAIT(EQ)
05095  DISPSTAT(4)
05100  STARTSCAN
05104  WSEC= ABS(RNGE-RNGS)/RATE
05105  WAIT(WSEC)
05120  STOPSCAN
05125  POTENTIAL=0
05130  STIRRER(On)
05140  DISPSTAT(5)
05150  NEXT IR
05160  GOTO 4000
05995  REM ******************************
09000  END
```

APPENDIX D - CHRPOT - chronopotentiometry program

```
00005  REM PROGRAM CHRPOT                                      VERSION 30.06.81
00010  REM Short program for doing chronopotentiometry.
00011  REM
00015  REM ********************************
00016  REM      INITIALIZE CONSTANTS
00017  REM ********************************
00100  INTEGER CHAN ADDR $EC1A,VOLTS ADDR $EC1D
00110  INTEGER ED,COUNT,K,I,TD,ECH,ECHAN(400)
00111  INTEGER EI,EQ,SECS,PURG
00120  INTEGER POTEN ADDR $EC14
00125  INTEGER CMAX,AV,AVMAX,Y,X,EMX,CH
00130  BYTE CRA ADDR $ED21,CRB ADDR $ED23
00140  BYTE DDRA ADDR $ED20,DDRB ADDR $ED22
00150  BYTE PDRA ADDR $ED20,PDRB ADDR $ED22
00155  BYTE SCREEN(22,80) ADDR $E000
00160  CRA=$0
00165  CRB=$0
00170  DDRA=$FF
00175  DDRB=$FF
00180  CRA=$4
00185  CRB=$4
00190  PDRA=$28
00195  PDRB=$1
00210  EQ=20
00239  GOTO 290
00240  REM *******************************
00241  REM     PROCEDURE: WAIT(SECS)
00242  REM *******************************
00243  DEF WAIT(SECS)
00244  IF SECS<=0 THEN  RETURN
00245  COUNT=0
00250  COUNT=COUNT+1
00255  FOR K=1 TO $19F0
00260  NEXT K
00265  IF COUNT#SECS THEN  GOTO 250
00270  RETURN
00290  REM *******************************
00291  REM     GET INPUT
00292  REM********************************
00300  INPUT "E-DEP (MV) ",ED
00310  INPUT "T-DEP (SECS) ",TD
00320  INPUT "PURGE (SECS) ",PURG
00335  REM *******************************
00336  REM     DEPOSITION STEP
00337  REM *******************************
00340  PDRA[4]=1 \ Purge
00342  WAIT(PURG)
00345  PDRA[4]=0
00348  POTEN=ED \ Set potential
00350  PDRB[2]=1 \ Cell on
00360  PDRA[3]=1
00365  REM
00400  WAIT(TD)
00500  PDRA[3]=0
00510  WAIT(EQ)
00600  PDRB[3]=1 \ Switch to galvanostatic mode.
00690  REM *******************************
00691  REM     COLLECT DATA
00692  REM *******************************
00700  CHAN=$0
00710  EI= FIX(-VOLTS)
00720  IF EI<1 THEN  GOTO 800
00730  ECHAN(EI)=ECHAN(EI)+1
00735  FOR K=1 TO 80
```

APPENDIX D - (continued)

```
00736  NEXT K
00740  GOTO 700
00800  PDRB[2]=0
00810  PDRB[3]=0
00820  PDRA[3]=1
01000  MAT SCREEN= SET [$20]
01005  CMAX=ECHAN(1)
01006  CH=0
01007  EMX=0
01010  FOR I=1 TO 400
01015  IF ECHAN(I)>=CMAX THEN EMX=I
01020  IF ECHAN(I)>=CMAX THEN CMAX=ECHAN(I)
01030  NEXT I
01040  FOR I=EMX-10 TO EMX+10
01050  CH=CH+ECHAN(I)
01060  NEXT I
01100  FOR I=1 TO 400
01110  ECHAN(I)= FIX(16*(ECHAN(I)/CMAX))
01130  NEXT I
01200  FOR ECH=0 TO 390 STEP 6
01210  AV=0
01220  FOR K=1 TO 6
01230  AV=AV+ECHAN(ECH+K)
01240  NEXT K
01250  Y=17- FIX(AV/6)+1
01255  X= FIX((ECH+6)/6)+5
01259  SCREEN(Y,X)=$2A
01260  FOR I=Y+1 TO 18
01262  SCREEN(I,X)=$21
01264  NEXT I
01270  NEXT ECH
01280  FOR K=4 TO 18
01284  SCREEN(K,72)=$7C
01285  SCREEN(K,5)=$7C
01286  NEXT K
01290  FOR K=5 TO 72
01292  SCREEN(19,K)=$2D
01293  SCREEN(4,K)=$5F
01294  NEXT K
01300  EMX= FIX(EMX*2.5)
01310  PRINT  USING "PEAK AT [4] ",EMX," MV";
01311  PRINT  USING "         CHARGE = [4] ",CH
01315  INPUT "ANOTHER RUN ",AN$
01320  IF AN$="Y" THEN  GOTO 100
01390  END
```

APPENDIX E - STRPOL - stripping polarography program

******** TO BE ADDED ********

APPENDIX F - PLOTR - linear curve smoothing program

```
00010  REM *****************************************************************
00020  REM    PROGRAM PROTR                                  VERSION 16.3.81
00030  REM
00040  REM    SMOOTHING FUNCTION USING 15 POINT MOVING AVERAGE.
00050  REM
00060  REM *****************************************************************
00070  INTEGER CURR(1010)
00080  INTEGER RECORDER ADDR $EC16
00090  INTEGER I,J,K,L
00100  INTEGER PARAM1(9)
00110  REM ****************************************
00120  REM *   INPUT DATA FROM DISK FILE
00130  INPUT "FILE NAME ",FNAM$
00140  OPEN #3,FNAM$,I
00150  FOR I=1 TO 9
00160  INPUT #3 ,PARAM1(I)
00170  NEXT I
00180  RNGT= ABS(PARAM1(4)-PARAM1(5))
00190  FOR J=1 TO RNGT
00200  INPUT #3 ,CURR(J)
00210  NEXT J
00220  REM ***************************************
00230  REM *   SMOOTHING LOOP
00235  FOR K=8 TO RNGT-7
00240  SUM=0
00250  FOR J=K-7 TO K+7
00260  SUM=SUM+CURR(J)
00270  NEXT J
00280  CURR(K)= FIX(SUM/15)
00290  NEXT K
00300  REM ***************************************
00310  REM *   OUTPUT TO PAPER RECORDER
00315  FOR K=1 TO RNGT
00320  PRINT CURR(K)
00330  RECORDER=CURR(K)
00340  NEXT K
00350  STOP
```

APPENDIX F - PLOTRQ - quadratic curve smoothing program

```
00100  REM **************************************************************
00200  REM    PROGRAM PLOTRQ                             VERSION 17.11.81
00300  REM
00400  REM    CONVOLUTES SMOOTHING USING QUADRATIC CUBIC FOR 15 POINTS.
00500  REM
00550  REM **************************************************************
00600  INTEGER CURR(1010)
00700  INTEGER RECORDER ADDR $EC16
00800  INTEGER I,J,K,L
00900  INTEGER PARAM1(9)
01000  INTEGER NP(15)
01050  REM**************************************************
01060  REM *   INITIALIZE CONVOLUTING INTEGERS
01100  NP(1)=-78
01200  NP(2)=-13
01300  NP(3)=42
01400  NP(4)=87
01500  NP(5)=122
01600  NP(6)=147
01700  NP(7)=162
01800  NP(8)=167
01900  NP(9)=NP(7)
02000  NP(10)=NP(6)
02100  NP(11)=NP(5)
02200  NP(12)=NP(4)
02300  NP(13)=NP(3)
02400  NP(14)=NP(2)
02500  NP(15)=NP(1)
02550  REM *************************************************
02560  REM *   INPUT DATA FROM DISK FILE
02600  INPUT "FILE NAME ",FNAM$
02700  OPEN #3,FNAM$,I
02800  FOR I=1 TO 9
02900  INPUT #3 ,PARAM1(I)
03000  NEXT I
03100  RNGT= ABS(PARAM1(4)-PARAM1(5))
03200  FOR J=1 TO RNGT
03300  INPUT #3 ,CURR(J)
03400  NEXT J
03500  REM *************************************************
03550  REM *   SMOOTHING LOOP
03600  FOR K=8 TO RNGT-7
03700  SUM=0
03800  FOR J=K-7 TO K+7
03900  SUM=SUM+(CURR(J)*NP(J-K+8))
04000  NEXT J
04100  CURR(K)= FIX(SUM/1105)
04200  NEXT K
04300  REM *************************************************
04350  REM *   OUTPUT TO RECORDER
04400  FOR K=1 TO RNGT
04500  RECORDER=CURR(K)
04600  PRINT CURR(K)
04700  NEXT K
04800  STOP
```

APPENDIX G - BLINE - baseline subtraction program

```
00005  REM ***************************************************************************
00006  REM   PROGRAM BLINE                                         VERSION 14.8.81
00007  REM
00009  REM   SUBTRACTS BASELINE DATA POINTS IN ONE DISK FILE FROM
00010  REM   DATA POINTS IN ANOTHER DISK FILE. SENDS OUTPUT TO
00011  REM   PAPER RECORDER.
00012  REM
00013  REM ***************************************************************************
00020  BYTE CRB ADDR $ED23
00025  BYTE DDRB ADDR $ED22
00030  BYTE PDRB ADDR $ED22
00035  CRB=0
00040  DDRB=$FF
00045  CRB=$4
00050  PDRB=0
00100  INTEGER I,J,K,HD1(9),HD2(9),RNGT
00110  INTEGER REC ADDR $EC16
00120  INTEGER BVAL(1010),DVAL(1010)
00124  REM *********************************************
00125  REM *   GET DATA FROM FILES
00130  INPUT "BASELINE FILE NAME",BNAM$
00140  INPUT "DATA FILE NAME",FNAM$
00150  OPEN #3,BNAM$,I
00155  OPEN #4,FNAM$,I
00160  FOR I=1 TO 9
00165  INPUT #3 ,HD1(I)
00170  INPUT #4 ,HD2(I)
00175  NEXT I
00180  RNGT= ABS(HD2(4)-HD2(5))
00190  FOR J=1 TO RNGT
00195  INPUT #3 ,BVAL(J)
00200  NEXT J
00210  FOR J=1 TO RNGT
00215  INPUT #4 ,DVAL(J)
00220  NEXT J
00222  REM *********************************************
00223  REM *   SUBTRACT AND OUTPUT TO RECORDER
00290  PDRB[1]=1 \ Recorder on
00300  FOR K=1 TO RNGT
00310  REC= FIX(DVAL(K)-BVAL(K))
00315  FOR I=1 TO 40
00316  NEXT I
00320  NEXT K
00330  PDRB[1]=0 \ Recorder off
00900  STOP
```

APPENDIX H - Solubility of elements in mercury *

Element	Weight %	Notes	Element	Weight %	Notes
Ag	0.066		Nb	0.001	
Al	0.002		Ni	4×10^{-5}	
As	0		Pb	1.10	
Au	0.131		Pd	0.006	
Ba	0.330		Pt	0.09	24°C
Be	1×10^{-6}	100°C	Rb	1.37	[27]
Bi	1.10		Re	0	
Ca	0.30	25°C	Rh	0.16	
Cd	5.30		Ru	0.353	
Ce	0.016		Sb	2.9×10^{-5}	
Co	1×10^{-6}	[109]	Si	0.001	
Cr	$<10^{-7}$	[109]	Sn	0.60	
Cs	4.0	25°C	Sr	1.04	
Cu	0.003		Ta	0	
Fe	$<10^{-7}$	[109]	Th	0.016	
Ga	1.13	22°C	Ti	5×10^{-6}	
Ge	0.027	350°C [109]	Tl	42.8	
In	57.0		V	5×10^{-5}	
Ir	$<10^{-5}$	[110]	W	1×10^{-5}	
K	0.395	0.46 [109]	Zn	1.99	
La	0.009	25°C	Zr	0.003	
Li	0.048	25°C			
Mg	0.310	17°C			
Mn	0.0018				
Na	0.57	25°C			

* All values taken from reference [27] and are for 20°C unless otherwise indicated.

APPENDIX I

Intermetallic compounds considered as good mercury-film substrates, but either not made or made and not used, for the reasons given.

SUBSTRATE	REASONS NOT MADE OR USED
Ni_2Ge	made but not used - extremely brittle
$PtSb_2$	not made - b.p. of Sb < m.p. of Pt
Au_2Be	not made - poisonous to RF-furnace
AuLa	not made - interaction with melting crucible
AuTe	not made - Te not available

Other miscellaneous types of substrates, already on hand, and whose mercury-film formation properties were sometimes well known, but tested for comparative reasons. (all substrates were fitted to the RDE Teflon tip, deposition was in 0.1M KNO_3 + 0.001M Hg^{++}, with other conditions as indicated below.

SUBSTRATE	REASONS NOT USED OR FURTHER TESTED
B_4C	Hg deposition between 0 to -1000mV always gave Hg spheres, surface difficult to polish, made of compressed powder, surface not homogen.
HgS	compressed powder, fell apart when placed in solution, application of 0 to -1000mV caused decomposition of surface into Hg and S
glas.C	Hg film formed at 0 to -1000mV always results in Hg spheres [55,75] (Sec.1.3)
Pt	Hg film formed, Pt-Hg formed [43-45] (Sec.1.3)

APPENDIX J - HALFWAVE - calculates log-plot parameters for polarographic curve

```
10   REM  **** Program HALFWAVE                          Version 28.08.84-spk
14   REM  **** Calculates the log-plot slope (theoretically = 59.2/n mV
15   REM       for a reversible polarogram at 25 deg.C), the halfwave
20   REM       potential E(1/2), and the correlation coefficient r, based
25   REM       on the premise that all current data including the
30   REM       limiting diffusion current have equal uncertainties.
35   REM       For other premises, alter LINE 170 as indicated in Table 2
40   REM       of reference:
45   REM
90   HOME :I(20),E(20)
100   INPUT "Number of I,E values (20 max) : ";N: PRINT
110   INPUT "Diffusion limited current (uA) : ";ID
130   HOME : HTAB 1: PRINT "E (mV)                 I (uA)": PRINT
135   FOR J = 1 TO N
140   HTAB 1: VTAB J + 2: PRINT "E(";J;") = ";: INPUT "";E(J)
145   HTAB 20: VTAB J + 2: PRINT "I(";J;") = ";: INPUT "";I(J)
147   NEXT J
150   GOSUB 400
151  S1 = 0:S2 = 0:S3 = 0:S4 = 0:S5 = 0:S6 = 0
152   POKE 33,80
153   PRINT : VTAB 1: POKE 1403,45: INVERSE : PRINT " For T = 25 deg.C ": NORMAL

155   FOR J = 1 TO N
160  Z = I(J) / ID
170  W = (Z * (1 - Z)) / ( SQR (1 + Z * Z))
180   IF W <  = 0 THEN  GOTO 270
190  W = W ^ 2
200  S1 = S1 + W
210  Y = W *  LOG ((1 - Z) / Z):S2 = S2 + Y
220  S3 = S3 + (Y ^ 2) / W
240  X = W * E(J):S4 = S4 + X
250  S5 = S5 + (X ^ 2) / W
260  S6 = S6 + X * Y / W
270   NEXT J
280  X = (S1 * S6) - (S2 * S4)
290  Y = (S1 * S5) - (S4 * S4)
300  B = (Y / X) * 2.303
310  EH = ((S4 * S6) - (S5 * S2)) / X
320  R = X /  SQR (Y * ((S1 * S3) - (S2 * S2)))
322  NE =  INT ((59.2 / B) * 10) / 10
325   VTAB 3: POKE 1403,45: CALL  - 868: PRINT "Slope = ";B;"/n mV"
330   VTAB 5: POKE 1403,45: CALL  - 868: PRINT "E(1/2) = ";EH;" mV"
340   VTAB 7: POKE 1403,45: CALL  - 868: PRINT "r = ";R
345   VTAB 9: POKE 1403,45: CALL  - 868: PRINT NE;" electron reaction"
346   POKE 33,40
350   GOSUB 800: GOTO 150
399   REM
400   VTAB 23: HTAB 1: CALL  - 868: PRINT "<M>odify, <C>alculate, <Q>uit ?
      ";: GET A$
410   PRINT A$;
420   IF A$ = "C" THEN  GOSUB 800: RETURN
425   IF A$ = "Q" THEN  GOSUB 800: POKE 33,80: END
430   IF A$ <  > "M" THEN  GOTO 400
440   GOSUB 800: PRINT "Which E,I value (1-";N;") : ";: INPUT "";J
442   IF J < 1 OR J > N THEN  GOTO 440
445   VTAB J + 2: HTAB 1: CALL  - 868: PRINT "E(";J;") = ";
446   VTAB J + 2: HTAB 20: PRINT "I(";J;") = "
450   VTAB J + 2: HTAB 1: PRINT "E(";J;") = ";: INPUT "";E(J)
455   VTAB J + 2: HTAB 20: PRINT "I(";J;") = ";: INPUT "";I(J)
460   GOTO 400
800   PRINT : VTAB 23: HTAB 1: CALL  - 868: RETURN
```

RESUME FRANCAIS

Les tentatives pour comprendre la distribution des espèces chimiques dans l'environnement aquatique peut profiter substantiellement des perfectionnements des capacités des techniques de voltammétrie inverse.

Les limitations les plus importantes pour l'interprétation des données obtenues, à partir de telles techniques, sont liées à la géométrie et à l'hydraudynamique de l'éléctrode, spécialement durant l'étape de déposition. Une électrode idéale peut être stable mécaniquement et chimiquement et posséder un surpotentiel d'hydrogène élévé. Des électrodes à gouttes et film de mercure possèdent une partie de ces propriétés et ont, donc, été généralement utilisées dans les études voltammétriques. Cependant, des sérieuses limitations existent pour les électrodes à gouttes de mercure dans les études de spéciation, particulièrement dans les limites de leur "masse" relative par rapport à la diffusion interne et leur hydrodynamique plutôt peu incontrôlé et non uniforme et de diffusion à leur surface sphérique.

La configuration idéale est sans doute un film mince de mercure avec un flux contrôllé sur sa surface. Un système hydrodynamique qui approche une surface hydraudynamiquement uniforme est le disque tournant. Ainsi la combinaison d'un film mince de mercure sur un disque tournant fournit certaines des propriétés désirées d'une "électrode idéale". Il semble que trouvant un substrait "approprié" sur lequel un film de mercure peut être formé a été, malgré tous les efforts de tant d'electrochimists, un but plutôt inatteignable.

Ce substrait doit: *i)* posséder une bonne mouillabilité par le mercure, et *ii)* être chimiquement inerte par rapport

au mercure et à tous les métaux devant être réduit dans le mercure. Ni l'un ni l'autre des substraits couramment utilisé, platine et carbone-vitreux, possèdent ces deux propriétés. Le premier est en réalité une électrode à film amalgamé, tandis que le dernier est une électrode à mono-couche de gouttelettes de mercure.

Etant donné que seul un nombre limité de matériaux on été testé comme substraits pour film de mercure, le but de ce travail de thèse est de comparer différents types de substraits, de selectionner le meilleur par rapport à sa facilité de maintenir un vrai film de mercure sur sa surface et de montrer son applicabilité potentiel à la spéciation de métaux en trace.

1. Dessein et Développement du Système Analytique

Le système complet, comme structuré pour cette recherche, se compose à la base, d'un micro-ordinateur avec deux interfaces spéciaux pour l'acquisition et le contrôle des données, un potentiostat/galvanostat, une cellule spéciale en plexiglasse, avec circulation de flux, et un microscope refléchissant inversé.

En contraste aux systèmes existants, il permet de contrôler simultanément le courant et le potentiel à une électrode, pendant l'observation microscopique "in-situ" de sa surface. D'autre part, la circulation de flux permet l'échange des solutions testés sans couper le contact électode-solution. Le système est surtout construit pour être facilement adaptable a une variété d'expériences électrochiméiques.

2. Sélection d'un Substrait pour un Film de Mercure

A première vue, il apparait que la plupart des matériaux qui supportent un bon film de mercure, le font plus précisément parce qu'ils sont solubles dans le mercure, et/ou forment un composé avec le mercure. Cependant, des interactions attractives s'observant à grande distance, dues aux forces de London-Van der Walls, peuvent aussi exister aux interfaces. Ces forces peuvent fournir dans le cas où aucune réaction et/ou solvation n'apparaisent un moyen de former un film de mercure stable.

Une sélection initiale des matériaux a été faite en se basant sur la faible solubilité, et sur l'interaction non-chimique du substrait avec le mercure comme défini par le fonction de travail électrochimique.

Les substraits sélectionnées pour les testes étaient: NiAl, NiSb, PtSi, PtSiCo et Ir.

Aucun des quatres alliages testés se comportent comme prédit. Ils possèdent tous les propriétés désirées étant insolubles (dans le mercure) et chimiquement non-réactifs avec le mercure, mais malheureusement, ils montrent aucune tendance à former un quelconque type de liasons favorisant le film. Dans le cas des deux alliages de Ni, ils subissent, également, une réaction électrochimique indésirable causant l'oxydation et/ou la détérioration de leurs surfaces.

Les résultats préliminaires obtenus pour le substrait d'iridium sont très prometteurs et indiquent qu'il possède simultanément les deux propriétés d'insolubilité et de liaison avec le mercure.

3. Caractérisation de l'Iridium comme Substrait pour un Film de Mercure

Le but de cette partie de la recherche est de quantifier les paramètres qui sont nécessaires à l'optimalisation de la formation d'un film de mercure sur un substrait d'iridium.

Un des paramètres le plus important dans la formation d'un film de mercure est le prétraitement de la surface. Les prétraitements peuvent être généralement décrit comme physiques, tel que le polissage, chimiques, tel que le nettoyage dans l'acide, et électriques, tel que l'application d'un potentiel positif ou négatif.

Pour mésurer l'efficacité du prétraitement, nous mesurons deux paramètres: l'angle de contact (θ), et le potentiel de demi-vague pour la réduction ($E_{1/2}$) du mercure sur le substrait d'iridium.

L'oxidation et la réduction des prétraitements affectent tous deux la surface similairement en fonction de $E_{1/2}$, mais quelque peu différemment en fonction de θ. Pour tous les types de prétraitements par oxydation, acide et électrique, il y a une diminuation substantielle de $E_{1/2}$ ($\approx$ 50 mV), spécialement avec l'augmentation de la force d'oxydation, mais seulement une faible diminution de θ ($\approx 2^{\circ}$). D'un autre coté, le prétraitement de cathodisation montre de très grande diminution des deux paramètres: $E_{1/2}$ ($\approx$ 60 mV) et θ ($\approx 9^{\circ}$). Ce comportement suggère que les deux prétraitements, chimique et électrochimique, produisent une couche d'oxyde sur la surface de l'iridium. Cette couche cause plus de difficultés pour la réduction du mercure(II), mais entraine aucune différence dans la capacité du mercure à s'étendre sur la surface (aucune diminution de θ). Ceci signifie éventuellement que, quand quelques nucléides sont formés, la réduction du mercure(II) continue sur ce nucléide de préférence à l'oxyde courrant la surface. Cette situation n'est pas favorable à la formation d'un film de mercure homogène. La cathodisation réduit la couche d'oxyde, facilitant l'étalement du mercure, mais causant les mêmes difficultés pour la réduction du mercure(II) que la couche d'oxyde. En combinant anodisation-cathodisation, nous avons probablement réduit seulement partiellement la surface anodisée, en conséquence, elle présente un comportement intermédiaire. Ainsi, à partir des résultats ci-dessus, une surface cathodisée semble fournir un meilleur substrait pour la formation d'un film de mercure.

Des voltammogrammes cycliques de la réduction de mercure(II) sur une surface d'iridium fraichement prétraitée donnent des vagues de réduction réversibles, avec un potentiel de demi-vague à 165 mV vs. SCE, n = 2, et une pente de 31 mV. L'oxydation du mercure(0) donne un pic à 410 mV vs. SCE.

Différents types d'électrolytes (acide, base, neutre et complexé) sont testés. Le choix final est $HClO_4$, étant le seul avec lequel un film de mercure reproductible est formé dans 50% des cas.

L'application d'un potentiel alternatif montre qu'un film de mercure peut etre plus facilement formé en utilisant des fréquences de 1000 à 5000 Hz à un potentiel de 50 mV et une amplitude de ±350 mV.

Finallement, un procédé complet est donné pour préparer une électrode à film de mercure sur Ir (Ir-MFE).

4. Applications de l'Iridium-MFE

L'objectif premier de ce travail décrit dans cette partie, est de fournir une évaluation quantitative de l'Ir-MFE, tout en montrant ses applications possibles. Ces études sont réalisées en se concentrant sur l'application éventuelle de l'électrode pour *i)* l'analyse quantitative de métaux en trace en utilisant l'ASV, et *ii)* leur spéciation en utilisant le "Stripping Polarography".

La première étude est une comparaison des courbes caractéristiques courant-potentiel de l'ASV avec les prédictions théoriques de De Vries et Van Dalen, pour les processus controlés par diffusion à des électrodes à film de mercure. Avec les résultats de nos expériences et ceux tirés de la littérature, nous montrons que la théorie de la MFE n'est pas, et ne peut pas être, appliquée à la MFE réelle puisque un film de mercure véritable ne peut pas exister pour un deposition de plus de ≈ 0.1µm de mercure.

Des interactions substrait-mercure directes peuvent lier une mono-couche d'atomes de mercure à la surface et des forces attractives s'observant à grande distance peuvent maintenir encore approx. 100 couches stables sur la surface. Cependant, le mercure ayant une viscosité très faible et une tension de surface très grande, tendra, quand il est laissé, à une forme sphérique. En prenant le rayon des atomes de mercure égale à $1.57x10^{-8}$ cm, nous pouvons estimer approxivement qu'une mono-couche est env. de 0.0003µm, et donc nous avons ≈ 3400 couches pour un film de 1µm et plus de $1x10^{5}$ couches pour un film de 30µm. Il semble évident cependant que la masse de mercure pour des films de plus de 0.5 µm est libre de prendre une forme semi-sphérique naturelle.

La seconde partie des applications étudiées démontrent que

l'iridium-MFE peut etre utilisée pour l'analyse quantitative du cadmium dans l'eau modele, et du zinc dans l'eau de mer naturelle. En même temps, une théorie simplifiée pour la "stripping polarography" sur un film de mercure est testée et se révèle valable.